NAVAL POSTGRADUATE SCHOOL

MONTEREY, CALIFORNIA

THESIS

NONLINEAR EFFECTS IN TRANSFORMATION OPTICS-BASED METAMATERIAL SHIELDS FOR COUNTER DIRECTED ENERGY WEAPON DEFENSE

by

Jacob D. Thompson

June 2016

Thesis Co-Advisors: James Luscombe
Brett Borden

THIS PAGE INTENTIONALLY LEFT BLANK

REPORT DOCUMENTATION PAGE

Form Approved OMB No. 0704–0188

1. AGENCY USE ONLY *(Leave Blank)*	2. REPORT DATE	3. REPORT TYPE AND DATES COVERED
	06-17-2016	Master's Thesis 07-07-2014 to 06-17-2016

4. TITLE AND SUBTITLE

NONLINEAR EFFECTS IN TRANSFORMATION OPTICS-BASED METAMATERIAL SHIELDS FOR COUNTER DIRECTED ENERGY WEAPON DEFENSE

5. FUNDING NUMBERS

6. AUTHOR(S)

Jacob D. Thompson

7. PERFORMING ORGANIZATION NAME(S) AND ADDRESS(ES)

Naval Postgraduate School
Monterey, CA 93943

8. PERFORMING ORGANIZATION REPORT NUMBER

9. SPONSORING / MONITORING AGENCY NAME(S) AND ADDRESS(ES)

N/A

10. SPONSORING / MONITORING AGENCY REPORT NUMBER

11. SUPPLEMENTARY NOTES

The views expressed in this document are those of the author and do not reflect the official policy or position of the Department of Defense or the U.S. Government. IRB Protocol Number: N/A.

12a. DISTRIBUTION / AVAILABILITY STATEMENT

Approved for public release; distribution is unlimited

12b. DISTRIBUTION CODE

13. ABSTRACT *(maximum 200 words)*

Transformation optics is the current method used to design metamaterial structures that manipulate the path of electromagnetic radiation. This approach, however, relies upon a completely linear response of the polarization and magnetization fields with respect to incident electromagnetic field intensities. As those field intensities rise, such as from a hypothetical directed energy weapon, nonlinear effects, which are unaccounted for in a completely linear theory, are observed. In order to investigate the behavior of a transformation optics–derived structure in such a high-field intensity regime, we propose to employ an iterative solution to the Maxwell equations for such a structure, and compare these results to those of the purely linear transformation optics model. Examining the first-order results of this approach, we observe a strong dependence of response field amplitude upon the wavelength of incident radiation.

14. SUBJECT TERMS

transformation optics, counter-directed energy weapons, metamaterials, electrodynamics, coordinate transformations

15. NUMBER OF PAGES 137

16. PRICE CODE

17. SECURITY CLASSIFICATION OF REPORT	18. SECURITY CLASSIFICATION OF THIS PAGE	19. SECURITY CLASSIFICATION OF ABSTRACT	20. LIMITATION OF ABSTRACT
Unclassified	Unclassified	Unclassified	UU

NSN 7540-01-280-5500

Standard Form 298 (Rev. 2–89)
Prescribed by ANSI Std. 239–18

THIS PAGE INTENTIONALLY LEFT BLANK

Approved for public release; distribution is unlimited

NONLINEAR EFFECTS IN TRANSFORMATION OPTICS-BASED METAMATERIAL SHIELDS FOR COUNTER DIRECTED ENERGY WEAPON DEFENSE

Jacob D. Thompson
Lieutenant, United States Navy
B.S., University of California, Santa Barbara, 2000

Submitted in partial fulfillment of the
requirements for the degree of

MASTER OF SCIENCE IN PHYSICS

from the

NAVAL POSTGRADUATE SCHOOL
June 2016

Approved by: James Luscombe
Thesis Co-Advisor

Brett Borden
Thesis Co-Advisor

Kevin B. Smith
Chair, Department of Physics

THIS PAGE INTENTIONALLY LEFT BLANK

ABSTRACT

Transformation optics is the current method used to design metamaterial structures that manipulate the path of electromagnetic radiation. This approach, however, relies upon a completely linear response of the polarization and magnetization fields with respect to incident electromagnetic field intensities. As those field intensities rise, such as from a hypothetical directed energy weapon, nonlinear effects, which are unaccounted for in a completely linear theory, are observed. In order to investigate the behavior of a transformation optics–derived structure in such a high-field intensity regime, we propose to employ an iterative solution to the Maxwell equations for such a structure, and compare these results to those of the purely linear transformation optics model. Examining the first-order results of this approach, we observe a strong dependence of response field amplitude upon the wavelength of incident radiation.

THIS PAGE INTENTIONALLY LEFT BLANK

Table of Contents

List of Figures

List of Acronyms and Abbreviations

CDEW	Counter-Directed Energy Weapons
DEW	Directed Energy Weapons
DOD	Department of Defense
HEL	High Energy Laser
HPM	High Power Microwave
HPRF	High Power Radio Frequency
NPS	Naval Postgraduate School
NRL	Naval Research Laboratory
ONR	Office of Naval Research
TO	Transformation Optics
USNA	United States Naval Academy

THIS PAGE INTENTIONALLY LEFT BLANK

Acknowledgments

I would like to express my gratitude to Professors James Luscombe and Brett Borden of the NPS Physics Department for their encouragement, patience, and guidance, as well as to all of the professors and lecturers of the Physics Department with whom I have worked for bringing me to this point in my studies. My sincere thanks as well to my grandfather, Robert Thompson, and aunt, Catherine Thompson, for their encouragement and support as I developed this work. For all of the days studying together and discussing this thesis, as well as for her unwavering confidence in me, my everlasting thanks to my fiancée.

THIS PAGE INTENTIONALLY LEFT BLANK

CHAPTER 1:
Introduction

As the Department of Defense (DOD) continues its development and implementation of a new category of weaponry, directed energy weapons (DEW), other nations are expected to follow suit [1]. The design method known as transformation optics (TO), developed by Pendry, Schurig, and Smith [2], provides a highly useful design tool for determining the electromagnetic material properties required in order to redirect incoming electromagnetic radiation along a more desirable path. This design method has proven effective in the fabrication of real world structures using metamaterials — materials engineered to possess properties which are not found in nature [3]. Although both powerful and elegant in its formulation, TO relies upon a purely linear formulation of the response of materials to electric and magnetic fields. It has been known since at least 1941 [4] that sufficiently large electric and magnetic field amplitudes induce nonlinear (i.e., second and higher order) material responses. As these high field amplitudes are naturally expected in an environment in which the concern is the countering of certain classes of DEW, such as high power lasers and microwave devices, a question of the effectiveness of TO derived redirection structures for counter-directed energy weapon (CDEW) applications arises. We attempt here to address this question of the utility of the transformation optics approach in a CDEW environment.

1.1 Directed Energy Weapons

A directed energy weapon is a weapon which delivers electromagnetic energy, rather than a traditional projectile, to its target. Typical examples of directed energy weapons include high power microwave (HPM) or high power radio frequency (HPRF) devices, designed to induce large voltages and currents in adversary electronic systems in order to render those systems inoperative, and high energy lasers (HEL), which ablate target material through the delivery of a focused high intensity beam of electromagnetic radiation onto a small area of the target. These weapon systems have been active areas of Navy research since the 1960s, and are the subject of ongoing development [1], [5]. As research into these devices proceeds, concern has grown regarding the ability of potential adversaries to field similar

weaponry, particularly within the realm of anti satellite applications [6].

1.2 Counter-Directed Energy Weapons

In response to this concern, the Office of Naval Research (ONR), in conjunction with the Naval Postgraduate School (NPS), United States Naval Academy (USNA), and Naval Research Laboratory (NRL) is "investigating basic research topics in counter threats from directed energy weapons systems, such as high-power lasers or microwaves" [7]. These research topics include, from [1],

> a. Advanced materials including nano- and/or nonlinear materials for enhanced HEL protection of sensors, optics, airframe, etc.
> b. Metamaterial structures for the control and mitigation of HEL and HPRF irradiation.
> c. Techniques for HEL mitigation such as use of plasmas and obscurants.
> d. HEL protection by degrading atmospheric transmission (e.g. thermal blooming, scattering, absorption aids, and turbulence).
> e. Modeling and sensing of off-axis detection and source geo-location.
> f. Novel instrumentation for detection of HEL and HPRF irradiation.
> g. Active/passive circuit protection and limiters for HPRF
> h. Modeling of HPRF and HEL effects to materials, electronics and sensors as applied to CDEW objectives.

1.2.1 Transformation Optics

The field of transformation optics, founded in [2] by Pendry, Schurig, and Smith, uses the form invariance of Maxwell's equations, the fundamental equations of electromagnetism, as well as the transformation properties of various electromagnetic fields and material properties under coordinate transformations, in order to determine the material properties necessary to force electromagnetic fields to behave in some desired fashion. A design tool for directing electromagnetic radiation along a specified path, transformation optics' potential for CDEW applications was quickly recognized. Just as quickly, the material parameters necessary to realize a working electromagnetic redirection structure (as seen below), were

discovered to be unlike those found in nature. Specifically, negative electric and magnetic susceptibility values are commonly required [2], [3], [8], [9], [10]. In addition, several applications require unrealistically diverging permittivity and permeability as an outer or inner edge of the structure is approached, as well as continuously (spatially) varying permittivity and permeability [8], [9]. Figure 1.1 illustrates both ideal and approximate material parameters required to achieve the cylindrical redirection structure of [9], as well as the simulated performance of the same structure with ideal material parameters.

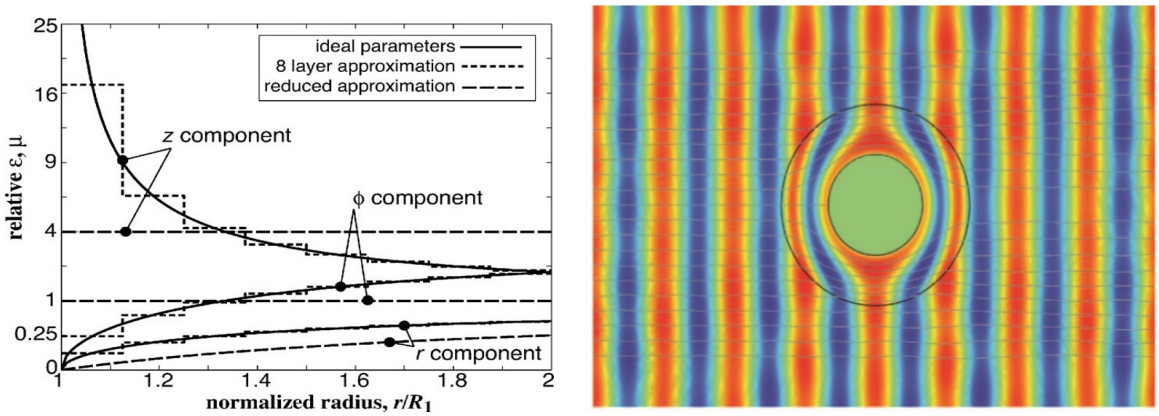

Figure 1.1: Left: Required ideal material properties for a cylindrical cloak of inner radius R_1 and outer radius of $R_2 = 2R_1$, as well as design compromises in order to make the structure realizeable. Right: Full-wave simulation of the performance of the idealized material parameters. Note that the waveform is undisturbed upon exiting the structure. Grey lines indicate the local direction of power flow. Source: [11].

While approximations and informed design compromises may effectively address the issue of diverging or continuously varying material properties [3], [12], the problem of material properties which are not observed in nature may be resolved through the use of metamaterials [12], [13]. Of particular note, however is the completely linear constitutive relation

$$P^i = \varepsilon_0 \chi_e^{ij} E_j \tag{1.1}$$

$$M^i = \chi_m^{ij} H_j \tag{1.2}$$

employed in TO, where $\vec{P}$ is the polarization, χ_e^{ij} are the components of the electric sus-

ceptibility, $\vec{E}$ is the electric field, $\vec{M}$ is the magnetization, χ_m^{ij} are the components of the magnetic susceptibility, and $\vec{H}$ is the magnetic field, and the Einstein summation convention is in use. A treatment of the theory of transformation optics is provided in Chapter 3 of this work.

1.2.2 Metamaterials

A metamaterial is a structure which is designed to possess aggregate material properties which have not yet been observed in nature. Within the context of electromagnetic interac-tions, these novel material responses are typically designed through the addition of struc-tural features which are smaller than the wavelength of radiation to be scattered. Specific to the negative permittivity and permeability often required for implementation of TO applications, an array of split-ring resonators, structures featuring two conducting, concentric, incomplete rings, is commonly used. In 2009, a cylindrical cloak operating at microwave frequencies, designed through TO and employing an array of split-ring resonators among other design features, was successfully demonstrated [3]. See Figure 1.2 for an example of this design.

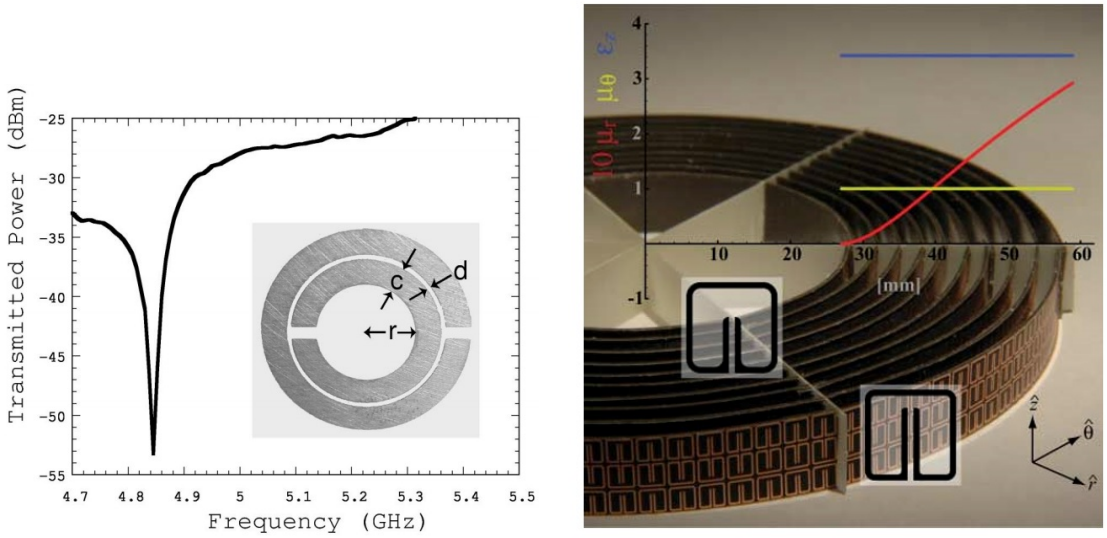

Figure 1.2: Left: Diagram of a split-ring resonator alongside its resonance curve (source: [14]). Right: Cylindrical microwave frequency cloak (source: [3]), with diagrams of split-ring resonator design based on radial position, and diagram of idealized material parameters.

Metamaterials may therefore be viewed as a promising set of structures with which we may realize a CDEW focused electromagnetic redirection device that has been designed through transformation optics.

1.3 Nonlinear Optics

As mentioned in the previous section, the TO design approach assumes a linear set of constitutive relations as given by (1.1) and (1.2). High amplitude electric and magnetic fields, however, are known to induce second order and higher effects typically modeled by, as an extension of (1.1),

$$P^i = \varepsilon_0 \left[\chi_e^{ij} E_j + \chi_e^{ijk} E_j E_k + \chi_e^{ijkl} E_j E_k E_l + ... \right] \tag{1.3}$$

where χ_e^{ijk} are the components of the second-order electric susceptibility and χ_e^{ijkl} are the components of the third-order electric susceptibility [15]. Second-order effects include frequency doubling, while third order effects include the Kerr effect, wherein refractive index varies with field strength [15]. The linear constitutive relations (1.1) and (1.2) do not allow for explicit realization of these observed phenomena. Therefore, the TO approach does not take nonlinear optical effects into account, and thus structures designed through TO may be expected to stray from design expectations as field strengths rise high enough for nonlinear effects to become non-negligible. As a potential DEW attack upon a TO designed redirection structure may involve electric and magnetic fields of sufficient intensity to trigger significant nonlinear effects, the question of applicability of the TO design method for CDEW applications arises. This question is the focus of the following chapters.

THIS PAGE INTENTIONALLY LEFT BLANK

CHAPTER 2:
Classical Electrodynamics in Matter

As TO describes a design method through which we may control the behavior of electromagnetic fields in matter, a description of the physical phenomenon of electromagnetic waves is in order. The objective of the following chapter will be the description of gen-eral electromagnetic phenomena via the Maxwell equations, followed by the application of these concepts to electromagnetic waves in free space as well as in media.

2.1 Maxwell's Equations

Maxwell's equations, the governing differential equations for all classical electrodynamic phenomena, are expressed as:

$$\nabla \cdot \vec{E} = \frac{\rho}{\varepsilon_0} \tag{2.1}$$

$$\nabla \times \vec{E} = -\frac{\partial \vec{B}}{\partial t} \tag{2.2}$$

$$\nabla \cdot \vec{B} = \vec{0} \tag{2.3}$$

$$\nabla \times \vec{B} = \mu_0 \vec{J} + \varepsilon_0 \mu_0 \frac{\partial \vec{E}}{\partial t} \tag{2.4}$$

where $\vec{E}$ is the electric field, $\vec{B}$ the magnetic flux density, ρ the charge density, $\vec{J}$ the current density, ε_o the permittivity of vacuum, and μ_o the permeability of vacuum. Note that overall charge conservation is consistent with the Maxwell equations as written: Taking the divergence of the Ampere-Maxwell law (2.4),

$$\nabla \cdot \left(\nabla \times \vec{B} \right) = \mu_0 \nabla \cdot \vec{J} + \varepsilon_0 \mu_0 \nabla \cdot \frac{\partial \vec{E}}{\partial t} \tag{2.5}$$

Since the divergence of a curl is always equal to zero, and the spatial and time derivatives are independent of each other,

$$\vec{0} = \mu_0 \nabla \cdot \vec{J} + \varepsilon_0 \mu_0 \frac{\partial \left(\nabla \cdot \vec{E} \right)}{\partial t} \tag{2.6}$$

Inserting Gauss' law (2.1) into the above relation,

$$\varepsilon_0 \frac{\partial \left(\frac{\rho}{\varepsilon_0} \right)}{\partial t} = -\nabla \cdot \vec{J} \tag{2.7}$$

$$\frac{\partial \rho}{\partial t} = -\nabla \cdot \vec{J} \tag{2.8}$$

2.2 Maxwell's Equations in Matter

While the Maxwell equations (2.1) – (2.4) provide a valid description of all electromagnetic phenomena, they are somewhat cumbersome when considering these fields in matter, where charge may be bound up in a material's constituent atoms. A more convenient approach is to first draw a distinction between ρ_f, the free charge density, and ρ_b, the bound charge density. Defining the polarization as

$$\vec{P} \equiv \frac{1}{V} \sum_i \vec{p}_i \tag{2.9}$$

where $\vec{p}_i$ is the electric dipole moment of a particular atom or molecule of interest. The bound charge density is defined as

$$\rho_b \equiv -\nabla \cdot \vec{P} \tag{2.10}$$

If charge is to be conserved, then

$$\frac{\partial \rho_b}{\partial t} = -\nabla \cdot \vec{J}_p \tag{2.11}$$

where $\vec{J}_p$ is the polarization current associated with the motion of bound charges. The above relationship thus requires

$$\vec{J}_p \equiv \frac{\partial \vec{P}}{\partial t} \tag{2.12}$$

yielding

$$\frac{\partial \rho_b}{\partial t} = \frac{\partial \left(-\nabla \cdot \vec{P}\right)}{\partial t} = -\nabla \cdot \left(\frac{\partial \vec{P}}{\partial t}\right) = -\nabla \cdot \vec{J}_p \tag{2.13}$$

The free charge density ρ_f is defined as any charge density which is not part of the bound charge density, giving

$$\rho_f + \rho_b = \rho \tag{2.14}$$

Similarly, the magnetization $\vec{M}$ is defined

$$\vec{M} \equiv \frac{1}{V}\sum_i \vec{m}_i \tag{2.15}$$

where $\vec{m}_i$ is the magnetic moment of an atom or molecule of interest. The bound current density $\vec{J}_b$ is

$$\vec{J}_b \equiv \nabla \times \vec{M} \tag{2.16}$$

The free current density $\vec{J}_f$ is the current density unaccounted for by the bound or polarization current densities. That is,

$$\vec{J} = \vec{J}_f + \vec{J}_p + \vec{J}_b \tag{2.17}$$

Inserting (2.14) into (2.1),

$$\nabla \cdot \vec{E} = \frac{\rho_f + \rho_b}{\varepsilon_0} \tag{2.18}$$

$$\nabla \cdot \vec{E} = \frac{\rho_f}{\varepsilon_0} - \frac{\nabla \cdot \vec{P}}{\varepsilon_0} \tag{2.19}$$

$$\nabla \cdot \left(\varepsilon_0 \vec{E} + \vec{P} \right) = \rho_f \tag{2.20}$$

The quantity $\varepsilon_0 \vec{E} + \vec{P}$ is the electric displacement field, denoted $\vec{D}$. Arriving at Gauss' Law for macroscopic media,

$$\nabla \cdot \vec{D} = \rho_f \tag{2.21}$$

Inserting (2.17) into (2.4),

$$\nabla \times \vec{B} = \mu_0 \left(\vec{J}_f + \vec{J}_p + \vec{J}_b \right) + \varepsilon_0 \mu_0 \frac{\partial \vec{E}}{\partial t} \tag{2.22}$$

$$\nabla \times \vec{B} = \mu_0 \left(\vec{J}_f + \frac{\partial \vec{P}}{\partial t} + \nabla \times \vec{M} \right) + \varepsilon_0 \mu_0 \frac{\partial \vec{E}}{\partial t} \tag{2.23}$$

$$\nabla \times \left(\frac{\vec{B}}{\mu_0} - \vec{M} \right) = \vec{J}_f + \frac{\partial \left(\varepsilon_0 \vec{E} + \vec{P} \right)}{\partial t} \tag{2.24}$$

$$\nabla \times \left(\frac{\vec{B}}{\mu_0} - \vec{M} \right) = \vec{J}_f + \frac{\partial \vec{D}}{\partial t} \tag{2.25}$$

The quantity $\frac{\vec{B}}{\mu_0} - \vec{M}$ is called the magnetic field and denoted $\vec{H}$. The Ampere-Maxwell law for macroscopic media is thus

$$\nabla \times \vec{H} = \vec{J}_f + \frac{\partial \vec{D}}{\partial t} \tag{2.26}$$

Replacing (2.1) with (2.21), and (2.4) with (2.26), we arrive at Maxwell's equations in matter

$$\nabla \cdot \vec{D} = \rho_f \tag{2.27}$$

$$\nabla \times \vec{E} = -\frac{\partial \vec{B}}{\partial t} \tag{2.28}$$

$$\nabla \cdot \vec{B} = \vec{0} \tag{2.29}$$

$$\nabla \times \vec{H} = \vec{J}_f + \frac{\partial \vec{D}}{\partial t} \tag{2.30}$$

2.3 The Wave Equations

2.3.1 The Wave Equations in Vacuum

Let us consider the Maxwell equations in vacuum in the absence of sources. Setting $\rho = 0$ and $\vec{J} = \vec{0}$,

$$\nabla \cdot \vec{E} = 0 \tag{2.31}$$

$$\nabla \times \vec{E} = -\frac{\partial \vec{B}}{\partial t} \tag{2.32}$$

$$\nabla \cdot \vec{B} = 0 \tag{2.33}$$

$$\nabla \times \vec{B} = \varepsilon_0 \mu_0 \frac{\partial \vec{E}}{\partial t} \tag{2.34}$$

Taking the curl of (2.32),

$$\nabla \times \nabla \times \vec{E} = -\nabla \times \left(\frac{\partial \vec{B}}{\partial t} \right) \tag{2.35}$$

Employing the vector identity $\nabla \times \nabla \times \vec{V} = -\nabla^2 \vec{V} + \nabla \left(\nabla \cdot \vec{V} \right)$,

$$-\nabla^2 \vec{E} + \nabla \left(\nabla \cdot \vec{E} \right) = -\frac{\partial \left(\nabla \times \vec{B} \right)}{\partial t} \tag{2.36}$$

Inserting (2.31) into the above relationship,

$$\nabla^2 \vec{E} = \frac{\partial \left(\nabla \times \vec{B} \right)}{\partial t} \tag{2.37}$$

Inserting the sourceless Ampere-Maxwell law (2.34) in vacuum into the above relationship,

$$\nabla^2 \vec{E} = \frac{\partial \left(\varepsilon_0 \mu_0 \frac{\partial \vec{E}}{\partial t} \right)}{\partial t} \tag{2.38}$$

$$\frac{\partial^2 \vec{E}}{\partial t^2} = \frac{1}{\varepsilon_0 \mu_0} \nabla^2 \vec{E} \tag{2.39}$$

Taking the curl of (2.34),

$$\nabla \times \nabla \times \vec{B} = \nabla \times \varepsilon_0 \mu_0 \frac{\partial \vec{E}}{\partial t} \tag{2.40}$$

$$-\nabla^2 \vec{B} + \nabla \left(\nabla \cdot \vec{B} \right) = \varepsilon_0 \mu_0 \frac{\partial \left(\nabla \times \vec{E} \right)}{\partial t} \tag{2.41}$$

Inserting Faraday's law (2.32) into the above relationship, and noting from (2.33) that $\nabla \cdot \vec{B} = 0$,

$$-\nabla^2 \vec{B} = \varepsilon_0 \mu_0 \frac{\partial \left(-\frac{\partial \vec{B}}{\partial t} \right)}{\partial t} \tag{2.42}$$

$$\frac{\partial^2 \vec{B}}{\partial t^2} = \frac{1}{\varepsilon_0 \mu_0} \nabla^2 \vec{B} \tag{2.43}$$

Recognizing (2.39) and (2.43) as wave equations for electric and magnetic fields which each propagate with velocity $\frac{1}{\sqrt{\varepsilon_0 \mu_0}} \equiv c$, which is experimentally equal to the speed of light in vacuum, we arrive at

$$\frac{\partial^2 \vec{E}}{\partial t^2} = c^2 \nabla^2 \vec{E} \tag{2.44}$$

$$\frac{\partial^2 \vec{B}}{\partial t^2} = c^2 \nabla^2 \vec{B} \tag{2.45}$$

2.3.2 The Wave Equations in Matter

Taking $\vec{E}$ and $\vec{H}$ as our primary fields, Gauss' law in matter (2.27) becomes

$$\nabla \cdot \left(\varepsilon_0 \vec{E} + \vec{P} \right) = \rho_f \tag{2.46}$$

$$\nabla \cdot \vec{E} = \frac{\rho_f}{\varepsilon_0} - \frac{1}{\varepsilon_0} \nabla \cdot \vec{P} \tag{2.47}$$

From Faraday's law in matter (2.28),

$$\nabla \times \vec{E} = -\mu_0 \frac{\partial \left(\vec{H} + \vec{M} \right)}{\partial t} \tag{2.48}$$

Equation (2.29) gives

$$\mu_0 \nabla \cdot \left(\vec{H} + \vec{M} \right) = \vec{0} \tag{2.49}$$

$$\nabla \cdot \vec{H} = -\nabla \cdot \vec{M} \tag{2.50}$$

The Ampere-Maxwell law in matter (2.30) may be expressed

$$\nabla \times \vec{H} = \vec{J}_f + \frac{\partial \left(\varepsilon_0 \vec{E} + \vec{P} \right)}{\partial t} \tag{2.51}$$

As was the case in vacuum, we assume our region of interest is free of sources - in this case, the free charge density and free current density ρ_f and $\vec{J}_f$, respectively. Taking $\rho_f = 0$ and $\vec{J}_f = 0$, Maxwell's equations now reduce to

$$\nabla \cdot \vec{E} = -\frac{1}{\varepsilon_0} \nabla \cdot \vec{P} \tag{2.52}$$

$$\nabla \times \vec{E} = -\mu_0 \frac{\partial \left(\vec{H} + \vec{M} \right)}{\partial t} \tag{2.53}$$

$$\nabla \cdot \vec{H} = -\nabla \cdot \vec{M} \tag{2.54}$$

$$\nabla \times \vec{H} = \frac{\partial \left(\varepsilon_0 \vec{E} + \vec{P} \right)}{\partial t} \tag{2.55}$$

Once again similar to the case in vacuum, we take the curl of the Maxwell equations involving the curl of the primary fields. Taking the curl of (2.48),

$$\nabla \times \nabla \times \vec{E} = -\mu_0 \nabla \times \frac{\partial \left(\vec{H} + \vec{M} \right)}{\partial t} \tag{2.56}$$

Again employing the vector identity $\nabla \times \nabla \times V = -\nabla^2 \vec{V} + \nabla \left(\nabla \cdot \vec{V} \right)$, and exploiting the independence of the temporal and spatial partial derivatives,

$$-\nabla^2 \vec{E} + \nabla \left(\nabla \cdot \vec{E} \right) = -\mu_0 \frac{\partial \left(\nabla \times \left(\vec{H} + \vec{M} \right) \right)}{\partial t} \tag{2.57}$$

Inserting (2.52) and (2.55) into the above relationship,

$$-\nabla^2 \vec{E} - \frac{1}{\varepsilon_0} \nabla \left(\nabla \cdot \vec{P} \right) = -\mu_0 \frac{\partial}{\partial t} \left[\frac{\partial \left(\varepsilon_0 \vec{E} + \vec{P} \right)}{\partial t} + \nabla \times \vec{M} \right] \tag{2.58}$$

$$\nabla^2 \vec{E} + \frac{1}{\varepsilon_0} \nabla \left(\nabla \cdot \vec{P} \right) = \mu_0 \varepsilon_0 \frac{\partial^2 \vec{E}}{\partial t^2} + \mu_0 \frac{\partial^2 \vec{P}}{\partial t^2} + \mu_0 \left(\nabla \times \frac{\partial \vec{M}}{\partial t} \right) \tag{2.59}$$

Forming the wave operator on the left, and identifying $c = \dfrac{1}{\sqrt{\varepsilon_0 \mu_0}}$ as previously,

$$\nabla^2 \vec{E} - \frac{1}{c^2}\frac{\partial^2 \vec{E}}{\partial t^2} = \mu_0 \frac{\partial^2 \vec{P}}{\partial t^2} + \mu_0 \left(\nabla \times \frac{\partial \vec{M}}{\partial t} \right) - \frac{1}{\varepsilon_0} \nabla \left(\nabla \cdot \vec{P} \right) \tag{2.60}$$

Taking the curl of (2.55),

$$\nabla \times \nabla \times \vec{H} = \nabla \times \frac{\partial \left(\varepsilon_0 \vec{E} + \vec{P} \right)}{\partial t} \tag{2.61}$$

$$-\nabla^2 \vec{H} + \nabla \left(\nabla \cdot \vec{H} \right) = \varepsilon_0 \frac{\partial \left(\nabla \times \vec{E} \right)}{\partial t} + \frac{\partial \left(\nabla \times \vec{P} \right)}{\partial t} \tag{2.62}$$

Inserting (2.53) and (2.54) into the above relationship,

$$-\nabla^2 \vec{H} - \nabla \left(\nabla \cdot \vec{M} \right) = \varepsilon_0 \frac{\partial}{\partial t} \left[-\mu_0 \frac{\partial \left(\vec{H} + \vec{M} \right)}{\partial t} \right] + \frac{\partial \left(\nabla \times \vec{P} \right)}{\partial t} \tag{2.63}$$

$$\nabla^2 \vec{H} + \nabla \left(\nabla \cdot \vec{M} \right) = \varepsilon_0 \mu_0 \frac{\partial^2 \vec{H}}{\partial t^2} + \varepsilon_0 \mu_0 \frac{\partial^2 \vec{M}}{\partial t^2} - \nabla \times \frac{\partial \vec{P}}{\partial t} \tag{2.64}$$

Once more taking $c = \dfrac{1}{\sqrt{\varepsilon_0 \mu_0}}$ and forming the wave operator on the left,

$$\nabla^2 \vec{H} - \frac{1}{c^2}\frac{\partial^2 \vec{H}}{\partial t^2} = \frac{1}{c^2}\frac{\partial^2 \vec{M}}{\partial t^2} - \nabla \times \frac{\partial \vec{P}}{\partial t} - \nabla \left(\nabla \cdot \vec{M} \right) \tag{2.65}$$

We have now obtained the wave equations in matter for $\vec{E}$ and $\vec{H}$.

$$\nabla^2 \vec{E} - \frac{1}{c^2}\frac{\partial^2 \vec{E}}{\partial t^2} = \mu_0 \frac{\partial^2 \vec{P}}{\partial t^2} + \mu_0 \left(\nabla \times \frac{\partial \vec{M}}{\partial t} \right) - \frac{1}{\varepsilon_0} \nabla \left(\nabla \cdot \vec{P} \right) \tag{2.66}$$

$$\nabla^2\vec{H} - \frac{1}{c^2}\frac{\partial^2\vec{H}}{\partial t^2} = \frac{1}{c^2}\frac{\partial^2\vec{M}}{\partial t^2} - \nabla\times\frac{\partial\vec{P}}{\partial t} - \nabla\left(\nabla\cdot\vec{M}\right) \tag{2.67}$$

This set of coupled hyperbolic inhomogeneous partial differential equations will prove resistant to the common methods of solution. Following an overview of transformation optics, which may be viewed as a method for circumventing a direct solution of the wave equations above for a desired propagation path, we will return to these expressions in an attempt to discover an iterative solution.

THIS PAGE INTENTIONALLY LEFT BLANK

CHAPTER 3:
An Overview of Transformation Optics

We now proceed to a description of transformation optics, the technique currently used in the design of metamaterial structures capable of redirecting electromagnetic radiation as desired through those structures.

As introduced by Pendry, Schurig, and Smith [2], transformation optics employs the invariance of the Maxwell equations under coordinate transformations to convert the free-space wave solutions in a coordinate-transformed system, referred to as "electromagnetic space" [9], to equally valid solutions in physical space with electric permittivity and magnetic permeability as determined solely by the coordinate transformation under consideration. A full understanding of the elegance, as well as the limitations, of the transformation optics approach will require a short overview of coordinate transformations as well as the covariant formulation of classical electrodynamics.

3.1 Coordinate Transformations

3.1.1 The Einstein Summation Convention

Throughout this chapter, repeated indices indicate summation over all components up to the dimension of the space in which we are working. That is,

$$a^i b_i \equiv \sum_{i=1}^{n} a^i b_i \tag{3.1}$$

where n is the dimension of the space, usually 3 (for classical mechanics) or 4 (for special relativistic applications). Furthermore, in order to avoid confusion between contravariant tensor components and exponents, should the need arise to express a tensor component raised to a power, the exponent will appear outside of a set of parentheses.

3.1.2 The Jacobian

Consider an invertible coordinate transformation in four dimensions from some coordinate system x^{α} into another coordinate system $x^{\alpha'}$ given by

$$x^{1'} = x^{1'}\left(x^0, x^1, x^2, x^3\right) \tag{3.2}$$

and similar for $x^{0'}, x^{2'}, x^{3'}$. Coordinate differentials in the new coordinate system are given by

$$dx^{\alpha'} = \frac{\partial x^{\alpha'}}{\partial x^{\alpha}} dx^{\alpha} \tag{3.3}$$

The expressions $\frac{\partial x^{\alpha'}}{\partial x^{\alpha}}$ form the elements of the Jacobian matrix

$$A^{\alpha'}_{\ \alpha} \equiv \frac{\partial x^{\alpha'}}{\partial x^{\alpha}} \tag{3.4}$$

$$dx^{\alpha'} = A^{\alpha'}_{\ \alpha} dx^{\alpha} \tag{3.5}$$

A contravariant vector, with components denoted V^{α} obeys the above transformation law.

$$V^{\alpha'} = A^{\alpha'}_{\ \alpha} V^{\alpha} \tag{3.6}$$

Just as the coordinate differentials comprise the primordial contravariant vector, the gradient serves as the prototypical covariant vector. Note that for some function f,

$$\partial_{\alpha'} f \equiv \frac{\partial f}{\partial x^{\alpha'}} = \frac{\partial f}{\partial x^{\alpha}} \frac{\partial x^{\alpha}}{\partial x^{\alpha'}} = A^{\alpha}_{\ \alpha'} \partial_{\alpha} f \tag{3.7}$$

A covariant vector, with components denoted V_{α} will obey the above transformation law.

3.1.3 The Metric Tensor

The covariant metric tensor g_{ij} is the collection of inner products of basis vectors in a given coordinate system. That is,

$$g_{ij} \equiv \mathbf{e}_i \cdot \mathbf{e}_j \tag{3.8}$$

Note that due to the commutative nature of the inner product, g_{ij} is symmetric. In addition,

$$ds^2 = g_{ij} dx^i dx^j \tag{3.9}$$

A metric g_{ij} therefore defines a geometry on the coordinate system in which we are interested [16]. Covariant vector elements may be related to their corresponding contravariant vector elements through the metric: For some vector $\mathbf{V}$,

$$V_i = g_{ij} V^j \tag{3.10}$$

$$V^i = g^{ij} V_j \tag{3.11}$$

These operations are commonly referred to as "lowering" or "raising" an index, respectively. We may apply these relations to extract a useful relationship between the covariant and contravariant metric.

$$V_i = g_{ij} V^j = g_{ij} g^{jk} V_k \tag{3.12}$$

$$\delta_i^k V_k = g_{ij} g^{jk} V_k \tag{3.13}$$

Where δ_i^k is the Kroneker delta.

$$(g_{ij}g^{jk} - \delta_i^k)V_k = 0 \tag{3.14}$$

Since **V** is arbitrary,

$$g_{ij}g^{jk} = \delta_i^k \tag{3.15}$$

and we conclude that $g^{\alpha\beta}$ is inverse to $g_{\alpha\beta}$.

3.1.4 Tensors

A contravariant tensor of rank 2 is a geometric object, denoted $T^{\alpha\beta}$ which transforms under the coordinate transformation given by the Jacobian $A^{\alpha'}_{\alpha}$ in the following manner

$$T^{\alpha'\beta'} = A^{\alpha'}_{\alpha}A^{\beta'}_{\beta}T^{\alpha\beta} \tag{3.16}$$

while a covariant tensor of rank 2 $T_{\alpha\beta}$ transforms as

$$T_{\alpha'\beta'} = A^{\alpha}_{\alpha'}A^{\beta}_{\beta'}T_{\alpha\beta} \tag{3.17}$$

This definition may be extended to contravariant and covariant tensors of higher rank by repeated applications of the Jacobian. For a contravariant tensor of rank n,

$$T^{a'_1a'_2\ldots a'_n} = A^{a'_1}_{a_1}A^{a'_2}_{a_2}\ldots A^{a'_n}_{a_n}T^{a_1a_2\ldots a_n} \tag{3.18}$$

while for a covariant tensor of rank n,

$$T_{a'_1a'_2\ldots a'_n} = A^{a_1}_{a'_1}A^{a_2}_{a'_2}\ldots A^{a_n}_{a'_n}T_{a_1a_2\ldots a_n} \tag{3.19}$$

A contravariant pseudotensor $\mathfrak{T}^{\alpha\beta}$ of weight w and rank n is an object with components

which transform as [16]

$$\mathfrak{T}^{\mathfrak{a}'_1\mathfrak{a}'_2\ldots\mathfrak{a}'_n} = |A|^w A^{a1'}_{a1} A^{a2'}_{a2} \ldots A^{a'_n}_{a_n} \mathfrak{T}^{\mathfrak{a}_1\mathfrak{a}_2\ldots\mathfrak{a}_n} \tag{3.20}$$

where $|A|$ is the determinant of the Jacobian. Pseudotensors of weight ± 1 are referred to as "tensor densities."

3.2 Covariant Electrodynamics

3.2.1 The Field Tensors

The covariant electromagnetic field tensor in Minkowski spacetime may be written

$$F_{\alpha\beta} = \begin{pmatrix} 0 & \frac{E_x}{c} & \frac{E_y}{c} & \frac{E_z}{c} \\ -\frac{E_x}{c} & 0 & -B_z & B_y \\ -\frac{E_y}{c} & B_z & 0 & -B_x \\ -\frac{E_z}{c} & -B_y & B_x & 0 \end{pmatrix} \tag{3.21}$$

in the basis (ct, x, y, z) with Minkowski metric

$$g_{\alpha\beta} = \begin{pmatrix} 1 & 0 & 0 & 0 \\ 0 & -1 & 0 & 0 \\ 0 & 0 & -1 & 0 \\ 0 & 0 & 0 & -1 \end{pmatrix} \tag{3.22}$$

The contravariant electromagnetic field tensor may be found through

$$F^{\alpha\beta} = g^{\alpha\mu} g^{\nu\beta} F_{\mu\nu} = \begin{pmatrix} 0 & -\frac{E_x}{c} & -\frac{E_y}{c} & -\frac{E_z}{c} \\ \frac{E_x}{c} & 0 & -B_z & B_y \\ \frac{E_y}{c} & B_z & 0 & -B_x \\ \frac{E_z}{c} & -B_y & B_x & 0 \end{pmatrix} \tag{3.23}$$

The contravariant magnetization-polarization tensor density (weight -1) $\mathfrak{M}^{\alpha\beta}$ is

$$\mathfrak{M}^{\alpha\beta} = \begin{pmatrix} 0 & P_x c & P_y c & P_z c \\ -P_x c & 0 & -M_z & M_y \\ -P_y c & M_z & 0 & -M_x \\ -P_z c & -M_y & M_x & 0 \end{pmatrix} \tag{3.24}$$

The contravariant displacement tensor density (weight -1) $\mathfrak{D}^{\alpha\beta}$ [16], [15] is, in this metric,

$$\mathfrak{D}^{\alpha\beta} = \begin{pmatrix} 0 & -D_x c & -D_y c & -D_z c \\ D_x c & 0 & -H_z & H_y \\ D_y c & H_z & 0 & -H_x \\ D_z c & -H_y & H_x & 0 \end{pmatrix} \tag{3.25}$$

The electromagnetic field tensor, magnetization-polarization tensor, and displacement tensor are related through

$$\mathfrak{D}^{\alpha\beta} = \frac{1}{\mu_0} F^{\alpha\beta} - \mathfrak{M}^{\alpha\beta} \tag{3.26}$$

3.2.2 The Maxwell Equations

The free current density (weight -1) four-vector is

$$J_f^{\nu} = \left(c\rho_f, \vec{J}_f \right) \tag{3.27}$$

From Gauss' Law (2.27) in matter,

$$\nabla \cdot \vec{D} = \rho_f \tag{3.28}$$

$$\partial_1 D_x + \partial_2 D_y + \partial_3 D_z = \rho_f \tag{3.29}$$

$$\partial_1 \frac{1}{c}\mathfrak{D}^{01} + \partial_2 \frac{1}{c}\mathfrak{D}^{02} + \partial_3 \frac{1}{c}\mathfrak{D}^{03} = \frac{1}{c}J_f^0 \tag{3.30}$$

$$\partial_1 \mathfrak{D}^{01} + \partial_2 \mathfrak{D}^{02} + \partial_3 \mathfrak{D}^{03} = J_f^0 \tag{3.31}$$

Since $\mathfrak{D}^{00} = 0$,

$$\partial_0 \mathfrak{D}^{00} + \partial_1 \mathfrak{D}^{01} + \partial_2 \mathfrak{D}^{02} + \partial_3 \mathfrak{D}^{03} = J_f^0 \tag{3.32}$$

While from the Ampere-Maxwell Law (2.30) in matter,

$$\nabla \times \vec{H} = \vec{J}_f + \frac{\partial \vec{D}}{\partial t} \tag{3.33}$$

The x-component of the above relation is

$$\partial_2 H_z - \partial_3 H_y = J_{f,x} + c\partial_0 D_x \tag{3.34}$$

$$\partial_2 H_z - \partial_3 H_y = J_f^1 - \partial_0 \mathfrak{D}^{01} \tag{3.35}$$

$$\partial_2 \mathfrak{D}^{21} + \partial_3 \mathfrak{D}^{31} = J_f^1 - \partial_0 \mathfrak{D}^{01} \tag{3.36}$$

But $\mathfrak{D}^{11} = 0$, and so

$$\partial_1 \mathfrak{D}^{11} + \partial_2 \mathfrak{D}^{21} + \partial_3 \mathfrak{D}^{31} = J_f^1 - \partial_0 \mathfrak{D}^{01} \tag{3.37}$$

$$\partial_0 \mathfrak{D}^{01} + \partial_1 \mathfrak{D}^{11} + \partial_2 \mathfrak{D}^{21} + \partial_3 \mathfrak{D}^{31} = J_f^1 \tag{3.38}$$

Similarly, the y-component of the Ampere-Maxwell Law in matter may be expressed

$$\partial_0 \mathfrak{D}^{02} + \partial_1 \mathfrak{D}^{12} + \partial_2 \mathfrak{D}^{22} + \partial_3 \mathfrak{D}^{32} = J_f^2 \tag{3.39}$$

While from the z-component,

$$\partial_0 \mathfrak{D}^{03} + \partial_1 \mathfrak{D}^{13} + \partial_2 \mathfrak{D}^{23} + \partial_3 \mathfrak{D}^{33} = J_f^3 \tag{3.40}$$

(3.32), (3.38), (3.39), and (3.40) may be summarized, in the Einstein summation convention,

$$\partial_\mu \mathfrak{D}^{\mu\nu} = J_f^\nu \tag{3.41}$$

We note that the above expression contains both Gauss' law and the Ampere-Maxwell law in linear media. Turning to the two sourceless Maxwell equations,

$$\nabla \cdot \vec{B} = \vec{0} \tag{3.42}$$

$$\nabla \times \vec{E} + \frac{\partial \vec{B}}{\partial t} = 0 \tag{3.43}$$

Note that (3.42) may be expressed

$$\partial_1 B_1 + \partial_2 B_2 + \partial_3 B_3 = 0 \tag{3.44}$$

$$\partial_1 F_{23} + \partial_2 F_{31} + \partial_3 F_{12} = 0 \tag{3.45}$$

While due to the antisymmetric nature of the electromagnetic field tensor (3.21),

$$\partial_1 F_{32} + \partial_2 F_{13} + \partial_3 F_{21} = 0 \tag{3.46}$$

From the x-component of Faraday's law,

$$\left[\nabla \times \vec{E} + \frac{\partial \vec{B}}{\partial t}\right]_1 = 0 \tag{3.47}$$

$$\partial_2 E_3 - \partial_3 E_2 + c\partial_0 B_1 = 0 \tag{3.48}$$

$$c\partial_2 F_{03} + c\partial_3 F_{20} + c\partial_0 F_{32} = 0 \tag{3.49}$$

$$\partial_2 F_{03} + \partial_3 F_{20} + \partial_0 F_{32} = 0 \tag{3.50}$$

Once again we exploit the antisymmetric nature of the electromagnetic field tensor to obtain

$$\partial_2 F_{30} + \partial_3 F_{02} + \partial_0 F_{23} = 0 \tag{3.51}$$

Similarly, from the y-component of Faraday's law we obtain

$$\partial_1 F_{30} + \partial_3 F_{01} + \partial_0 F_{13} = 0 \tag{3.52}$$

$$\partial_1 F_{03} + \partial_3 F_{10} + \partial_0 F_{31} = 0 \tag{3.53}$$

And from the z-component of Faraday's law

$$\partial_1 F_{02} + \partial_2 F_{10} + \partial_0 F_{21} = 0 \tag{3.54}$$

$$\partial_1 F_{20} + \partial_2 F_{01} + \partial_0 F_{12} = 0 \tag{3.55}$$

Equations (3.45), (3.46), and (3.50)–(3.55) contain all possible three-element cyclic permutations of the four spacetime indices, and may be encapsulated as

$$\partial_\alpha F_{\beta\sigma} + \partial_\beta F_{\sigma\alpha} + \partial_\sigma F_{\alpha\beta} = 0 \tag{3.56}$$

Or equivalently,

$$\partial_\alpha \left(\frac{1}{2} \varepsilon^{\alpha\beta\gamma\delta} F_{\gamma\delta} \right) = 0 \tag{3.57}$$

where $\varepsilon^{\alpha\beta\gamma\delta}$ is the four dimensional Levi-Civita symbol. The quantity $\frac{1}{2}\varepsilon^{\alpha\beta\gamma\delta}F_{\gamma\delta} \equiv \mathscr{F}^{\alpha\beta}$ is denoted as the dual tensor to the electromagnetic field tensor.

$$\partial_\alpha \mathscr{F}^{\alpha\beta} = 0 \tag{3.58}$$

We note that the dual electromagnetic tensor

$$\mathscr{F}^{\alpha\beta} = \begin{pmatrix} 0 & B_x & B_y & B_z \\ -B_x & 0 & -\frac{E_z}{c} & \frac{E_y}{c} \\ -B_y & \frac{E_z}{c} & 0 & -\frac{E_x}{c} \\ -B_z & -\frac{E_y}{c} & \frac{E_x}{c} & 0 \end{pmatrix} \tag{3.59}$$

may be obtained from the components of $F^{\alpha\beta}$ through $\vec{B} \to E$, $\frac{1}{c}\vec{E} \to \frac{1}{c}\vec{B}$. Equation (3.58) contains both Faraday's law and $\nabla \cdot \vec{B} = \vec{0}$. Maxwell's equations in matter may thus be

expressed in covariant form as

$$\partial_\mu \mathfrak{D}^{\mu\nu} = J_f^\nu \tag{3.60}$$

$$\partial_\alpha \mathscr{F}^{\alpha\beta} = 0 \tag{3.61}$$

3.2.3 The Covariant Constitutive Relations

The constitutive relations linking the primary fields to the material response fields are taken as

$$\vec{P} = \varepsilon_0 \chi_e \vec{E} \tag{3.62}$$

$$\vec{M} = \chi_m \vec{H} \tag{3.63}$$

for homogenous, isotropic, linear media, where the scalar values χ_e and χ_m are the electric and magnetic susceptibilities of the material under consideration. For anisotropic linear media, we take these susceptibilities as second rank tensors, leading to the relations

$$\vec{P} = \varepsilon_0 \boldsymbol{\chi}_\mathbf{e} * \vec{E} \tag{3.64}$$

$$\vec{M} = \boldsymbol{\chi}_\mathbf{m} * \vec{H} \tag{3.65}$$

where $*$ indicates tensor contraction. By components,

$$P^i = \varepsilon_0 \chi_e^{ij} E_j \tag{3.66}$$

$$M^i = \chi_m^{ij} H_j \tag{3.67}$$

The covariant representation of these relations may be given as [4], [10]

$$\mathfrak{M}^{\mu\nu} = \chi^{\mu\nu\alpha\beta} F_{\alpha\beta} \tag{3.68}$$

where $\chi^{\mu\nu\alpha\beta}$ are the components of the rank four contravariant susceptibility. We may conclude from the known nature of $\mathfrak{M}$ as a tensor density of weight -1 and the tensor quotient theorem [16], that χ must also transform as a tensor density of weight -1. The traditional permittivity and permeability of the material in question may be extracted from the susceptibility tensor density: Inserting (3.26) into (3.68) [10],

$$\mathfrak{D}^{\alpha\beta} = \frac{1}{\mu_0} F^{\alpha\beta} - \mathfrak{M}^{\alpha\beta} = \frac{1}{\mu_0} F^{\alpha\beta} - \chi^{\alpha\beta\mu\nu} F_{\mu\nu} \tag{3.69}$$

Since $F^{\alpha\beta}$ is antisymmetric, it may be expressed [10]

$$F^{\alpha\beta} = \frac{1}{2}\left(F^{\alpha\beta} - F^{\beta\alpha}\right) \tag{3.70}$$

$$F^{\alpha\beta} = \frac{1}{2}\left(g^{\alpha\mu} g^{\beta\nu} - g^{\beta\mu} g^{\alpha\nu}\right) F_{\mu\nu} \tag{3.71}$$

Inserting this relationship into (3.69),

$$\mathfrak{D}^{\alpha\beta} = \frac{1}{2\mu_0}\left(g^{\alpha\mu} g^{\beta\nu} - g^{\beta\mu} g^{\alpha\nu} - \chi^{\alpha\beta\mu\nu}\right) F_{\mu\nu} \tag{3.72}$$

Defining $X^{\alpha\beta\gamma\delta}$ as [10]

$$X^{\alpha\beta\gamma\delta} \equiv \frac{1}{2\mu_0}\left(g^{\alpha\gamma}g^{\beta\delta} - g^{\beta\gamma}g^{\alpha\delta} - \chi^{\alpha\beta\gamma\delta}\right) \tag{3.73}$$

Note that the displacement tensor density elements are, in terms of this new susceptibility tensor,

$$\mathfrak{D}^{\alpha\beta} = X^{\alpha\beta\mu\nu}F_{\mu\nu} \tag{3.74}$$

We will take the above relationship as our covariant constitutive relationship. Note again from the quotient theorem that since $\mathfrak{D}$ transforms as a tensor density of weight -1 that $\mathbf{X}$ must also transform as a tensor density of weight -1.

We pause for a moment to observe that *our constitutive relationship above is completely linear and therefore does not explicitly account for observed nonlinear effects* e.g., self-focusing, frequency doubling.

We may extract the traditional bianisotropic coupling coefficients, such as the permittivity and permeability from the elements of $\mathbf{X}$. From, for example, the $(\alpha\beta) = (01)$ term [10],

$$\mathfrak{D}^{01} = X^{01\mu\nu}F_{\mu\nu} \tag{3.75}$$

$$-cD_x = X^{01\mu\nu}F_{\mu\nu} \tag{3.76}$$

$$\begin{aligned} -cD_x = {} & X^{0100}F_{00} + X^{0101}F_{01} + X^{0102}F_{02} + X^{0103}F_{03} \\ & + X^{0110}F_{10} + X^{0111}F_{11} + X^{0112}F_{12} + X^{0113}F_{13} \\ & + X^{0120}F_{20} + X^{0121}F_{21} + X^{0122}F_{22} + X^{0123}F_{23} \\ & + X^{0130}F_{30} + X^{0131}F_{31} + X^{0132}F_{32} + X^{0133}F_{33} \end{aligned} \tag{3.77}$$

$$-cD_x = -X^{0101}\frac{E_x}{c} - X^{0102}\frac{E_y}{c} - X^{0103}\frac{E_z}{c} + X^{0110}\frac{E_x}{c} - X^{0112}B_z + X^{0113}B_y \\ + X^{0120}\frac{E_y}{c} + X^{0121}B_z - X^{0123}B_x + X^{0130}\frac{E_z}{c} - X^{0131}B_y + \chi^{0132}B_x \quad (3.78)$$

$$cD_x = \left(X^{0101} - X^{0110}\right)\frac{E_x}{c} + \left(X^{0102} - X^{0120}\right)\frac{E_y}{c} + \left(X^{0103} - X^{0130}\right)\frac{E_z}{c} \\ + \left(X^{0123} - X^{0132}\right)B_x + \left(X^{0131} - X^{0113}\right)B_y + \left(X^{0112} - X^{0121}\right)B_z \quad (3.79)$$

Comparing this relationship to the common bianisotropic constitutive relationship [15]

$$\vec{D} = \varepsilon\vec{E} + \xi\vec{H} \quad (3.80)$$

$$\vec{B} = \mu\vec{H} + \zeta\vec{E} \quad (3.81)$$

where $\varepsilon, \xi, \mu, \zeta$ are the spatial tensors which couple the electric displacement and magnetic fields to the electric and magnetic fields,

$$\varepsilon^{1j} = \frac{1}{c^2}\left(X^{010j} - X^{01j0}\right) \quad (3.82)$$

Note that since the electromagnetic field tensor $\mathbf{F}$ is antisymmetric, our constitutive relationship (3.74) requires that $X^{\alpha\beta\,\mu\nu}$ be antisymmetric with respect to the pairs $\mu\nu$. Therefore

$$\varepsilon^{1j} = \frac{2}{c^2}X^{010j} \quad (3.83)$$

Similar calculations yield expressions for the remaining components of the permittivity [10]

$$\varepsilon^{ij} = \frac{2}{c^2} X^{0i0j} \tag{3.84}$$

3.3 Transformation Optics

Having constructed the contravariant rank 4 modified susceptibility tensor density $X^{\alpha\beta\gamma\delta}$ [15], and analyzed the transformation properties of tensors [16], we may now investigate the transformation properties of the material parameters contained within the susceptibility tensor. As a contravariant tensor density of rank 4 and weight -1, under a coordinate transformation described by the Jacobian $A^{\alpha'}_{\alpha}$, the contravariant components of the redefined susceptibility $\mathbf{X}$ transform as [10]

$$X^{\alpha'\beta'\gamma'\delta'} = |A|^{-1} A^{\alpha'}_{\alpha} A^{\beta'}_{\beta} A^{\gamma'}_{\gamma} A^{\delta'}_{\delta} X^{\alpha\beta\gamma\delta} \tag{3.85}$$

We now investigate the way in which the Maxwell equations in media transform under such a coordinate transformation. From (3.60) and (3.61),

$$\partial_\mu \mathfrak{D}^{\mu\nu} = J_f^\nu \tag{3.86}$$

$$\partial_\alpha \mathscr{F}^{\alpha\beta} = 0 \tag{3.87}$$

Applying the coordinate transformation given by the Jacobian with elements $A^{\alpha'}_{\alpha}$ to the left hand side of the Gauss-Ampere-Maxwell law (3.84),

$$\partial_{\mu'} \mathfrak{D}^{\mu'\nu'} = |A|^{-1} A^{\mu}_{\ \mu'} A^{\mu'}_{\mu} A^{\nu'}_{\ \nu} \partial_\mu \mathfrak{D}^{\mu\nu} = |A|^{-1} A^{\mu}_{\ \mu'} A^{\mu'}_{\mu} A^{\nu'}_{\ \nu} J_f^\nu \tag{3.88}$$

But

$$A^{\mu}{}_{\mu'}A^{\mu'}{}_{\mu} = \frac{\partial x^{\mu}}{\partial x^{\mu'}}\frac{\partial x^{\mu'}}{\partial x^{\mu}} = \frac{\partial x^{\mu}}{\partial x^{\mu}} = 1 \tag{3.89}$$

and so

$$\partial_{\mu'}\mathfrak{D}^{\mu'\nu'} = |A|^{-1}A^{\nu'}_{\nu}J^{\nu}_{f} \tag{3.90}$$

Since the four-current density is a tensor density of rank 1, weight -1, it will transforms as

$$J^{\alpha'}_{f} = |A|^{-1}A^{\alpha'}{}_{\alpha}J^{\alpha}_{f} \tag{3.91}$$

The Gauss-Ampere-Maxwell law therefore transforms as

$$\partial_{\mu'}\mathfrak{D}^{\mu'\nu'} = J^{\nu'}_{f} \tag{3.92}$$

and is thus form invariant under coordinate transformations. Turning to the Faraday-Gauss law,

$$\partial_{\alpha'}\mathscr{F}^{\alpha'\beta'} = A^{\alpha}{}_{\alpha'}A^{\alpha'}_{\alpha}A^{\beta'}{}_{\beta}\partial_{\alpha}\mathscr{F}^{\alpha\beta} = 0 \tag{3.93}$$

All of the Maxwell equations are therefore form invariant under coordinate transformations, as we might expect of such a set of tensor relationships. A valid solution set $\mathscr{F}^{\alpha\beta}, \mathfrak{D}^{\alpha\beta}, X^{\alpha\beta\gamma\delta}$ to Maxwell's equations in one coordinate system will provide a valid solution set $\mathscr{F}^{\alpha'\beta'}, \mathfrak{D}^{\alpha'\beta'}, X^{\alpha'\beta'\gamma'\delta'}$ in another coordinate system according to our transformation properties [10]

$$\mathscr{F}^{\alpha'\beta'} = A^{\alpha'}_{\alpha}A^{\beta'}{}_{\beta}\mathscr{F}^{\alpha\beta} \tag{3.94}$$

$$\mathfrak{D}^{\alpha'\beta'} = |A|^{-1} A^{\alpha'}_{\ \alpha} A^{\beta'}_{\ \beta} \mathfrak{D}^{\alpha\beta} \tag{3.95}$$

$$X^{\alpha'\beta'\gamma'\delta'} = |A|^{-1} A^{\alpha'}_{\ \alpha} A^{\beta'}_{\ \beta} A^{\gamma'}_{\ \gamma} A^{\delta'}_{\ \delta} X^{\alpha\beta\gamma\delta} \tag{3.96}$$

The form invariance of the Maxwell equations and the resulting transformation properties of the modified susceptibility tensor density **X** is the concept at the heart of Transformation Optics.

3.3.1 Spatial Transformations

Turning now to the special case of transformations which do not involve the time:

$$t' = t \quad x' = x'(x,y,z) \quad y' = y'(x,y,z) \quad z' = z'(x,y,z) \tag{3.97}$$

Note that under this set of restrictions

$$A^{0'}_{\ 0} = 1 \quad A^{0'}_{\ i} = 0 \tag{3.98}$$

for all i from 1 to 3 (spatial index). From (3.84) the components of the electrical permittivity transform as

$$\varepsilon^{i'j'} = \frac{2}{c^2} X^{0'i'0'j'} = \frac{2}{c^2} |A|^{-1} A^{0'}_{\ \alpha} A^{i'}_{\ \beta} A^{0'}_{\ \gamma} A^{j'}_{\ \delta} X^{\alpha\beta\gamma\delta} \tag{3.99}$$

From (3.98), the only α or γ which survive the summation are $\alpha = 0$ and $\gamma = 0$.

$$\varepsilon^{i'j'} = \frac{2}{c^2} |A|^{-1} A^{i'}_{\ \beta} A^{j'}_{\ \delta} X^{0\beta0\delta} \tag{3.100}$$

But from (3.84), $\frac{2}{c^2} X^{0\beta0\delta} = \varepsilon^{\beta\delta}$. Reindexing, [10]

$$\varepsilon^{i'j'} = |A|^{-1} A^{i'}{}_{i} A^{j'}{}_{j} \varepsilon^{ij} \tag{3.101}$$

3.3.2 Application: Cylindrical Cloak

As our first investigation into the design of an electromagnetic redirection structure, we follow the development of a right circular cylindrical device in [9]. Let unprimed coordinates represent physical space and primed coordinates represent our electromagnetic space. We consider a coordinate transformation of the form

$$r = \frac{b-a}{b} r' + a \tag{3.102}$$

$$\phi = \phi' \tag{3.103}$$

$$z = z' \tag{3.104}$$

$$ct = ct' \tag{3.105}$$

in cylindrical coordinates, where a and b are positive real numbers, with $b > a$. Such a transform maps the line $r' = 0$ onto the circular cylinder $r = a$ and the circular cylinder $r' = b$ onto the circular cylinder $r = b$. Figure 3.1 illustrates such a coordinate transformation.

Let us assume vacuum in the electromagnetic space. Then $\varepsilon^{i'j'} = \varepsilon_0 \delta^{i'}_{j'}$ and $\mu^{i'j'} = \mu_0 \delta^{i'}_{j'}$. As the transformation (3.102) does not involve the time, we may apply (3.101) in order to determine the transformed permittivity in physical space

$$\varepsilon^{ij} = |A|^{-1} A^{i}{}_{i'} A^{j}{}_{j'} \varepsilon^{i'j'} \tag{3.106}$$

The Elements $A^{\alpha}{}_{\alpha'}$ of the Jacobian are

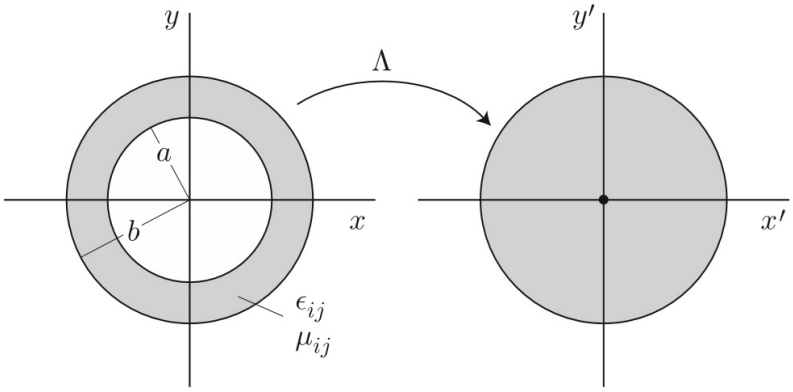

Figure 3.1: Transformation for Cylindrical Cloaking Structure. Source: [9]

.

$$A^{\alpha}{}_{\alpha'} = \frac{\partial x^{\alpha}}{\partial x^{\alpha'}} \tag{3.107}$$

And so

$$A^{0}{}_{0'} = \frac{\partial (ct)}{\partial (ct')} = 1 \tag{3.108}$$

$$A^{0}{}_{i'} = \frac{\partial (ct)}{\partial x^{i'}} = 0 \tag{3.109}$$

$$A^{i}{}_{0'} = \frac{\partial x^{i}}{\partial (ct')} = 0 \tag{3.110}$$

for all spatial indices i,$i' = 1,2,3$. Computing the remaining elements of this Jacobian,

$$A^{1}{}_{1'} = \frac{\partial x}{\partial x'} = \frac{\partial (r\cos(\phi))}{\partial x'} \tag{3.111}$$

$$A^1{}_{1'} = \frac{\partial\left(r\cos\left(\phi\right)\right)}{\partial r'}\frac{\partial r'}{\partial x'} + \frac{\partial\left(r\cos\left(\phi\right)\right)}{\partial \phi'}\frac{\partial \phi'}{\partial x'} + \frac{\partial\left(r\cos\left(\phi\right)\right)}{\partial z'}\frac{\partial z'}{\partial x'} \tag{3.112}$$

$$A^1{}_{1'} = \frac{\partial}{\partial r'}\left[\frac{b-a}{b}r'\cos\left(\phi'\right) + a\cos\left(\phi'\right)\right]\frac{\partial r'}{\partial x'} + \frac{\partial\left(r\cos\left(\phi'\right)\right)}{\partial \phi'}\frac{\partial \phi'}{\partial x'} \tag{3.113}$$

Let $R \equiv \dfrac{b-a}{b}$.

$$A^1{}_{1'} = R\cos\left(\phi'\right)\frac{\partial r'}{\partial x'} - r\sin\left(\phi'\right)\frac{\partial \phi'}{\partial x'} \tag{3.114}$$

$$A^1{}_{1'} = R\cos\left(\phi'\right)\frac{\partial\left(\sqrt{x'^2+y'^2}\right)}{\partial x'} - r\sin\left(\phi'\right)\frac{\partial\left(\tan^{-1}\left(\frac{y'}{x'}\right)\right)}{\partial x'} \tag{3.115}$$

$$A^1{}_{1'} = R\cos\left(\phi'\right)\frac{x'}{r'} + r\sin\left(\phi'\right)\frac{y'}{x'^2\left(1+\frac{y'^2}{x'^2}\right)} \tag{3.116}$$

$$A^1{}_{1'} = R\cos^2\left(\phi'\right) + \frac{r}{r'}\sin^2\left(\phi'\right) \tag{3.117}$$

$$A^1{}_{2'} = \frac{\partial x^1}{\partial x^{2'}} = \frac{\partial\left(r\cos\left(\phi\right)\right)}{\partial y'} \tag{3.118}$$

$$A^1{}_{2'} = \frac{\partial}{\partial y'}\left[Rr'\cos\left(\phi'\right) + a\cos\left(\phi'\right)\right] \tag{3.119}$$

$$A^1{}_{2'} = \left(Rr'+a\right)\frac{\partial\left(\cos\left(\phi'\right)\right)}{\partial y'} + R\cos\left(\phi'\right)\frac{\partial r'}{\partial y'} \tag{3.120}$$

$$A^1{}_{2'} = \left(Rr' + a\right) \frac{\partial \left(\frac{x'}{r'}\right)}{\partial y'} + R\cos\left(\phi'\right) \frac{\partial \left(\sqrt{x'^2 + y'^2}\right)}{\partial y'} \tag{3.121}$$

$$A^1{}_2 = -\left(Rr' + a\right) \frac{x'}{r'^2} \frac{\partial \left(\sqrt{x'^2 + y'^2}\right)}{\partial y'} + R\cos\left(\phi'\right) \frac{\partial \left(\sqrt{x'^2 + y'^2}\right)}{\partial y'} \tag{3.122}$$

$$A^1{}_{2'} = -\left(Rr' + a\right) \frac{x'y'}{r'^3} + R\cos\left(\phi'\right) \frac{y'}{r'} \tag{3.123}$$

$$A^1{}_{2'} = -\left(Rr' + a\right) \frac{\cos\left(\phi'\right)\sin\left(\phi'\right)}{r'} + R\cos\left(\phi'\right)\sin\left(\phi'\right) \tag{3.124}$$

$$A^1{}_{2'} = -\frac{a}{r'}\cos\left(\phi'\right)\sin\left(\phi'\right) = \frac{Rr' - r}{r'}\cos\left(\phi'\right)\sin\left(\phi'\right) \tag{3.125}$$

$$A^1{}_{2'} = \left(R - \frac{r}{r'}\right)\cos\left(\phi'\right)\sin\left(\phi'\right) \tag{3.126}$$

$$A^1{}_{3'} = \frac{\partial x^1}{\partial x^{3'}} = \frac{\partial x}{\partial z'} = 0 \tag{3.127}$$

$$A^2{}_{1'} = \frac{\partial \left(r\sin\left(\phi'\right)\right)}{\partial x'} = \frac{\partial}{\partial x'}\left[\left(Rr' + a\right)\sin\left(\phi'\right)\right] \tag{3.128}$$

$$A^2{}_{1'} = \left(Rr' + a\right) \frac{\partial \left(\sin\left(\phi'\right)\right)}{\partial x'} + R\sin\left(\phi'\right) \frac{\partial r'}{\partial x'} \tag{3.129}$$

$$A^2{}_{1'} = \left(Rr' + a\right) \frac{\partial \left(\frac{y'}{r'}\right)}{\partial x'} + R\sin\left(\phi'\right) \frac{\partial r'}{\partial x'} \tag{3.130}$$

$$A^2{}_{1'} = -\left(Rr'+a\right)\frac{y'}{r'^2}\frac{\partial r'}{\partial x'} + R\sin\left(\phi'\right)\frac{\partial r'}{\partial x'} \tag{3.131}$$

$$A^2{}_{1'} = \left(-\left(Rr'+a\right)\frac{\sin\left(\phi'\right)}{r'} + R\sin\left(\phi'\right)\right)\frac{\partial r'}{\partial x'} \tag{3.132}$$

$$A^2{}_{1'} = -\frac{a}{r'}\sin\left(\phi'\right)\frac{\partial r'}{\partial x'} = -\frac{ax'}{r'^2}\sin\left(\phi'\right) \tag{3.133}$$

$$A^2{}_{1'} = \frac{\left(Rr'-r\right)}{r'}\cos\left(\phi'\right)\sin\left(\phi'\right) \tag{3.134}$$

$$A^2{}_{1'} = \left(R-\frac{r}{r'}\right)\cos\left(\phi'\right)\sin\left(\phi'\right) \tag{3.135}$$

$$A^2{}_{2'} = \frac{\partial\left(r\sin\left(\phi'\right)\right)}{\partial y'} = \frac{\partial}{\partial y'}\left[\left(Rr'+a\right)\sin\left(\phi'\right)\right] \tag{3.136}$$

$$A^2{}_{2'} = \left(Rr'+a\right)\frac{\partial\left(\sin\left(\phi'\right)\right)}{\partial y'} + R\sin\left(\phi'\right)\frac{\partial r'}{\partial y'} \tag{3.137}$$

$$A^2{}_{2'} = \left(Rr'+a\right)\frac{\partial\left(\frac{y'}{r'}\right)}{\partial y'} + R\sin\left(\phi'\right)\frac{\partial r'}{\partial y'} \tag{3.138}$$

$$A^2{}_{2'} = \left(Rr'+a\right)\left(-\frac{y'}{r'^2}\frac{\partial r'}{\partial y'} + \frac{1}{r'}\right) + R\sin\left(\phi'\right)\frac{\partial r'}{\partial y'} \tag{3.139}$$

$$A^2{}_{2'} = \left(Rr'+a\right)\left(-\frac{y'^2}{r'^3} + \frac{1}{r'}\right) + R\sin\left(\phi'\right)\frac{y'}{r'} \tag{3.140}$$

$$A^2{}_{2'} = \left(Rr' + a\right) \frac{1 - \sin^2\left(\phi'\right)}{r'} + R\sin^2\left(\phi'\right) \tag{3.141}$$

$$A^2{}_{2'} = \left(Rr' + a\right) \frac{\cos^2\left(\phi'\right)}{r'} + R\sin^2\left(\phi'\right) \tag{3.142}$$

$$A^2{}_{2'} = R\sin^2\left(\phi'\right) + \frac{r}{r'}\cos^2\left(\phi'\right) \tag{3.143}$$

$$A^2{}_{3'} = \frac{\partial y}{\partial z'} = 0 \tag{3.144}$$

The remaining components of the Jacobian are somewhat simpler. For $i' = 1, 2$, we obtain

$$A^3{}_{i'} = \frac{\partial z}{\partial x^{i'}} = 0 \tag{3.145}$$

While

$$A^3{}_{3'} = \frac{\partial z}{\partial z'} = 1 \tag{3.146}$$

Our Jacobian therefore takes the form

$$A = \begin{pmatrix} R\cos^2\left(\phi'\right) + \frac{r}{r'}\sin^2\left(\phi'\right) & \left(R - \frac{r}{r'}\right)\cos\left(\phi'\right)\sin\left(\phi'\right) & 0 \\ \left(R - \frac{r}{r'}\right)\cos\left(\phi'\right)\sin\left(\phi'\right) & R\sin^2\left(\phi'\right) + \frac{r}{r'}\cos^2\left(\phi'\right) & 0 \\ 0 & 0 & 1 \end{pmatrix} \tag{3.147}$$

The determinant $|A|$ of this Jacobian is

$$|A| = \left(R\cos^2\left(\phi'\right) + \frac{r}{r'}\sin^2\left(\phi'\right)\right)\left(R\sin^2\left(\phi'\right) + \frac{r}{r'}\cos^2\left(\phi'\right)\right) - \left(R - \frac{r}{r'}\right)^2\cos^2\left(\phi'\right)\sin^2\left(\phi'\right) \tag{3.148}$$

$$|A| = \left(R^2 + \frac{r^2}{r'^2}\right)\cos^2\left(\phi'\right)\sin^2\left(\phi'\right) + \frac{Rr}{r'}\left(\cos^4\left(\phi'\right) + \sin^4\left(\phi'\right)\right) - \left(R - \frac{r}{r'}\right)^2\cos^2\left(\phi'\right)\sin^2\left(\phi'\right) \tag{3.149}$$

$$|A| = \frac{Rr}{r'}\left(\cos^4\left(\phi'\right) + \sin^4\left(\phi'\right)\right) + 2\frac{Rr}{r'}\cos^2\left(\phi'\right)\sin^2\left(\phi'\right) \tag{3.150}$$

$$|A| = \frac{Rr}{r'}\left(\cos^2\left(\phi'\right) + \sin^2\left(\phi'\right)\right)^2 \tag{3.151}$$

$$|A| = \frac{Rr}{r'} \tag{3.152}$$

Applying our transformation relationship (3.106) for purely spatial transformations, with $\varepsilon^{i'j'} = \varepsilon_0\delta^{i'}_{j'}$,

$$\varepsilon^{ij} = |A|^{-1}A^i{}_{i'}A^j{}_{j'}\varepsilon_0\delta^{i'}_{j'} \tag{3.153}$$

$$\varepsilon^{ij} = |A|^{-1}A^i{}_{j'}A^j{}_{j'}\varepsilon_0 \tag{3.154}$$

$$\varepsilon^{ij} = \varepsilon_0|A|^{-1}A^i{}_{j'}\left(A^T\right)^j_{j'} \tag{3.155}$$

$$\varepsilon^{ij} = \varepsilon_0|A|^{-1}\left(AA^T\right)^{ij} \tag{3.156}$$

$$\varepsilon = \varepsilon_0 |A|^{-1} AA^T \tag{3.157}$$

$$\begin{aligned}\varepsilon = \varepsilon_0 \frac{r'}{Rr} &\begin{pmatrix} R\cos^2(\phi') + \frac{r}{r'}\sin^2(\phi') & \left(R - \frac{r}{r'}\right)\cos(\phi')\sin(\phi') & 0 \\ \left(R - \frac{r}{r'}\right)\cos(\phi')\sin(\phi') & R\sin^2(\phi') + \frac{r}{r'}\cos^2(\phi') & 0 \\ 0 & 0 & 1 \end{pmatrix} \\ &\times \begin{pmatrix} R\cos^2(\phi') + \frac{r}{r'}\sin^2(\phi') & \left(R - \frac{r}{r'}\right)\cos(\phi')\sin(\phi') & 0 \\ \left(R - \frac{r}{r'}\right)\cos(\phi')\sin(\phi') & R\sin^2(\phi') + \frac{r}{r'}\cos^2(\phi') & 0 \\ 0 & 0 & 1 \end{pmatrix}\end{aligned} \tag{3.158}$$

$$\varepsilon^{11} = \varepsilon_0 \frac{r'}{Rr}\left(\left(R\cos^2(\phi') + \frac{r}{r'}\sin^2(\phi')\right)^2 + \left(R - \frac{r}{r'}\right)^2 \cos^2(\phi')\sin^2(\phi')\right) \tag{3.159}$$

$$\varepsilon^{11} = \varepsilon_0 \frac{r'}{Rr}\left(R^2\cos^4(\phi') + \frac{r^2}{r'^2}\sin^4(\phi') + \left(R^2 + \frac{r^2}{r'^2}\right)\cos^2(\phi')\sin^2(\phi')\right) \tag{3.160}$$

$$\varepsilon^{11} = \varepsilon_0 \frac{r'}{Rr}\left(R^2\cos^2(\phi')\left(\cos^2(\phi') + \sin^2(\phi')\right) + \frac{r^2}{r'^2}\sin^2(\phi')\left(\sin^2(\phi') + \cos^2(\phi')\right)\right) \tag{3.161}$$

$$\varepsilon^{11} = \varepsilon_0 \frac{r'}{Rr}\left(R^2\cos^2(\phi') + \frac{r^2}{r'^2}\sin^2(\phi')\right) \tag{3.162}$$

$$\varepsilon^{12} = \varepsilon_0 \frac{r'}{Rr}\left(R\left(R-\frac{r}{r'}\right)\cos^3\left(\phi'\right)\sin\left(\phi'\right) + \frac{r}{r'}\left(R-\frac{r}{r'}\right)\cos\left(\phi'\right)\sin^3\left(\phi'\right) \right.$$
$$\left. + R\left(R-\frac{r}{r'}\right)\cos\left(\phi'\right)\sin^3\left(\phi'\right) + \frac{r}{r'}\left(R-\frac{r}{r'}\right)\cos^3\left(\phi'\right)\sin\left(\phi'\right) \right) \quad (3.163)$$

$$\varepsilon^{12} = \varepsilon_0 \frac{r'}{Rr}\left(R\left(R-\frac{r}{r'}\right)\cos\left(\phi'\right)\sin\left(\phi'\right) + \frac{r}{r'}\left(R-\frac{r}{r'}\right)\cos\left(\phi'\right)\sin\left(\phi'\right)\right)\left(\cos^2\left(\phi'\right)+\sin^2\left(\phi'\right)\right) \quad (3.164)$$

$$\varepsilon^{12} = \varepsilon_0 \frac{r'}{Rr}\left(R+\frac{r}{r'}\right)\left(R-\frac{r}{r'}\right)\cos\left(\phi'\right)\sin\left(\phi'\right) \quad (3.165)$$

$$\varepsilon^{12} = \varepsilon_0 \frac{r'}{Rr}\left(R^2-\frac{r^2}{r'^2}\right)\cos\left(\phi'\right)\sin\left(\phi'\right) \quad (3.166)$$

$$\varepsilon^{13} = 0 \quad (3.167)$$

$$\varepsilon^{21} = \varepsilon_0 \frac{r'}{Rr}\left(R\left(R-\frac{r}{r'}\right)\cos^3\left(\phi'\right)\sin\left(\phi'\right) + \frac{r}{r'}\left(R-\frac{r}{r'}\right)\cos\left(\phi'\right)\sin^3\left(\phi'\right) + \right.$$
$$\left. R\left(R-\frac{r}{r'}\right)\cos\left(\phi'\right)\sin^3\left(\phi'\right) + \frac{r}{r'}\left(R-\frac{r}{r'}\right)\cos^3\left(\phi'\right)\sin\left(\phi'\right) \right) \quad (3.168)$$

$$\varepsilon^{21} = \varepsilon_0 \frac{r'}{Rr}\left(R\left(R-\frac{r}{r'}\right)\cos\left(\phi'\right)\sin\left(\phi'\right) + \frac{r}{r'}\left(R-\frac{r}{r'}\right)\cos\left(\phi'\right)\sin\left(\phi'\right)\right)\left(\cos^2\left(\phi'\right)+\sin^2\left(\phi'\right)\right) \quad (3.169)$$

$$\varepsilon^{21} = \varepsilon_0 \frac{r'}{Rr}\left(R+\frac{r}{r'}\right)\left(R-\frac{r}{r'}\right)\cos\left(\phi'\right)\sin\left(\phi'\right) \quad (3.170)$$

$$\varepsilon^{21} = \varepsilon_0 \frac{r'}{Rr}\left(R^2 - \frac{r^2}{r'^2}\right)\cos\left(\phi'\right)\sin\left(\phi'\right) \tag{3.171}$$

$$\varepsilon^{22} = \varepsilon_0 \frac{r'}{Rr}\left(\left(R - \frac{r}{r'}\right)^2 \cos^2\left(\phi'\right)\sin^2\left(\phi'\right) + \left(R\sin^2\left(\phi'\right) + \frac{r}{r'}\cos^2\left(\phi'\right)\right)^2\right) \tag{3.172}$$

$$\varepsilon^{22} = \varepsilon_0 \frac{r'}{Rr}\left(\left(R^2 + \frac{r^2}{r'^2}\right)\cos^2\left(\phi'\right)\sin^2\left(\phi'\right) + R^2\sin^4\left(\phi'\right) + \frac{r^2}{r'^2}\cos^4\left(\phi'\right)\right) \tag{3.173}$$

$$\varepsilon^{22} = \varepsilon_0 \frac{r'}{Rr}\left(R^2\sin^2\left(\phi'\right)\left(\cos^2\left(\phi'\right) + \sin^2\left(\phi'\right)\right) + \frac{r^2}{r'^2}\cos^2\left(\phi'\right)\left(\sin^2\left(\phi\right) + \cos^2\left(\phi'\right)\right)\right) \tag{3.174}$$

$$\varepsilon^{22} = \varepsilon_0 \frac{r'}{Rr}\left(R^2\sin^2\left(\phi'\right) + \frac{r^2}{r'^2}\cos^2\left(\phi'\right)\right) \tag{3.175}$$

$$\varepsilon^{31} = \varepsilon^{32} = 0 \tag{3.176}$$

$$\varepsilon^{33} = 1 \tag{3.177}$$

Collecting the elements of ε,

$$\varepsilon = \varepsilon_0 \frac{r'}{Rr}\begin{pmatrix} R^2\cos^2\left(\phi'\right) + \frac{r^2}{r'^2}\sin^2\left(\phi'\right) & \left(R^2 - \frac{r^2}{r'^2}\right)\cos\left(\phi'\right)\sin\left(\phi'\right) & 0 \\ \left(R^2 - \frac{r^2}{r'^2}\right)\cos\left(\phi'\right)\sin\left(\phi'\right) & R^2\sin^2\left(\phi'\right) + \frac{r^2}{r'^2}\cos^2\left(\phi'\right) & 0 \\ 0 & 0 & 1 \end{pmatrix} \tag{3.178}$$

in accordance with results claimed in [9]. Note that since $r' \to 0$ as $r \to a$, the susceptibility components $\chi^{11}, \chi^{12}, \chi^{21}$, and χ^{22} are expected to diverge. This divergence indicates a possible issue which may arise when performing numerical computations in order to determine the response fields (see Chapter 5). Specifically, we anticipate the possibility that the value attained from those calculations may vary considerably depending on the fineness of our mesh.

Converting to cylindrical coordinates in the basis (r, ϕ, z),

$$\varepsilon^{i'j'} = |A|^{-1} A^{i'}{}_{i} A^{j'}{}_{j} \varepsilon^{ij} \tag{3.179}$$

$$\left(\varepsilon^{i'j'}\right) = |A|^{-1} A \varepsilon_{cartesian} (A)^T \tag{3.180}$$

where A is the Jacobian from Cartesian to cylindrical coordinates, given by the transformation

$$r = \sqrt{x^2 + y^2} \ , \ \phi = \tan^{-1}\left(\frac{y}{x}\right), \quad z = z \tag{3.181}$$

Computing the Jacobian,

$$A^{i'}{}_{j} = \frac{\partial x^{i'}}{\partial x^{j}} \to A = \begin{pmatrix} \frac{\partial r}{\partial x} & \frac{\partial r}{\partial y} & \frac{\partial r}{\partial z} \\ \frac{\partial \phi}{\partial x} & \frac{\partial \phi}{\partial y} & \frac{\partial \phi}{\partial z} \\ \frac{\partial z}{\partial x} & \frac{\partial z}{\partial y} & \frac{\partial z}{\partial z} \end{pmatrix} \tag{3.182}$$

$$A = \begin{pmatrix} \frac{x}{r} & \frac{y}{r} & 0 \\ \frac{-y}{r^2} & \frac{x}{r^2} & 0 \\ 0 & 0 & 1 \end{pmatrix} = \begin{pmatrix} \cos(\phi) & \sin(\phi) & 0 \\ \frac{-\sin(\phi)}{r} & \frac{\cos(\phi)}{r} & 0 \\ 0 & 0 & 1 \end{pmatrix} \tag{3.183}$$

The permittivity in cylindrical coordinates is thus

$$\left(\varepsilon^{i'j'}\right) = \varepsilon_0 \frac{r'}{R} \begin{pmatrix} \cos(\phi) & \sin(\phi) & 0 \\ -\frac{\sin(\phi)}{r} & \frac{\cos(\phi)}{r} & 0 \\ 0 & 0 & 1 \end{pmatrix} \begin{pmatrix} R^2\cos^2(\phi) + \frac{r^2}{r'^2}\sin^2(\phi) & \left(R^2 - \frac{r^2}{r'^2}\right)\cos(\phi)\sin(\phi) & 0 \\ \left(R^2 - \frac{r^2}{r'^2}\right)\cos(\phi)\sin(\phi) & R^2\sin^2(\phi) + \frac{r^2}{r'^2}\cos^2(\phi) & 0 \\ 0 & 0 & 1 \end{pmatrix} \times \begin{pmatrix} \cos(\phi) & -\frac{\sin(\phi)}{r} & 0 \\ \sin(\phi) & \frac{\cos(\phi)}{r} & 0 \\ 0 & 0 & 1 \end{pmatrix} \quad (3.184)$$

$$\left(\varepsilon^{i'j'}\right) = \varepsilon_0 \frac{r'}{R} \begin{pmatrix} R^2\cos(\phi) & R^2\sin(\phi) & 0 \\ -\frac{r\sin(\phi)}{r'^2} & \frac{r\cos(\phi)}{r'^2} & 0 \\ 0 & 0 & 1 \end{pmatrix} \begin{pmatrix} \cos(\phi) & -\frac{\sin(\phi)}{r} & 0 \\ \sin(\phi) & \frac{\cos(\phi)}{r} & 0 \\ 0 & 0 & 1 \end{pmatrix} \quad (3.185)$$

$$\left(\varepsilon^{i'j'}\right) = \varepsilon_0 \frac{r'}{R} \begin{pmatrix} R^2 & 0 & 0 \\ 0 & \frac{1}{r'^2} & 0 \\ 0 & 0 & 1 \end{pmatrix} = \varepsilon_0 \begin{pmatrix} r'R & 0 & 0 \\ 0 & \frac{1}{r'R} & 0 \\ 0 & 0 & \frac{r'}{R} \end{pmatrix} \quad (3.186)$$

$$\left(\varepsilon^{i'j'}\right) = \varepsilon_0 \begin{pmatrix} r-a & 0 & 0 \\ 0 & \frac{1}{r-a} & 0 \\ 0 & 0 & \frac{r-a}{R^2} \end{pmatrix} \quad (3.187)$$

Note that these results are not in accordance with [9], although both results are diagonal in cylindrical coordinates. We attribute the discrepancy (of a factor r) to the author's neglect of the tensor density nature of the permittivity and subsequent omission of the necessary factor $|A|^{-1} = r$. Regardless, the permittivity is diagonal in cylindrical coordinates, as we might have predicted based upon symmetry requirements. Again we see that at least one component of the susceptibility is expected to diverge at $r = a$.

THIS PAGE INTENTIONALLY LEFT BLANK

CHAPTER 4:
An Iterative Approach to the Wave Equations

In this chapter we will discuss an alternative approach to the wave equations in matter as determined in chapter two. We will then consider this approach when applied to the problem of scattering of a pure plane electromagnetic plane wave from a structure of known geometry and electromagnetic susceptibilities.

4.1 The Helmholtz Equation

From equations (2.66) and (2.67), our wave equations for $\vec{E}$ and $\vec{H}$ in matter,

$$\nabla^2\vec{E} - \frac{1}{c^2}\frac{\partial^2\vec{E}}{\partial t^2} = \mu_0\frac{\partial^2\vec{P}}{\partial t^2} + \mu_0(\nabla\times\frac{\partial\vec{M}}{\partial t}) - \frac{1}{\varepsilon_0}\nabla(\nabla\cdot\vec{P}) \tag{4.1}$$

$$\nabla^2\vec{H} - \frac{1}{c^2}\frac{\partial^2\vec{H}}{\partial t^2} = \frac{1}{c^2}\frac{\partial^2\vec{M}}{\partial t^2} - \nabla\times\frac{\partial\vec{P}}{\partial t} - \nabla(\nabla\cdot\vec{M}) \tag{4.2}$$

Fourier transforming (4.1) with respect to time, leaving the spatial coordinates untransformed,

$$\int_{-\infty}^{\infty}\left(\nabla^2\vec{E} - \frac{1}{c^2}\frac{\partial^2\vec{E}}{\partial t^2}\right)e^{-i\omega t}\,dt = \int_{-\infty}^{\infty}\left(\mu_0\frac{\partial^2\vec{P}}{\partial t^2} + \mu_0\left(\nabla\times\frac{\partial\vec{M}}{\partial t}\right) - \frac{1}{\varepsilon_0}\nabla(\nabla\cdot\vec{P})\right)e^{-i\omega t}\,dt \tag{4.3}$$

Exploiting the properties of the Fourier transform (see appendix A),

$$\nabla^2\tilde{\vec{E}} + \frac{\omega^2}{c^2}\tilde{\vec{E}} = -\mu_0\omega^2\tilde{\vec{P}} - i\mu_0\omega\left(\nabla\times\tilde{\vec{M}}\right) - \frac{1}{\varepsilon_0}\nabla\left(\nabla\cdot\tilde{\vec{P}}\right) \tag{4.4}$$

where a tilde above a vector quantity implies that vector quantity exists in the position,

frequency domain.

$$\nabla^2\vec{\tilde{E}} + k^2\vec{\tilde{E}} = -\frac{k^2}{\varepsilon_0}\vec{\tilde{P}} - i\omega\mu_0\left(\nabla\times\vec{\tilde{M}}\right) - \frac{1}{\varepsilon_0}\nabla\left(\nabla\cdot\vec{\tilde{P}}\right) \tag{4.5}$$

where $k \equiv \dfrac{\omega}{c}$ and we have used the relationship $c \equiv \dfrac{1}{\sqrt{\varepsilon_0\mu_0}}$. Similarly, from the time$\rightarrow$ frequency Fourier transform of (4.2),

$$\nabla^2\vec{\tilde{H}} + \frac{\omega^2}{c^2}\vec{\tilde{H}} = -\frac{\omega^2}{c^2}\vec{\tilde{M}} + i\omega\left(\nabla\times\vec{\tilde{P}}\right) - \nabla\left(\nabla\cdot\vec{\tilde{M}}\right) \tag{4.6}$$

$$\nabla^2\vec{\tilde{H}} + k^2\vec{\tilde{H}} = -k^2\vec{\tilde{M}} + i\omega\left(\nabla\times\vec{\tilde{P}}\right) - \nabla\left(\nabla\cdot\vec{\tilde{M}}\right) \tag{4.7}$$

where k is again equal to $\dfrac{\omega}{c}$. We recognize (3.5) and (3.7) as a set of inhomogeneous, coupled Helmholtz equations for the components of $\vec{\tilde{E}}$ and $\vec{\tilde{H}}$.

4.2 Constitutive Relations

We wish now to introduce a set of constitutive relations between the polarization and magnetization fields $\vec{\tilde{P}}$ and $\vec{\tilde{M}}$, and the electromagnetic fields $\vec{\tilde{E}}$ and $\vec{\tilde{H}}$, respectively. In linear, isotropic media, the relations

$$\vec{\tilde{P}} = \varepsilon_0\chi^e\vec{\tilde{E}}$$

$$\vec{\tilde{M}} = \chi^m\vec{\tilde{H}}$$

where χ^e and χ^m are the electric and magnetic susceptibilities, and are employed to describe the response of the polarization and magnetization to the fields. In order to account for the possible anisotropy of our media, we express each of the susceptibilities as the second-rank tensors χ^e and χ^m. The constitutive relations now read

$$\vec{\tilde{P}} = \varepsilon_0 \chi^e * \vec{\tilde{E}} \tag{4.8}$$

$$\vec{\tilde{M}} = \chi^m * \vec{\tilde{H}} \tag{4.9}$$

where $*$ denotes tensor contraction. By components,

$$P_\alpha = \varepsilon_0 \sum_{\beta=1}^{3} \chi^e_{\alpha\beta} \tilde{E_\beta} \tag{4.10}$$

$$M_\alpha = \sum_{\beta=1}^{3} \chi^m_{\alpha\beta} \tilde{H_\beta} \tag{4.11}$$

Our Fourier-transformed wave equations now read

$$\nabla^2 \vec{\tilde{E}} + k^2 \vec{\tilde{E}} = -k^2 \left(\chi^e * \vec{\tilde{E}} \right) - i\omega\mu_0 \left(\nabla \times \left(\chi^m * \vec{\tilde{H}} \right) \right) - \nabla \left(\nabla \cdot \left(\chi^e * \vec{\tilde{E}} \right) \right) \tag{4.12}$$

$$\nabla^2 \vec{\tilde{H}} + k^2 \vec{\tilde{H}} = -k^2 \left(\chi^m * \vec{\tilde{H}} \right) + i\omega\varepsilon_0 \left(\nabla \times \left(\chi^e * \vec{\tilde{E}} \right) \right) - \nabla \left(\nabla \cdot \left(\chi^m * \vec{\tilde{H}} \right) \right) \tag{4.13}$$

4.3 Incident and Response Fields

We now consider separately the incident fields and the material responses to those fields. That is,

$$\vec{\tilde{E}} \equiv \vec{\tilde{E}}_0 + \vec{\tilde{E}}_r \tag{4.14}$$

$$\vec{\tilde{H}} \equiv \vec{\tilde{H}}_0 + \vec{\tilde{H}}_r \tag{4.15}$$

where $\vec{\tilde{E}}_0, \vec{\tilde{H}}_0$ are the incident fields and $\vec{\tilde{E}}_r, \vec{\tilde{H}}_r$ the fields due to the material response. From (4.12),

$$\begin{aligned}&\nabla^2\left(\vec{\tilde{E}}_0+\vec{\tilde{E}}_r\right)+k^2\left(\vec{\tilde{E}}_0+\vec{\tilde{E}}_r\right)=\\&-k^2\left(\chi^e*\left(\vec{\tilde{E}}_0+\vec{\tilde{E}}_r\right)\right)-i\omega\mu_0\left(\nabla\times\left(\chi^m*\left(\vec{\tilde{H}}_0+\vec{\tilde{H}}_r\right)\right)\right)-\nabla\left(\nabla\cdot\left(\chi^e*\left(\vec{\tilde{E}}_0+\vec{\tilde{E}}_r\right)\right)\right)\end{aligned} \tag{4.16}$$

Let us model the incident fields as arriving through vacuum. Then the incident fields are expected to obey the sourceless Helmholtz equations:

$$\nabla^2\vec{\tilde{E}}_0+k^2\vec{\tilde{E}}_0=\vec{0} \tag{4.17}$$

Thus,

$$\begin{aligned}&\nabla^2\vec{\tilde{E}}_r+k^2\vec{\tilde{E}}_r=\\&-k^2\left(\chi^e*\left(\vec{\tilde{E}}_0+\vec{\tilde{E}}_r\right)\right)-i\omega\mu_0\left(\nabla\times\left(\chi^m*\left(\vec{\tilde{H}}_0+\vec{\tilde{H}}_r\right)\right)\right)-\nabla\left(\nabla\cdot\left(\chi^e*\left(\vec{\tilde{E}}_0+\vec{\tilde{E}}_r\right)\right)\right)\end{aligned} \tag{4.18}$$

Similarly, from (4.13)

$$\begin{aligned}&\nabla^2\vec{\tilde{H}}_r+k^2\vec{\tilde{H}}_r=\\&-k^2\left(\chi^m*\left(\vec{\tilde{H}}_0+\vec{\tilde{H}}_r\right)\right)+i\omega\varepsilon_0\left(\nabla\times\left(\chi^e*\left(\vec{\tilde{E}}_0+\vec{\tilde{E}}_r\right)\right)\right)-\nabla\left(\nabla\cdot\left(\chi^m*\left(\vec{\tilde{H}}_0+\vec{\tilde{H}}_r\right)\right)\right)\end{aligned} \tag{4.19}$$

Note the near symmetry in the source terms of the above two equations for the response

fields. We define

$$F_1\left(\vec{X},\vec{Y}\right) \equiv -k^2\left(\chi^e * \vec{X}\right) - i\omega\mu_0\left(\nabla \times \left(\chi^m * \vec{Y}\right)\right) - \nabla\left(\nabla \cdot \left(\chi^e * \vec{X}\right)\right) \tag{4.20}$$

$$F_2\left(\vec{X},\vec{Y}\right) \equiv -k^2\left(\chi^m * \vec{X}\right) + i\omega\varepsilon_0\left(\nabla \times \left(\chi^e * \vec{Y}\right)\right) - \nabla\left(\nabla \cdot \left(\chi^m * \vec{X}\right)\right) \tag{4.21}$$

Note that

$$\begin{aligned} &F_1\left(\vec{X}_1+\vec{X}_2,\vec{Y}_1+\vec{Y}_2\right) = \\ &-k^2\left(\chi^e * \left(\vec{X}_1+\vec{X}_2\right)\right) - i\omega\mu_0\left(\nabla \times \left(\chi^m * \left(\vec{Y}_1+\vec{Y}_2\right)\right)\right) - \nabla\left(\nabla \cdot \left(\chi^e * \left(\vec{X}_1+\vec{X}_2\right)\right)\right) \end{aligned} \tag{4.22}$$

$$\begin{aligned} = -k^2\left(\chi^e * \vec{X}_1\right) - k^2\left(\chi^e * \vec{X}_2\right) - i\omega\mu_0\left(\nabla \times \left(\chi^m * \vec{Y}_1\right)\right) - i\omega\mu_0\left(\nabla \times \left(\chi^m * \vec{Y}_2\right)\right) \\ - \nabla\left(\nabla \cdot \left(\chi^e * \vec{X}_1\right)\right) - \nabla\left(\nabla \cdot \left(\chi^e * \vec{X}_2\right)\right) \end{aligned}$$

$$F_1\left(\vec{X}_1+\vec{X}_2,\vec{Y}_1+\vec{Y}_2\right) = F_1\left(\vec{X}_1,\vec{Y}_1\right) + F_1\left(\vec{X}_2,\vec{Y}_2\right) \tag{4.23}$$

And similar for F_2. From (4.18) and (4.19),

$$\nabla^2\vec{\tilde{E}}_r + k^2\vec{\tilde{E}}_r = F_1\left(\vec{\tilde{E}}_0,\vec{\tilde{H}}_0\right) + F_1\left(\vec{\tilde{E}}_r,\vec{\tilde{H}}_r\right) \tag{4.24}$$

$$\nabla^2\vec{\tilde{H}}_r + k^2\vec{\tilde{H}}_r = F_2\left(\vec{\tilde{H}}_0,\vec{\tilde{E}}_0\right) + F_2\left(\vec{\tilde{H}}_r,\vec{\tilde{E}}_r\right) \tag{4.25}$$

4.4 An Integral Equation

The Green Function for the Helmholtz equation in two dimensions is known (see Appendix A) to be given by

$$G_{k_0}\left(\vec{r},\vec{r}'\right) = \frac{i}{4}H_0^{(1)}\left(k_0\left|\vec{r}-\vec{r}'\right|\right) \tag{4.26}$$

For the Helmholtz operator $\nabla^2 + k_0$, where ${H_0}^{(1)}$ is the first Hankel function of the first kind. With this Green function in hand, we may express the solution to our inhomogeneous Helmholtz equations (4.24) and (4.25) as

$$\vec{\tilde{E}}_r = \int_{-\infty}^{\infty} G_k\left(\vec{r},\vec{r}'\right)\left(F_1\left(\vec{\tilde{E}}_0\left(\vec{r}'\right),\vec{\tilde{H}}_0\left(\vec{r}'\right)\right) + F_1\left(\vec{\tilde{E}}_r\left(\vec{r}'\right),\vec{\tilde{H}}_r\left(\vec{r}'\right)\right)\right) d^2\vec{r}' \tag{4.27}$$

$$\vec{\tilde{H}}_r = \int_{-\infty}^{\infty} G_k\left(\vec{r},\vec{r}'\right)\left(F_2\left(\vec{\tilde{H}}_0\left(\vec{r}'\right),\vec{\tilde{E}}_0\left(\vec{r}'\right)\right) + F_2\left(\vec{\tilde{H}}_r\left(\vec{r}'\right),\vec{\tilde{E}}_r\left(\vec{r}'\right)\right)\right) d^2\vec{r}' \tag{4.28}$$

We have now converted our differential equations for the response fields in equations (4.24) and (4.25) into a set of coupled integral equations for these fields. In an attempt to keep our expressions under control, we further introduce the notation

$$F_1^{\vec{r}}\left(\vec{X},\vec{Y}\right) \equiv F_1\left(\vec{X}\left(\vec{r}\right),\vec{Y}\left(\vec{r}\right)\right) \tag{4.29}$$

and similar for F_2. Our integral equations for the response fields now read

$$\vec{\tilde{E}}_r = \int_{-\infty}^{\infty} G_k\left(\vec{r},\vec{r}'\right) F_1^{\vec{r}'}\left(\vec{\tilde{E}}_0,\vec{\tilde{H}}_0\right) d^2\vec{r}' + \int_{-\infty}^{\infty} G_k\left(\vec{r},\vec{r}'\right) F_1^{\vec{r}'}\left(\vec{\tilde{E}}_r,\vec{\tilde{H}}_r\right) d^2\vec{r}' \tag{4.30}$$

$$\vec{\tilde{H}}_r = \int_{-\infty}^{\infty} G_k\left(\vec{r},\vec{r}'\right) F_2^{\vec{r}'}\left(\vec{\tilde{H}}_0,\vec{\tilde{E}}_0\right) d^2\vec{r}' + \int_{-\infty}^{\infty} G_k\left(\vec{r},\vec{r}'\right) F_2^{\vec{r}'}\left(\vec{\tilde{H}}_r,\vec{\tilde{E}}_r\right) d^2\vec{r}' \tag{4.31}$$

4.5 The Neumann Series

We propose to attain an approximate solution to equations (4.24) and (4.25) for the response fields through the following iteration method: Insert the entirety of equation (4.27) and (4.28) for $\vec{\tilde{E}}_r$ and $\vec{\tilde{H}}_r$, respectively, back into the last terms of (4.27) and (4.28). This method produces what is known in mathematics as a Neumann series, which is often employed in the approximate solution of integral equations [17]. The technique is also commonly used for quantum scattering problems, where truncation of all but the first term of the resulting series is known as the Born approximation [18].

$$\begin{aligned}\vec{\tilde{E}}_r &= \int_{-\infty}^{\infty} G_k\left(\vec{r},\vec{r}'\right) F_1^{\vec{r}'}\left(\vec{\tilde{E}}_0,\vec{\tilde{H}}_0\right) d^2\vec{r}' \\ &+ \int_{\infty}^{\infty} G_k\left(\vec{r},\vec{r}'\right) F_1^{\vec{r}'}\left(\left(\int_{-\infty}^{\infty} G_k\left(\vec{r}',\vec{r}''\right) F_1^{\vec{r}''}\left(\vec{\tilde{E}}_0,\vec{\tilde{H}}_0\right) d^2\vec{r}'' + \int_{-\infty}^{\infty} G_k\left(\vec{r}',\vec{r}''\right) F_1^{\vec{r}''}\left(\vec{\tilde{E}}_r,\vec{\tilde{H}}_r\right) d^2\vec{r}''\right),\right. \\ &\left.\left(\int_{-\infty}^{\infty} G_k\left(\vec{r}',\vec{r}''\right) F_2^{\vec{r}''}\left(\vec{\tilde{H}}_0,\vec{\tilde{E}}_0\right) d^2\vec{r}'' + \int_{-\infty}^{\infty} G_k\left(\vec{r}',\vec{r}''\right) F_2^{\vec{r}''}\left(\vec{\tilde{H}}_r,\vec{\tilde{E}}_r\right) d^2\vec{r}''\right)\right) d^2\vec{r}' \end{aligned} \quad (4.32)$$

$$\begin{aligned}\vec{\tilde{E}}_r &= \int_{-\infty}^{\infty} G_k\left(\vec{r},\vec{r}'\right) F_1^{\vec{r}'}\left(\vec{\tilde{E}}_0,\vec{\tilde{H}}_0\right) d^2\vec{r}' \\ &+ \int_{-\infty}^{\infty} G_k\left(\vec{r},\vec{r}'\right) F_1^{\vec{r}'}\left(\int_{-\infty}^{\infty} G_k\left(\vec{r}',\vec{r}''\right) F_1^{\vec{r}''}\left(\vec{\tilde{E}}_0,\vec{\tilde{H}}_0\right) d^2\vec{r}'', \int_{-\infty}^{\infty} G_k\left(\vec{r}',\vec{r}''\right) F_2^{\vec{r}''}\left(\vec{\tilde{H}}_0,\vec{\tilde{E}}_0\right) d^2\vec{r}''\right) d^2\vec{r}' \\ &+ \int_{-\infty}^{\infty} G_k\left(\vec{r},\vec{r}'\right) F_1^{\vec{r}'}\left(\int_{-\infty}^{\infty} G_k\left(\vec{r}',\vec{r}''\right) F_1^{\vec{r}''}\left(\vec{\tilde{E}}_r,\vec{\tilde{H}}_r\right) d^2\vec{r}'', \int_{-\infty}^{\infty} G_k\left(\vec{r}',\vec{r}''\right) F_2^{\vec{r}''}\left(\vec{\tilde{H}}_r,\vec{\tilde{E}}_r\right) d^2\vec{r}''\right) d^2\vec{r}' \end{aligned} \quad (4.33)$$

where we have used the linearity of the function F_1 from equation (4.23) in the last step. Provided the convergence of the resulting series, we may continue this iteration process as we wish in order to attain an approximate solution for $\vec{\tilde{E}}_r$. Similarly, for the response magnetic field $\vec{\tilde{H}}_r$,

$$\vec{\tilde{H}}_r = \int_{-\infty}^{\infty} G_k\left(\vec{r},\vec{r}'\right) F_2^{\vec{r}'}\left(\vec{\tilde{H}}_0,\vec{\tilde{E}}_0\right) d^2\vec{r}'$$
$$+\int_{\infty}^{\infty} G_k\left(\vec{r},\vec{r}'\right) F_2^{\vec{r}'}\left(\left(\int_{-\infty}^{\infty} G_k\left(\vec{r}',\vec{r}''\right) F_2^{\vec{r}''}\left(\vec{\tilde{H}}_0,\vec{\tilde{E}}_0\right) d^2\vec{r}'' + \int_{-\infty}^{\infty} G_k\left(\vec{r}',\vec{r}''\right) F_2^{\vec{r}''}\left(\vec{\tilde{H}}_r,\vec{\tilde{E}}_r\right) d^2\vec{r}''\right),\right.$$
$$\left.\left(\int_{-\infty}^{\infty} G_k\left(\vec{r}',\vec{r}''\right) F_1^{\vec{r}''}\left(\vec{\tilde{E}}_0,\vec{\tilde{H}}_0\right) d^2\vec{r}'' + \int_{-\infty}^{\infty} G_k\left(\vec{r}',\vec{r}''\right) F_1^{\vec{r}''}\left(\vec{\tilde{E}}_r,\vec{\tilde{H}}_r\right) d^2\vec{r}''\right)\right) d^2\vec{r}' \quad (4.34)$$

$$\vec{\tilde{H}}_r = \int_{-\infty}^{\infty} G_k\left(\vec{r},\vec{r}'\right) F_2^{\vec{r}'}\left(\vec{\tilde{H}}_0,\vec{\tilde{E}}_0\right) d^2\vec{r}'$$
$$+\int_{-\infty}^{\infty} G_k\left(\vec{r},\vec{r}'\right) F_2^{\vec{r}'}\left(\int_{-\infty}^{\infty} G_k\left(\vec{r}',\vec{r}''\right) F_2^{\vec{r}''}\left(\vec{\tilde{H}}_0,\vec{\tilde{E}}_0\right) d^2\vec{r}'', \int_{-\infty}^{\infty} G_k\left(\vec{r}',\vec{r}''\right) F_1^{\vec{r}''}\left(\vec{\tilde{E}}_0,\vec{\tilde{H}}_0\right) d^2\vec{r}''\right) d^2\vec{r}'$$
$$+\int_{-\infty}^{\infty} G_k\left(\vec{r},\vec{r}'\right) F_2^{\vec{r}'}\left(\int_{-\infty}^{\infty} G_k\left(\vec{r}',\vec{r}''\right) F_2^{\vec{r}''}\left(\vec{\tilde{H}}_r,\vec{\tilde{E}}_r\right) d^2\vec{r}'', \int_{-\infty}^{\infty} G_k\left(\vec{r}',\vec{r}''\right) F_1^{\vec{r}''}\left(\vec{\tilde{E}}_r,\vec{\tilde{H}}_r\right) d^2\vec{r}''\right) d^2\vec{r}' \quad (4.35)$$

Identifying the first term of (4.33) and (4.35) as the first-order response in χ, second term as the second-order response, and the final term the remaining higher-order response, we may continue the iteration process as we desire by inserting each of (4.33) and (4.35) into the expressions for the response fields of each of these expressions, each time attaining the next higher order solution to our wave equation.

4.6 Incident Plane Wave

As a precursor to our implementation of the iteration scheme outlined above (see Chapter 5), let us consider the material response of a two-dimensional structure embedded in the x-y plane when subject to an incident electromagnetic plane wave, polarized in the $\hat{z}$ direction, with angular frequency ω_0, travelling in the $\hat{x}$ direction, and arriving through vacuum.

$$\vec{E}_0 = E_0 e^{i\left(\vec{k}_0\cdot\vec{r}-\omega_0 t\right)}\hat{z} \quad (4.36)$$

where $\vec{k_0}$ is the wave vector, oriented in the direction of propagation, with magnitude given by $k_0 = \dfrac{\omega_0}{c}$.

4.6.1 First Order Response

The temporal Fourier transform $\vec{\tilde{E}}_0(\vec{r},\omega)$ with respect to waves propagating outward is

$$\vec{\tilde{E}}_0 = \int_{-\infty}^{\infty} E_0 e^{i(k_0 x - \omega_0 t)} e^{i\omega t}\, dt\, \hat{z} \tag{4.37}$$

$$\vec{\tilde{E}}_0 = E_0 e^{ik_0 x} \int_{-\infty}^{\infty} e^{i(\omega-\omega_0)t}\, dt\, \hat{z} \tag{4.38}$$

$$\vec{\tilde{E}}_0 = 2\pi E_0 e^{ik_0 x} \delta(\omega - \omega_0)\, \hat{z} \tag{4.39}$$

where $\delta(\omega-\omega_0)$ is the Dirac delta distribution. For plane electromagnetic waves, $\vec{H}_0$ is determined by our choice of polarization and propagation directions to be

$$\vec{H}_0 = -H_0 e^{i(k_0 x - \omega_0 t)}\, \hat{y} \tag{4.40}$$

Where $H_0 = \dfrac{E_0}{\mu_0 c} = E_0\sqrt{\dfrac{\varepsilon_0}{\mu_0}} = \varepsilon_0 c E_0$. The temporal Fourier transform of this incident plane wave is

$$\vec{\tilde{H}}_0 = -2\pi H_0 e^{ik_0 x} \delta(\omega - \omega_0)\, \hat{y} \tag{4.41}$$

We now take $\chi^e = \chi^m$ in order to ensure that the structure is impedance matched to free space, eliminating reflection – a desired property in a CDEW application. The first-order response electric field is thus, from (4.33),

$$\vec{\tilde{E}}_{r,1} = \int_{-\infty}^{\infty} G_k\left(\vec{r},\vec{r}'\right) F_1^{\vec{r}'}\left(\vec{\tilde{E}}_0, \vec{\tilde{H}}_0\right) d^2\vec{r}' \tag{4.42}$$

$$\vec{\vec{E}}_{r,1} = \int_{-\infty}^{\infty} \frac{i}{4} H_0^{(1)}\left(k\left|\vec{r}-\vec{r}'\right|\right)$$
$$\times\left(-k^2\left(\chi * \vec{\vec{E}}_0\left(\vec{r}'\right)\right) - i\omega\mu_0\left(\nabla\times\left(\chi * \vec{\vec{H}}_0\left(\vec{r}'\right)\right)\right) - \nabla\left(\nabla\cdot\left(\chi * \vec{\vec{E}}_0\left(\vec{r}'\right)\right)\right)\right) d^2\vec{r}' \quad (4.43)$$

$$\vec{\vec{E}}_{r,1} = \frac{-i}{4}\int_{-\infty}^{\infty} H_0^{(1)}\left(k\left|\vec{r}-\vec{r}'\right|\right)$$
$$\times\left(k^2\left(\chi_e * \vec{\vec{E}}_0\left(\vec{r}'\right)\right) + i\omega\mu_0\left(\nabla\times\left(\chi_m * \vec{\vec{H}}_0\left(\vec{r}'\right)\right)\right) + \nabla\left(\nabla\cdot\left(\chi_e * \vec{\vec{E}}_0\left(\vec{r}'\right)\right)\right)\right) d^2\vec{r}' \quad (4.44)$$

Inserting the expressions (4.39) and (4.41) for $\vec{\vec{E}}_0$ and $\vec{\vec{H}}_0$, respectively, and exploiting the relation $\chi_e = \chi_m$ for nonreflectance,

$$\vec{\vec{E}}_{r,1} = -\delta(\omega-\omega_0)\frac{\pi i}{2}\int_{-\infty}^{\infty} H_0^{(1)}\left(k\left|\vec{r}-\vec{r}'\right|\right)$$
$$\left(k^2\left(\chi * \left(E_0 e^{ik_0x'}\hat{z}\right)\right) - i\omega\mu_0\left(\nabla\times\left(\chi * H_0 e^{ik_0x'}\hat{y}\right)\right) + \nabla\left(\nabla\cdot\left(\chi * \left(E_0 e^{ik_0x'}\hat{z}\right)\right)\right)\right) d^2\vec{r}' \quad (4.45)$$

$$\vec{\vec{E}}_{r,1} = -\delta(\omega-\omega_0)\frac{\pi i}{2}\int_{-\infty}^{\infty} H_0^{(1)}\left(k\left|\vec{r}-\vec{r}'\right|\right)$$
$$\left(k^2 E_0\left(\chi * \left(e^{ik_0x'}\hat{z}\right)\right) - i\omega\mu_0 H_0\left(\nabla\times\left(\chi * e^{ik_0x'}\hat{y}\right)\right) + E_0\nabla\left(\nabla\cdot\left(\chi * \left(e^{ik_0x'}\hat{z}\right)\right)\right)\right) d^2\vec{r}' \quad (4.46)$$

Let us express χ in the basis $\{x,y,z\}$ as

$$\chi = \begin{pmatrix} \chi_{11} & \chi_{12} & 0 \\ \chi_{21} & \chi_{22} & 0 \\ 0 & 0 & \chi_{33} \end{pmatrix} \tag{4.47}$$

since all of the TO–derived susceptibilities under consideration in this work take the above form. Furthermore, since all of the components χ_{ij} have no z-dependence, the tensor contractions of equation (4.46) are

$$\chi * \left(e^{ik_0 x} \hat{z} \right) = e^{ik_0 x} \chi_{33} \hat{z} \tag{4.48}$$

$$\nabla \cdot \left(\chi * e^{ik_0 x} \hat{z} \right) = \nabla \cdot \left(e^{ik_0 x} \chi_{33} \hat{z} \right) = \frac{\partial \left(e^{ik_0 x} \chi_{33} \right)}{\partial z} \tag{4.49}$$

$$\nabla \cdot \left(\chi * e^{ik_0 x} \hat{z} \right) = e^{ik_0 x} \frac{\partial \chi_{33}}{\partial z} \hat{z} \tag{4.50}$$

As stated, χ_{33} does not vary with z, and so

$$\nabla \cdot \left(\chi * e^{ik_0 x} \hat{z} \right) = 0 \tag{4.51}$$

Turning to the curl term in (4.46),

$$\chi * e^{ik_0 x} \hat{y} = e^{ik_0 x} \left(\chi_{12} \hat{x} + \chi_{22} \hat{y} \right) \tag{4.52}$$

$$\left[\nabla \times \left(\chi * \left(e^{ik_0 x} \hat{y} \right) \right) \right]_j = \varepsilon_{jkl} \frac{\partial \left(e^{ik_0 x} \left(\chi_{12} \delta_{l,1} + \chi_{22} \delta_{l,2} \right) \right)}{\partial x_k} \tag{4.53}$$

$$\nabla \times \left(\chi * \left(e^{ik_0 x}\hat{y}\right)\right) = \left(-\frac{\partial\left(e^{ik_0 x}\chi_{22}\right)}{\partial z}\right)\hat{x} + \frac{\partial\left(e^{ik_0 x}\chi_{12}\right)}{\partial z}\hat{y} + \left(\frac{\partial\left(e^{ik_0 x}\chi_{22}\right)}{\partial x} - \frac{\partial\left(e^{ik_0 x}\chi_{12}\right)}{\partial y}\right)\hat{z} \tag{4.54}$$

Once more exploiting the z-independence of the susceptibility components,

$$\nabla \times \left(\chi * \left(e^{ik_0 x}\hat{y}\right)\right) = \left(\frac{\partial\left(e^{ik_0 x}\chi_{22}\right)}{\partial x} - \frac{\partial\left(e^{ik_0 x}\chi_{12}\right)}{\partial y}\right)\hat{z} \tag{4.55}$$

$$\nabla \times \left(\chi * \left(e^{ik_0 x}\hat{y}\right)\right) = \left(e^{ik_0 x}\frac{\partial \chi_{22}}{\partial x} + ik_0\chi_{22}e^{ik_0 x} - e^{ik_0 x}\frac{\partial \chi_{12}}{\partial y}\right)\hat{z} \tag{4.56}$$

Inserting (4.48), (4.51), and (4.56) into our expression for the first-order response electric field (4.46), taking $B_0 = \frac{E_0}{c} \rightarrow \mu_0 H_0 = \frac{E_0}{c} \rightarrow H_0 = \sqrt{\frac{\varepsilon_0}{\mu_0}}E_0$,

$$\vec{\tilde{E}}_{r,1} = -\delta(\omega - \omega_0)\frac{\pi E_0 i}{2}\int_{-\infty}^{\infty} H_0^{(1)}\left(k\left|\vec{r} - \vec{r}'\right|\right)e^{ik_0 x'}\left(k^2\chi_{33} - i\frac{\omega}{c}\left(\frac{\partial \chi_{22}}{\partial x} + ik_0\chi_{22} - \frac{\partial \chi_{12}}{\partial y}\right)\right)\hat{z}\,d^2\vec{r}' \tag{4.57}$$

But $k = \frac{\omega}{c}$, so

$$\vec{\tilde{E}}_{r,1} = -\delta(\omega - \omega_0)\frac{\pi E_0 i}{2}\int_{-\infty}^{\infty} H_0^{(1)}\left(k\left|\vec{r} - \vec{r}'\right|\right)e^{ik_0 x'}\left(k^2\chi_{33} - ik\frac{\partial \chi_{22}}{\partial x} + k_0 k\chi_{22} + ik\frac{\partial \chi_{12}}{\partial y}\right)\hat{z}\,d^2\vec{r}' \tag{4.58}$$

4.6.2 Second Order Response

Returning to equation (4.33), the second order response electric field is

$$\vec{\tilde{E}}_{r,2} = \int_{-\infty}^{\infty} G_k\left(\vec{r},\vec{r}'\right)F_1^{\vec{r}'}\left(\int_{-\infty}^{\infty} G_k\left(\vec{r}',\vec{r}''\right)F_1^{\vec{r}''}\left(\vec{\tilde{E}}_0,\vec{\tilde{H}}_0\right)d^2\vec{r}'', \int_{-\infty}^{\infty} G_k\left(\vec{r}',\vec{r}''\right)F_2^{\vec{r}''}\left(\vec{\tilde{H}}_0,\vec{\tilde{E}}_0\right)d^2\vec{r}''\right)d^2\vec{r}' \tag{4.59}$$

The first integral over $\vec{r}''$ is identical in structure to the first order response field, given in (4.58).

$$\int_{-\infty}^{\infty} G_k\left(\vec{r}',\vec{r}''\right) F_1^{\vec{r}''}\left(\vec{\tilde{E}}_0,\vec{\tilde{H}}_0\right) d^2\vec{r}'' =$$
$$-\delta\left(\omega-\omega_0\right)\frac{\pi E_0 i}{2}\int_{-\infty}^{\infty} H_0^{(1)}\left(k\left|\vec{r}'-\vec{r}''\right|\right) e^{ik_0 x''}\left(k^2\chi_{33}-ik\frac{\partial\chi_{22}}{\partial x}+k_0 k\chi_{22}+ik\frac{\partial\chi_{12}}{\partial y}\right)\hat{z}\,d^2\vec{r}'' \tag{4.60}$$

Focusing on the second integral over $\vec{r}''$,

$$\int_{-\infty}^{\infty} G_k\left(\vec{r}',\vec{r}''\right) F_2^{\vec{r}''}\left(\vec{\tilde{H}}_0,\vec{\tilde{E}}_0\right) d^2\vec{r}'' =$$
$$\int_{-\infty}^{\infty} G_k\left(\vec{r}',\vec{r}''\right)\left(-k^2\left(\chi*\vec{\tilde{H}}_0\right)+i\omega\varepsilon_0\left(\nabla\times\left(\chi^e*\vec{\tilde{E}}_0\right)\right)-\nabla\left(\nabla\cdot\left(\chi^m*\vec{\tilde{H}}_0\right)\right)\right) d^2\vec{r}'' \tag{4.61}$$

$$= 2\pi\delta\left(\omega-\omega_0\right)\int_{-\infty}^{\infty} G_k\left(\vec{r}',\vec{r}''\right) e^{ik_0 x''}\Big(-k^2\chi*(-H_0\hat{y})+i\omega\varepsilon_0\nabla\times(\chi^e*(E_0\hat{z}))$$
$$-\nabla\left(\nabla\cdot(\chi^m*(-H_0\hat{y}))\right)\Big) d^2\vec{r}''$$

$$= \frac{\pi E_0 i}{2}\delta\left(\omega-\omega_0\right)\int_{-\infty}^{\infty} H_0^{(1)}\left(k\left|\vec{r}'-\vec{r}''\right|\right) e^{ik_0 x''}\Big(k^2\sqrt{\frac{\varepsilon_0}{\mu_0}}\chi*\hat{y}+i\omega\varepsilon_0\nabla\times(\chi^e*\hat{z})$$
$$+\sqrt{\frac{\varepsilon_0}{\mu_0}}\nabla\left(\nabla\cdot(\chi^m*\hat{y})\right)\Big) d^2\vec{r}''$$

$$= \frac{\pi E_0 i}{2} \delta(\omega - \omega_0) \int_{-\infty}^{\infty} H_0^{(1)}\left(k\left|\vec{r}' - \vec{r}''\right|\right) e^{ik_0 x''} \left(k^2 \sqrt{\frac{\varepsilon_0}{\mu_0}} (\chi_{12}\hat{x} + \chi_{22}\hat{y}) + i\omega\varepsilon_0 \nabla \times (\chi_{33}\hat{z}) \right.$$
$$\left. + \sqrt{\frac{\varepsilon_0}{\mu_0}} \nabla (\nabla \cdot (\chi_{12}\hat{x} + \chi_{22}\hat{y})) \right) d^2\vec{r}''$$

$$= \frac{\pi E_0 i}{2} \delta(\omega - \omega_0) \int_{-\infty}^{\infty} H_0^{(1)}\left(k\left|\vec{r}' - \vec{r}''\right|\right) e^{ik_0 x''}$$
$$\left(k^2 \sqrt{\frac{\varepsilon_0}{\mu_0}} (\chi_{12}\hat{x} + \chi_{22}\hat{y}) + i\omega\varepsilon_0 \left(\frac{\partial \chi_{33}}{\partial y''}\hat{x} - \frac{\partial \chi_{33}}{\partial x''}\hat{y} \right) \right.$$
$$\left. + \sqrt{\frac{\varepsilon_0}{\mu_0}} \nabla \left(\frac{\partial \chi_{12}}{\partial x''} + \frac{\partial \chi_{22}}{\partial y''} \right) \right) d^2\vec{r}''$$

$$\int_{-\infty}^{\infty} G_k\left(\vec{r}', \vec{r}''\right) F_2^{\vec{r}''}\left(\vec{\tilde{H}}_0, \vec{\tilde{E}}_0\right) d^2\vec{r}'' =$$
$$\frac{\pi E_0 i}{2} \delta(\omega - \omega_0) \int_{-\infty}^{\infty} H_0^{(1)}\left(k\left|\vec{r}' - \vec{r}''\right|\right) e^{ik_0 x''} \left(k^2 \sqrt{\frac{\varepsilon_0}{\mu_0}} (\chi_{12}\hat{x} + \chi_{22}\hat{y}) + i\omega\varepsilon_0 \left(\frac{\partial \chi_{33}}{\partial y''}\hat{x} - \frac{\partial \chi_{33}}{\partial x''}\hat{y} \right) \right.$$
$$\left. + \sqrt{\frac{\varepsilon_0}{\mu_0}} \left(\left[\frac{\partial^2 \chi_{12}}{\partial \left(x''\right)^2} + \frac{\partial^2 \chi_{22}}{\partial x'' \partial y''} \right] \hat{x} + \left[\frac{\partial^2 \chi_{12}}{\partial y'' \partial x''} + \frac{\partial^2 \chi_{22}}{\partial \left(y''\right)^2} \right] \hat{y} \right) \right) d^2\vec{r}'' \quad (4.62)$$

Inserting (4.60) and (4.62) into (4.59) yields

$$\vec{\bar{E}}_{r,2} = \int_{-\infty}^{\infty} G_k\left(\vec{r},\vec{r}'\right) \times$$
$$F_1^{\vec{r}'}\left(-\delta\left(\omega-\omega_0\right)\frac{\pi E_0 i}{2}\int_{-\infty}^{\infty} H_0^{(1)}\left(k\left|\vec{r}'-\vec{r}''\right|\right) e^{ik_0 x''}\left(k^2\chi_{33} - ik\frac{\partial \chi_{22}}{\partial x} + k_0 k\chi_{22} + ik\frac{\partial \chi_{12}}{\partial y}\right)\hat{z}\, d^2\vec{r}'', \right.$$
$$\frac{\pi E_0 i}{2}\delta\left(\omega-\omega_0\right)\int_{-\infty}^{\infty} H_0^{(1)}\left(k\left|\vec{r}'-\vec{r}''\right|\right) e^{ik_0 x''}\left(k^2\sqrt{\frac{\varepsilon_0}{\mu_0}}\left(\chi_{12}\hat{x}+\chi_{22}\hat{y}\right) + i\omega\varepsilon_0\left(\frac{\partial \chi_{33}}{\partial y''}\hat{x} - \frac{\partial \chi_{33}}{\partial x''}\hat{y}\right) + \right.$$
$$\left.\left.\sqrt{\frac{\varepsilon_0}{\mu_0}}\left(\left[\frac{\partial^2\chi_{12}}{\partial\left(x''\right)^2} + \frac{\partial^2\chi_{22}}{\partial x''\partial y''}\right]\hat{x} + \left[\frac{\partial^2\chi_{12}}{\partial y''\partial x''} + \frac{\partial^2\chi_{22}}{\partial\left(y''\right)^2}\right]\hat{y}\right)\right) d^2\vec{r}''\right) d^2\vec{r}' \quad (4.63)$$

$$\vec{\bar{E}}_{r,2} = \int_{-\infty}^{\infty} G_k\left(\vec{r},\vec{r}'\right)\delta\left(\omega-\omega_0\right)\left[k^2\frac{\pi E_0 i}{2}\times\right.$$
$$\left(\chi * \left(\int_{-\infty}^{\infty} H_0^{(1)}\left(k\left|\vec{r}'-\vec{r}''\right|\right) e^{ik_0 x''}\left(k^2\chi_{33} - ik\frac{\partial \chi_{22}}{\partial x} + k_0 k\chi_{22} + ik\frac{\partial \chi_{12}}{\partial y}\right)\hat{z}\, d^2\vec{r}''\right)\right) +$$
$$\frac{\pi E_0}{2}\omega\mu_0\nabla\times\left(\int_{\infty}^{\infty} H_0^{(1)}\left(k\left|\vec{r}-\vec{r}''\right|\right) e^{ik_0 x''}\left(k^2\sqrt{\frac{\varepsilon_0}{\mu_0}}\left(\chi_{12}\hat{x}+\chi_{22}\hat{y}\right)\right) + \right.$$
$$i\omega\varepsilon_0\left(\frac{\partial \chi_{33}}{\partial y''}\hat{x} - \frac{\partial \chi_{33}}{\partial x''}\hat{y}\right) + \sqrt{\frac{\varepsilon_0}{\mu_0}}\left(\left[\frac{\partial^2\chi_{12}}{\partial\left(x''\right)^2} + \frac{\partial^2\chi_{22}}{\partial x''\partial y''}\right]\hat{x} + \left[\frac{\partial^2\chi_{12}}{\partial y''\partial x''} + \frac{\partial^2\chi_{22}}{\partial\left(y''\right)^2}\right]\hat{y}\right)\Big) +$$
$$\left.\left.\frac{\pi E_0 i}{2}\nabla\left(\nabla\cdot\left(\chi * \int_{-\infty}^{\infty} H_0^{(1)}\left(k\left|\vec{r}'-\vec{r}''\right|\right) e^{ik_0 x''}\left(k^2\chi_{33} - ik\frac{\partial \chi_{22}}{\partial x} + k_0 k\chi_{22} + ik\frac{\partial \chi_{12}}{\partial y}\right)\hat{z}\, d^2\vec{r}''\right)\right)\right] \quad (4.64)$$

We may observe from the relative complexity of the above result that the second and higher order terms of the response fields (4.33) and (4.35) will be computationally taxing for all but the simplest structures and material parameters. We will therefore focus our efforts in the following chapter on characterizing first order responses for the TO-derived structures which appear in the literature.

THIS PAGE INTENTIONALLY LEFT BLANK

CHAPTER 5:
Applications

In this chapter we will apply the iterative approach outlined in Chapter 4 to some basic electromagnetic redirection structures and analyze the results in an attempt to quantify the error fields which result from nonlinear effects in these TO derived devices.

5.1 Cylindrical Shield

We will attempt to apply the iterative method of Chapter 4 to the cylindrical structure presented in [9] in Cartesian coordinates, followed by an analysis of the same structure in the coordinate system most suited to such a structure, cylindrical coordinates.

5.1.1 Cartesian Coordinates

From equation (3.178) the electric permittivity ε is, in the basis (x,y,z),

$$\boldsymbol{\varepsilon} = \varepsilon_0 \frac{r'}{Rr} \begin{pmatrix} R^2\cos^2(\phi) + \frac{r^2}{r'^2}\sin^2(\phi) & \left(R^2 - \frac{r^2}{r'^2}\right)\cos(\phi)\sin(\phi) & 0 \\ \left(R^2 - \frac{r^2}{r'^2}\right)\cos(\phi)\sin(\phi) & R^2\sin^2(\phi) + \frac{r^2}{r'^2}\cos^2(\phi) & 0 \\ 0 & 0 & 1 \end{pmatrix} \tag{5.1}$$

The electric susceptibility $\chi_{\mathbf{e}}$ corresponding to this permittivity is

$$\chi_e = \frac{1}{\varepsilon_0}\varepsilon - \begin{pmatrix} 1 & 0 & 0 \\ 0 & 1 & 0 \\ 0 & 0 & 1 \end{pmatrix} \tag{5.2}$$

$$\chi_{\mathbf{e}} = \begin{pmatrix} \frac{Rr'}{r}\cos^2(\phi) + \frac{r}{Rr'}\sin^2(\phi) - 1 & \left(\frac{Rr'}{r} - \frac{r}{Rr'}\right)\cos(\phi)\sin(\phi) & 0 \\ \left(\frac{Rr'}{r} - \frac{r}{Rr'}\right)\cos(\phi)\sin(\phi) & \frac{Rr'}{r}\sin^2(\phi) + \frac{r}{Rr'}\cos^2(\phi) - 1 & 0 \\ 0 & 0 & \frac{r'}{Rr} - 1 \end{pmatrix} \tag{5.3}$$

$$\chi_{\mathbf{e}} = \begin{pmatrix} \frac{r-a}{r}\cos^2(\phi) + \frac{r}{r-a}\sin^2(\phi) - 1 & \left(\frac{r-a}{r} - \frac{r}{r-a}\right)\cos(\phi)\sin(\phi) & 0 \\ \left(\frac{r-a}{r} - \frac{r}{r-a}\right)\cos(\phi)\sin(\phi) & \frac{r-a}{r}\sin^2(\phi) + \frac{r}{r-a}\cos^2(\phi) - 1 & \\ 0 & 0 & \frac{r-a}{R^2 r} - 1 \end{pmatrix} \quad (5.4)$$

where we have used the transformation relation (3.102) in the last step. The permittivity is, as for the case of the square structure of [8], of the form

$$\chi_{\mathbf{e}} = \begin{pmatrix} \chi_{11} & \chi_{12} & 0 \\ \chi_{21} & \chi_{22} & 0 \\ 0 & 0 & \chi_{33} \end{pmatrix} \quad (5.5)$$

and so our result (4.58) for the first order response to an incident plane wave, polarized in the $\hat{z}$-direction will apply to this cylindrical structure as well.

$$\vec{\tilde{E}}_{r,1} = \delta(\omega - \omega_0)\frac{\pi E_0 i}{2}\int_{-\infty}^{\infty} H_0^{(1)}\left(k\left|\vec{r} - \vec{r}'\right|\right) e^{ik_0 x'}\left(k^2\chi_{33} - ik\frac{\partial \chi_{22}}{\partial x} + k_0 k\chi_{22} + ik\frac{\partial \chi_{12}}{\partial y}\right)\hat{z}\, d^2\vec{r}' \quad (5.6)$$

Constructing the permittivity as per [9] (see MATLAB code, Appendix B) for a structure of inner radius 1 meter and outer radius of 1.5 meter, we note immediately from Figure 5.1 the sharp peaks at the inner radius (set to 1 meter in this simulation). The mathematical form of the electric susceptibility from equation (5.16) suggests that these peaks are an artifact of the rectangular grid enforced upon an inherently cylindrical structure. That the location and height of these peaks, in addition, varies with mesh size (see Figure 5.1), provides further evidence of a granularity problem. This granularity issue and the resultant inablility of this model to accurately determine susceptibility values according to the TO prescription suggests that any application of the iterative approach outlined in Chapter 4 which uses these susceptibility values should be suspect. As seen in Figure 5.2, the attained first order response field does not exhibit any of the expected behavior of a TO-derived redirection structure. We attribute this incongruence to the issue of representing a

a circular structure on a rectangular grid.

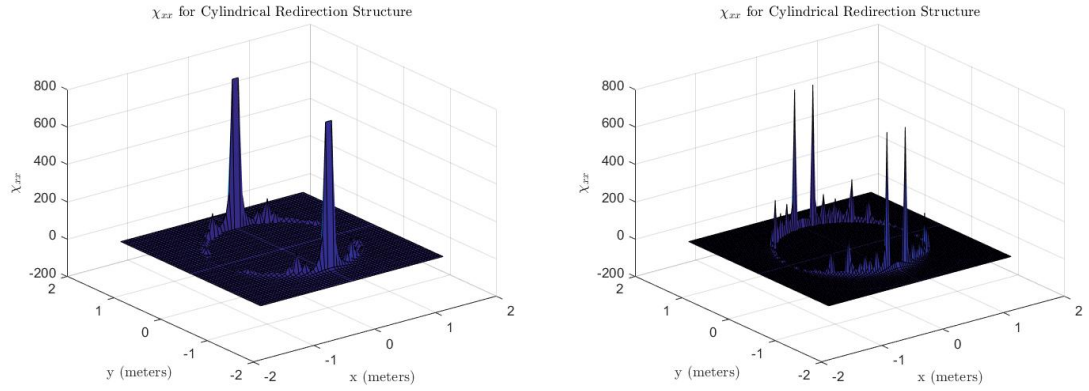

Figure 5.1: Left: xx component of the electric susceptibility as computed in cartesian coordinates, for a redirection structure of inner radius 1 meter, outer radius 1.5 meter, and mesh size of 0.05 meter. Right: The same simulation, with a mesh size of 0.03 meter. Note the sharp peaks which arise due to the granularity of the simulation regardless of mesh size.

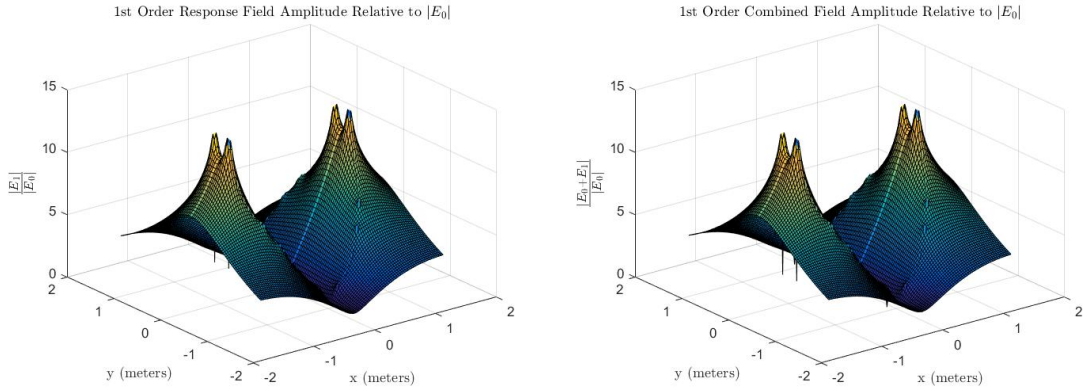

Figure 5.2: Left: First order response field for incident $\hat{z}$-polarized plane wave with wavenumber $1 \times 10^{-2} m^{-1}$, in Cartesian coordinates, mesh size 0.03 meter Right: Combined response field. Note that the jagged peaks of Figure 5.1, an artifact of the Cartesian grid imposed on the structure, have carried over to the response field

5.1.2 Cylindrical Coordinates

In an effort to address the granularity issue which has likely compromised the usefulness of the treatment seen in the previous subsection, we turn to the coordinate system naturally

suited to a cylindrical structure — cylindrical polar coordinates. Constructing a cylindrical coordinate grid and inputting the susceptibility values determined from (3.189) and [9] (see, once again, MATLAB code, Appendix B), we observe that the sharp peaks characteristic of the susceptibility in a Cartesian grid system appear to have been eliminated in favor of the expected smoothly varying values from (3.178), as we may see in Figure 5.3.

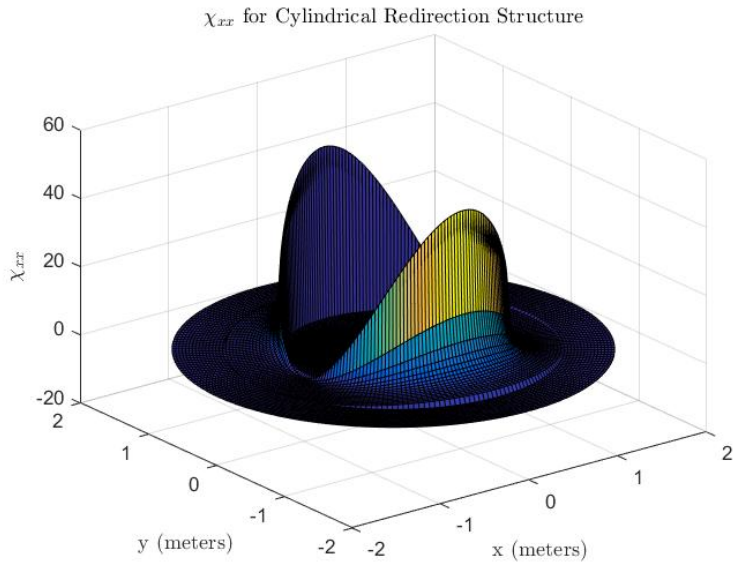

Figure 5.3: xx componenet of the electric susceptibility for the same cylindrical structure as seen in Figure 5.1, in cylindrical coordinates. Mesh size is 0.03 meter in the radial direction, $\frac{2\pi}{200}$ radian azimuthally.

From equation(4.47), for an incident plane wave polarized along the $\hat{z}$-direction,

$$\vec{\tilde{E}}_{r,1} = \delta(\omega-\omega_0)\frac{\pi i}{2}\int_{-\infty}^{\infty} H_0^{(1)}\left(k\left|\vec{r}-\vec{r}'\right|\right)$$
$$\left(k^2E_0\left(\chi * \left(e^{ik_0x'}\hat{z}\right)\right) - i\omega\mu_0H_0\left(\nabla\times\left(\chi * e^{ik_0x'}\hat{y}\right)\right) + E_0\nabla\left(\nabla\cdot\left(\chi * \left(e^{ik_0x'}\hat{z}\right)\right)\right)\right)d^2\vec{r}' \tag{5.7}$$

Performing the computation (5.9) with this cylindrical mesh, we note that although the

overall combined (incident and first order response) electric field amplitude shows overall promising behavior, falling rapidly within the structure, the resultant fields can be made to vary over several orders of magnitude depending upon the choice of mesh fineness. See Figures 5.4-5.6 for a comparison of the combined electric field for various mesh sizes.

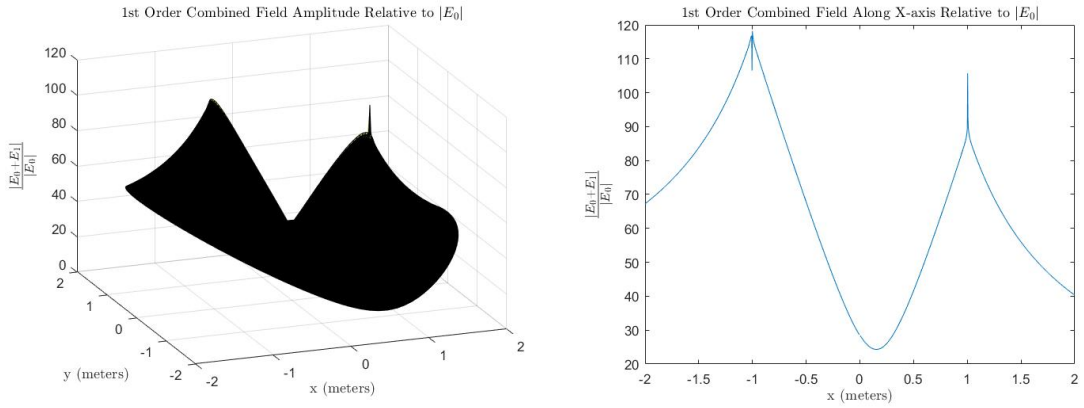

Figure 5.4: Left: Surface plot of the combined (incident and first order response) electric field amplitude for the cylindrical structure. Meshsize is 0.003 meter in the radial direction, $\frac{2\pi}{100}$ azimuthally. Wavenumber is $0.01\,m^{-1}$. Right: The response field for the same meshsize, along the x-axis.

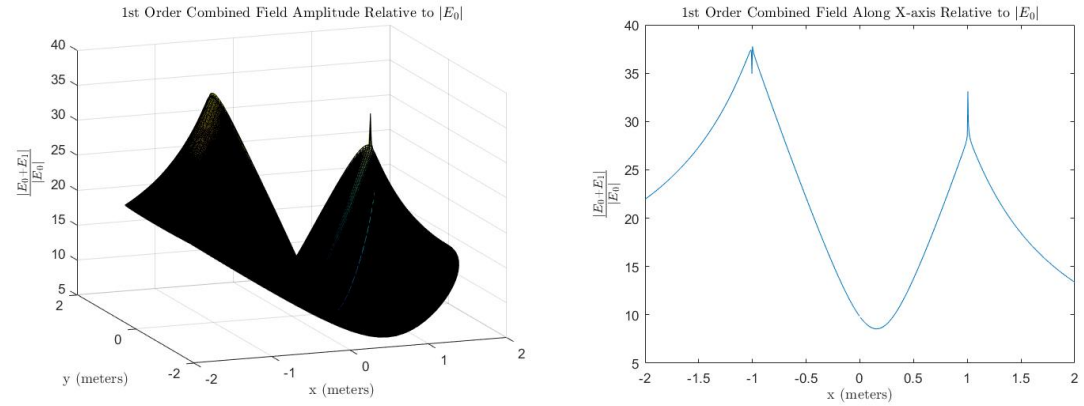

Figure 5.5: Surface plot and two dimensional plot along the x-axis for the same structure as in Figure 5.4, with a meshsize of 0.005 meter in the radial direction.

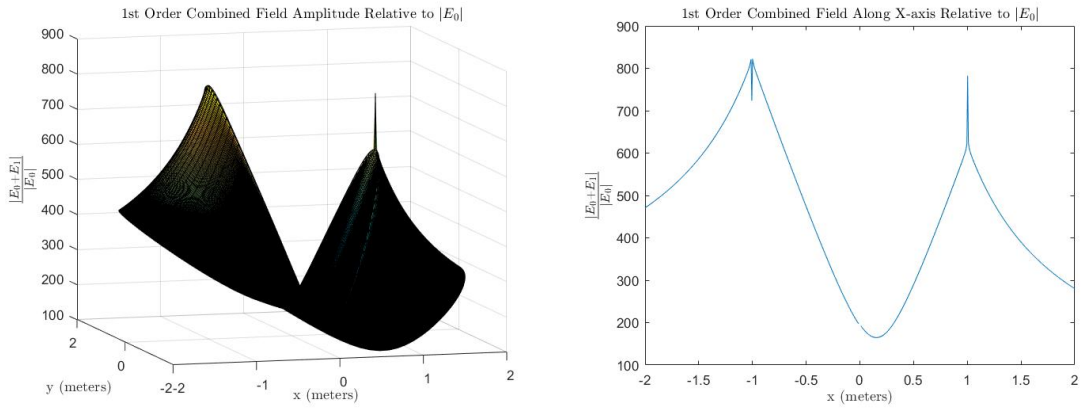

Figure 5.6: Surface plot and two dimensional plot along the x-axis for the same structure as in Figure 5.4, with a meshsize of 0.007 meter in the radial direction.

In addition, our results appear strongly dependent upon our choice of incident wavenumber, as shown in Figures 5.7-5.10.

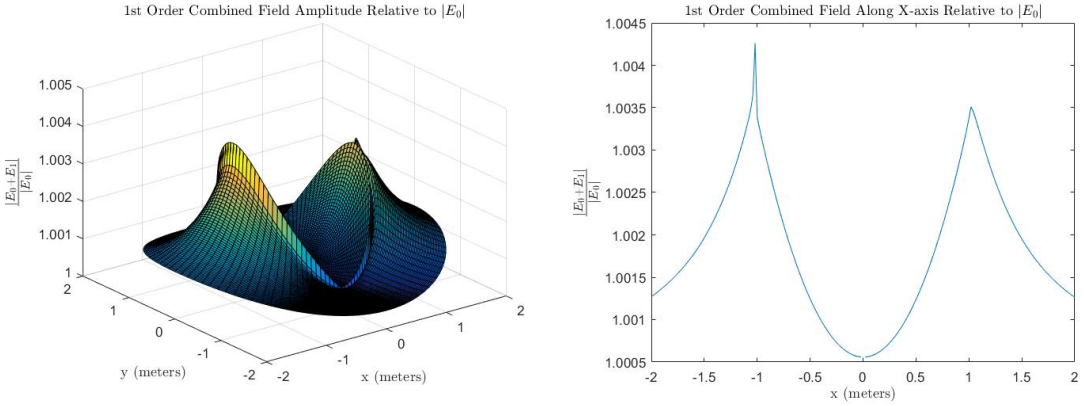

Figure 5.7: Surface plot and two dimensional plot along the x-axis of the amplitude of the combined (through first order) electric field, relative to incident field amplitude, for the cylindrical redirection structure simulation, with cylindrical mesh, radial meshsize of 0.02 meter, azimuthal meshsize $\frac{2\pi}{100}$, and wavenumber $0.001m^{-1}$.

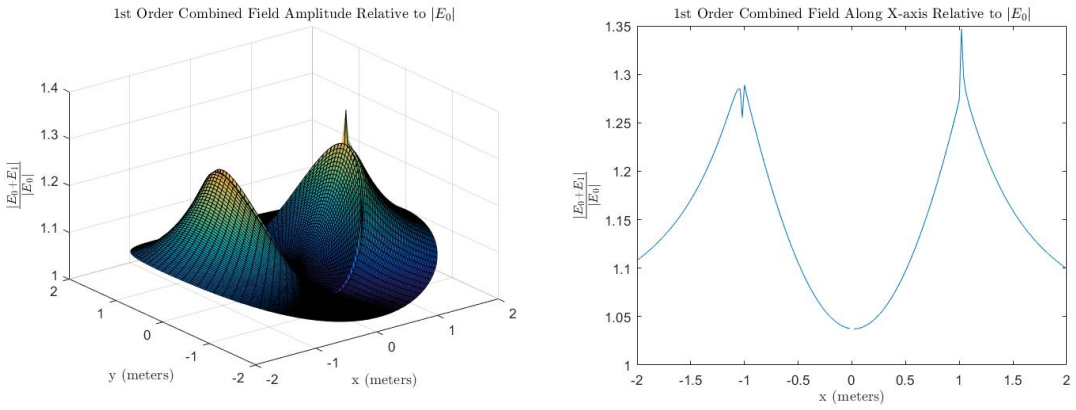

Figure 5.8: Surface plot and two dimensional plot along the x-axis of the amplitude of the combined (through first order) electric field, relative to incident field amplitude, for the cylindrical redirection structure simulation, with cylindrical mesh, radial meshsize of 0.02 meter, azimuthal meshsize $\frac{2\pi}{100}$, and wavenumber $0.01m^{-1}$.

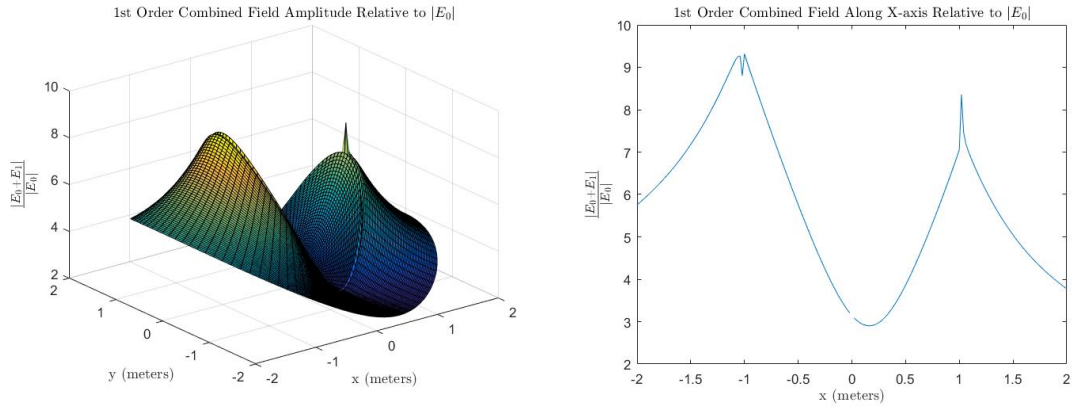

Figure 5.9: Surface plot and two dimensional plot along the x-axis of the amplitude of the combined (through first order) electric field, relative to incident field amplitude, for the cylindrical redirection structure simulation, with cylindrical mesh, radial meshsize of 0.02 meter, azimuthal meshsize $\frac{2\pi}{100}$, and wavenumber $0.1m^{-1}$.

We note from Figure 5.10 that as the wavelength falls to less than three orders of magnitude relative to the radial mesh size, the simulation appears to break down altogether. We attribute this failure to the inability of the (now relatively coarse) mesh to fully extract the necessary data from our model for the incident electromagnetic wave.

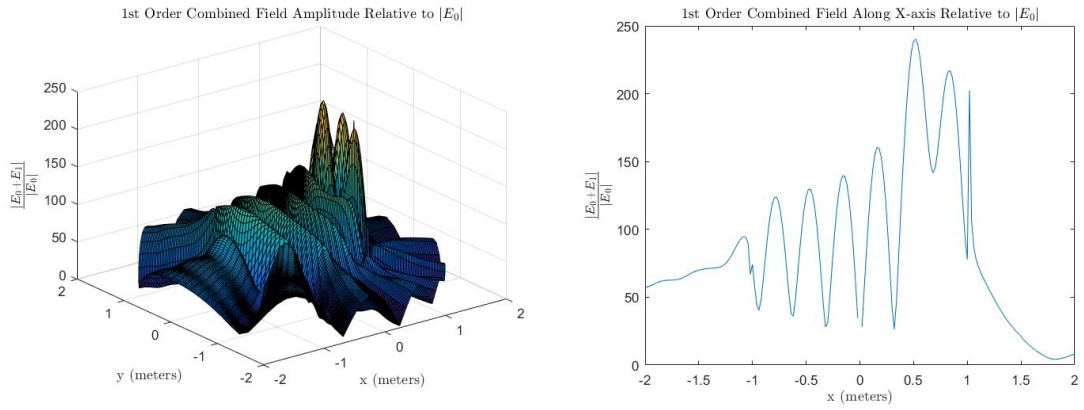

Figure 5.10: Surface plot and two dimensional plot along the x-axis of the amplitude of the combined (through first order) electric field, relative to incident field amplitude, for the cylindrical redirection structure simulation, with cylindrical mesh, radial meshsize of 0.02 meter, azimuthal meshsize $\frac{2\pi}{100}$, and wavenumber $1m^{-1}$.

5.2 Reduced Material Parameter Cylindrical Shield

In an effort to eliminate the influence of diverging material parameters upon our results, we turn to an approach discussed in [3] and [11]. Enforcing $\mu^{\phi\phi} = 1$, Cummer et al. have shown that although the non-reflectance condition $\frac{\varepsilon^{ij}}{\varepsilon_0} = \frac{\mu^{ij}}{\mu_0}$ is no longer met, the remaining relevant material parameters in cylindrical coordinates reduce to

$$\varepsilon^{zz} = \left(\frac{b}{b-a}\right)^2 = \frac{1}{R^2} \tag{5.8}$$

$$\mu^{rr} = \left(\frac{r-a}{r}\right)^2 \tag{5.9}$$

The absence of electrical permittivity components other than ε^{zz} will prove a useful simplification when considering the structure's response to a plane wave polarized along the $\hat{z}$ direction.

We note that these reduced material parameters involve only one cylindrical coordinate component which varies with position through the structure, and that none of the components of the prescribed susceptibilities diverge anywhere within the structure (see Figure 5.11). These reduced parameters are therefore expected to be advantageous from a manufacturing standpoint [11], as arbitrarily large electromagnetic material parameters are not currently realizable. In simulations, the reflected intensity arising from now nonzero impedance mismatch between surroundings and structure is somewhat minor [11].

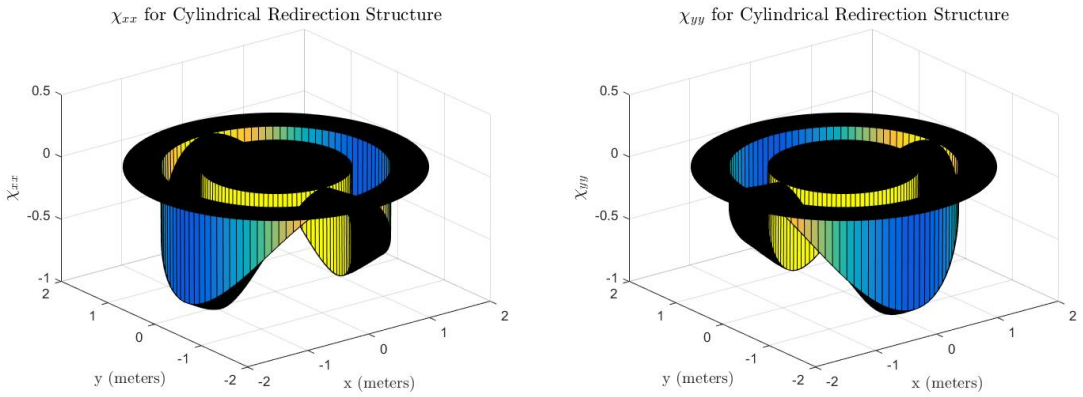

Figure 5.11: $\chi_{m,xx}$ and $\chi_{m,yy}$ for the reduced material parameter cylindrical structure. Unlike the material parameter solutions of the previous section, these susceptibiity components do not diverge as we approach the inner boundary.

Since, for this application, $\chi_e \neq \chi_m$, the general first order response (4.44) becomes, following development identical in form to that of equations (4.45) to (4.58),

$$\vec{\tilde{E}}_{r,1} = -\delta(\omega-\omega_0)\frac{\pi E_0 i}{2}\int_{-\infty}^{\infty} H_0^{(1)}\left(k\left|\vec{r}-\vec{r}'\right|\right)e^{ik_0x'}\left(k^2\chi_{e,33} - ik\frac{\partial\chi_{22}}{\partial x} + k_0k\chi_{m,22} + ik\frac{\partial\chi_{m,12}}{\partial y}\right)\hat{z}\,d^2\vec{r}' \tag{5.10}$$

Implementation of this expression for the first order response electric field in MATLAB (Appendix B) and analysis of the resulting combined (incident and first order) electric field demonstrates that the previously observed large variation of results with respect to meshsize has been eliminated. See Figures 5.12-5.14 for a depiction of this simulation stability with

respect to meshsize.

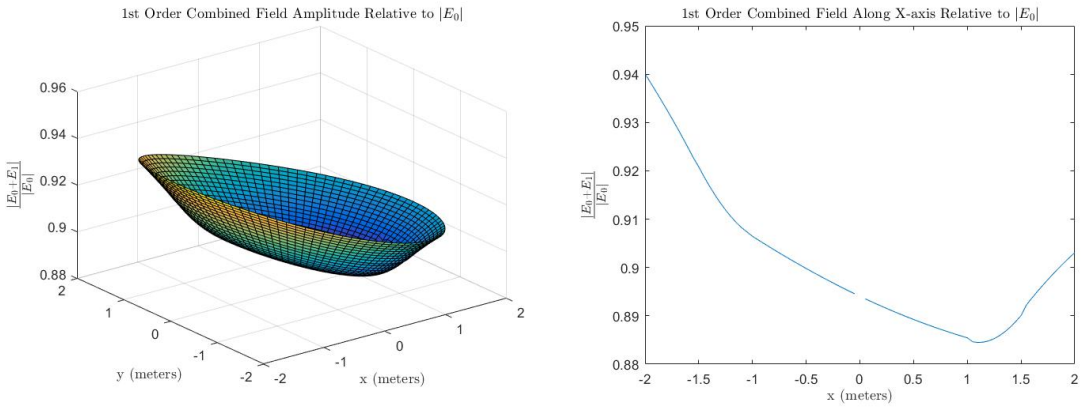

Figure 5.12: Surface plot and two dimensional plot along the x-axis of the amplitude of the combined (through first order) electric field, relative to incident field amplitude, for the MATLAB simulation of the cylindrical reduced material parameter redirection structure, inner radius 1 meter, outer radius 1.5 meter, with cylindrical mesh, radial meshsize of 0.05 meter, azimuthal meshsize $\frac{2\pi}{100}$, and wavenumber $0.1m^{-1}$.

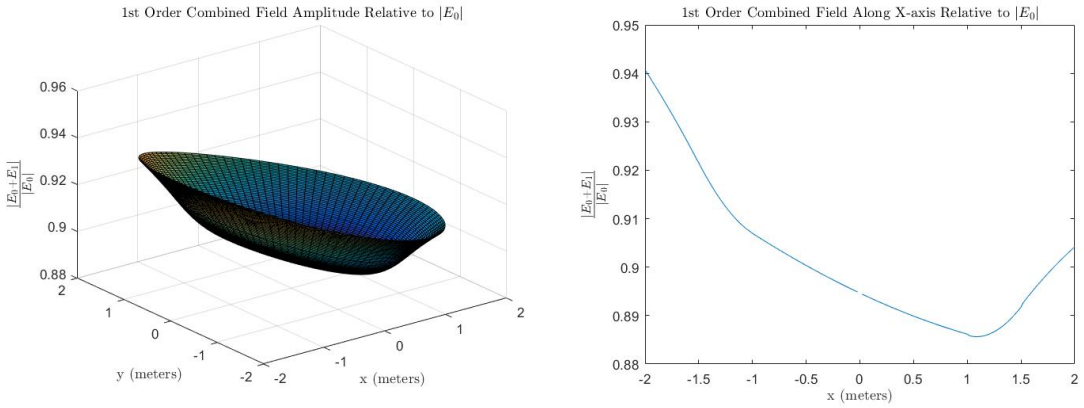

Figure 5.13: Surface plot and two dimensional plot along the x-axis of the amplitude of the combined (through first order) electric field, relative to incident field amplitude, for the MATLAB simulation of the cylindrical reduced material parameter redirection structure, inner radius 1 meter, outer radius 1.5 meter, with cylindrical mesh, radial meshsize of 0.02 meter, azimuthal meshsize $\frac{2\pi}{100}$, and wavenumber $0.1m^{-1}$.

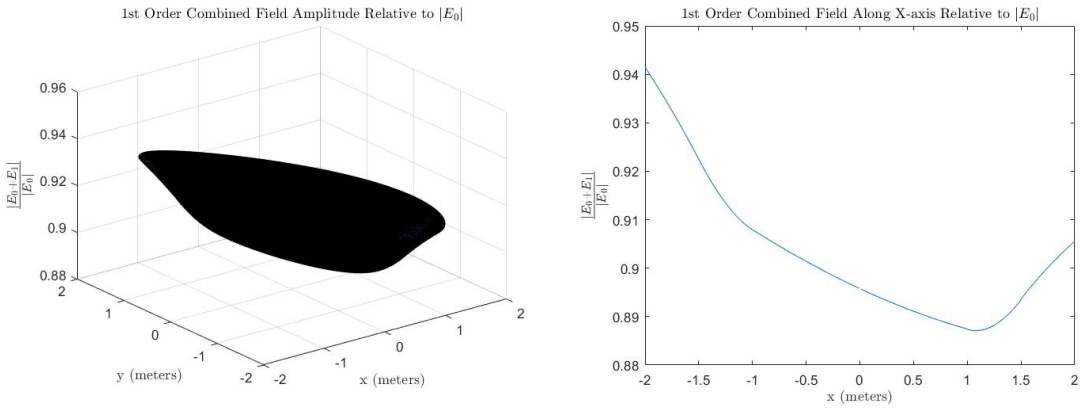

Figure 5.14: Surface plot and two dimensional plot along the x-axis of the amplitude of the combined (through first order) electric field, relative to incident field amplitude, for the MATLAB simulation of the cylindrical reduced material parameter redirection structure, inner radius 1 meter, outer radius 1.5 meter, with cylindrical mesh, radial meshsize of 0.008 meter, azimuthal meshsize $\frac{2\pi}{100}$, and wavenumber $0.1m^{-1}$.

We still observe, however, a very strong dependence of our results on the choice of incident wavenumber. See Figures 5.15-5.19 for a review of simulation dependence upon incident wavenumber.

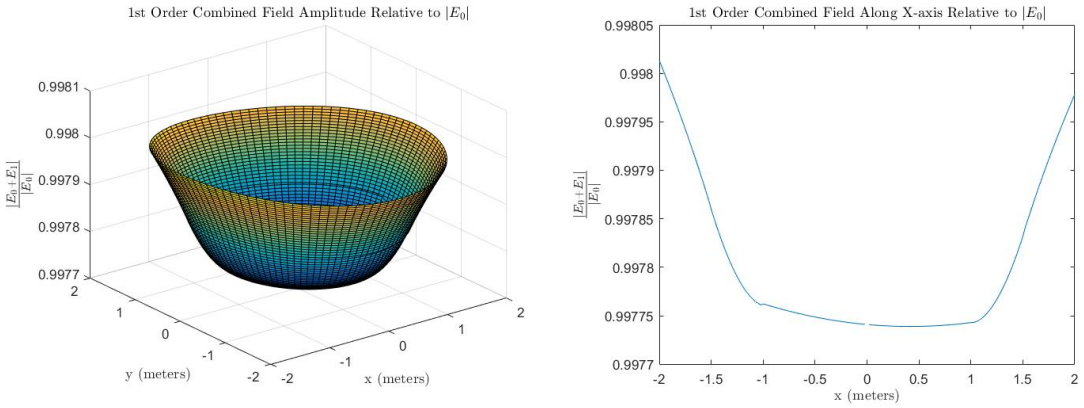

Figure 5.15: Surface plot and two dimensional plot along the x-axis of the amplitude of the combined (through first order) electric field, relative to incident field amplitude, for the MATLAB simulation of the cylindrical reduced material parameter redirection structure, inner radius 1 meter, outer radius 1.5 meter, with cylindrical mesh, radial meshsize of 0.02 meter, azimuthal meshsize $\frac{2\pi}{100}$, and wavenumber $0.01m^{-1}$.

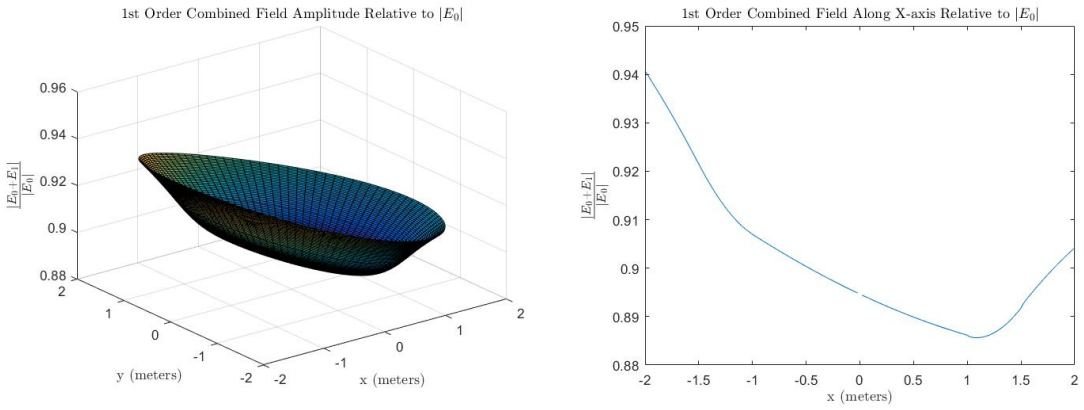

Figure 5.16: Surface plot and two dimensional plot along the x-axis of the amplitude of the combined (through first order) electric field, relative to incident field amplitude, for the MATLAB simulation of the cylindrical reduced material parameter redirection structure, inner radius 1 meter, outer radius 1.5 meter, with cylindrical mesh, radial meshsize of 0.02 meter, azimuthal meshsize $\frac{2\pi}{100}$, and wavenumber $0.1m^{-1}$.

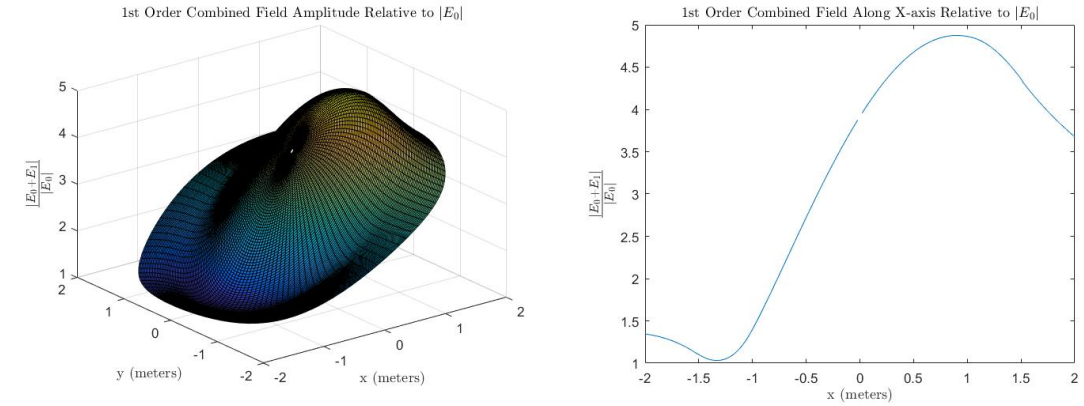

Figure 5.17: Surface plot and two dimensional plot along the x-axis of the amplitude of the combined (through first order) electric field, relative to incident field amplitude, for the MATLAB simulation of the cylindrical reduced material parameter redirection structure, inner radius 1 meter, outer radius 1.5 meter, with cylindrical mesh, radial meshsize of 0.02 meter, azimuthal meshsize $\frac{2\pi}{100}$, and wavenumber $1m^{-1}$.

As previously, the simulation appears to breakdown as the incident wavelength falls to within three orders of magnitude of the radial meshsize.

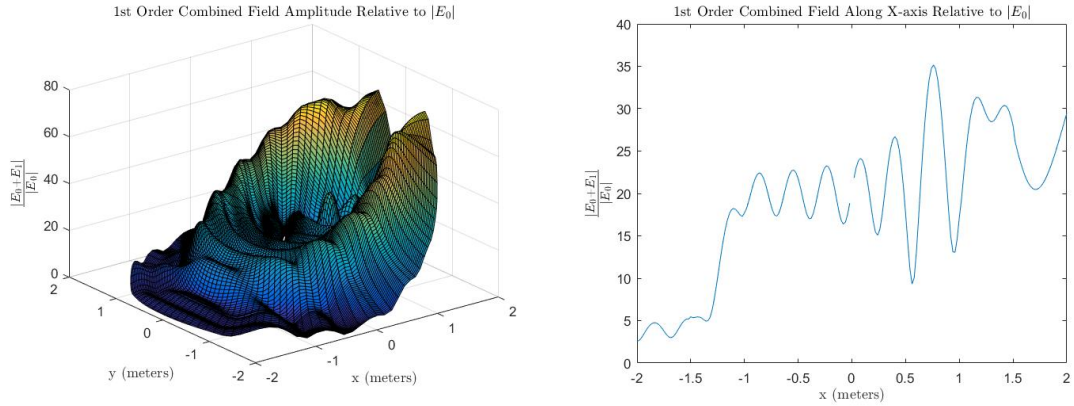

Figure 5.18: Surface plot and two dimensional plot along the x-axis of the amplitude of the combined (through first order) electric field, relative to incident field amplitude, for the MATLAB simulation of the cylindrical reduced material parameter redirection structure, inner radius 1 meter, outer radius 1.5 meter, with cylindrical mesh, radial meshsize of 0.02 meter, azimuthal meshsize $\frac{2\pi}{100}$, and wavenumber $10m^{-1}$.

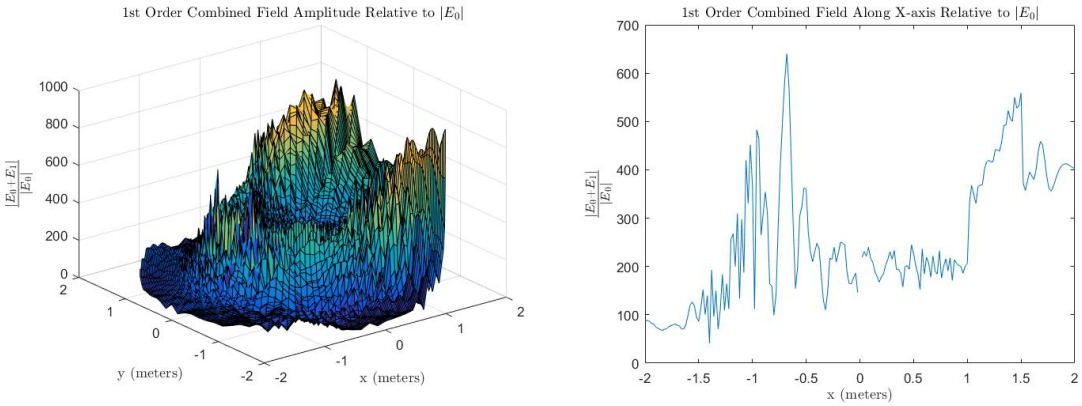

Figure 5.19: Surface plot and two dimensional plot along the x-axis of the amplitude of the combined (through first order) electric field, relative to incident field amplitude, for the MATLAB simulation of the cylindrical reduced material parameter redirection structure, inner radius 1 meter, outer radius 1.5 meter, with cylindrical mesh, radial meshsize of 0.02 meter, azimuthal meshsize $\frac{2\pi}{100}$, and wavenumber $100m^{-1}$.

Based upon the above results, we hypothesize that the strong dependence on meshsize observed in Section 5.1 is a result arising from the divergence of the material parameters

observed in those structures. As our mesh becomes finer, it incorporates a greater portion of the region near the inner boundary, where susceptibility values diverge, leading to rising response field values, as we have seen. The simulation results obtained in the case of the reduced parameter structure, which do not involve diverging electric or magnetic susceptibility, appear highly stable with respect to meshsize variation. A common feature to both approaches, however, is the strong dependence of our results upon incident wavenumber.

5.3 Square Shield

We now consider the square electromagnetic redirection structure outlined in [8]. Note that as for the unreduced parameter cylindrical structure, some components of the susceptibility diverge as we approach the inner surface. In Cartesian coordinates, the susceptibility tensor χ may be expressed as

$$\chi = \begin{pmatrix} \chi_{11} & \chi_{12} & 0 \\ \chi_{21} & \chi_{22} & 0 \\ 0 & 0 & \chi_{33} \end{pmatrix} \tag{5.11}$$

For an incident plane wave polarized in the $\hat{z}$-direction, the first order response is given by equation (4.58) as

$$\vec{\tilde{E}}_{r,1} = \delta(\omega - \omega_0)\frac{\pi E_0 i}{2}\int_{-\infty}^{\infty} H_0^{(1)}\left(k\left|\vec{r}-\vec{r}'\right|\right) e^{ik_0 x'}\left(k^2\chi_{33} - ik\frac{\partial \chi_{22}}{\partial x} + k_0 k\chi_{22} + ik\frac{\partial \chi_{12}}{\partial y}\right)\hat{z}\,d^2\vec{r}' \tag{5.12}$$

Results of simulations (Appendix B) for this structure are similar to those observed for the Cylindrical structure once an appropriate mesh shape was imposed upon it. We again observe similar overall behavior between all structures, displaying some of the desired combined field behavior (field amplitude falls to a minimum rapidly upon entering the inner area of the structure), with amplitudes strongly dependent upon meshsize, as shown in Figures 5.20-5.22.

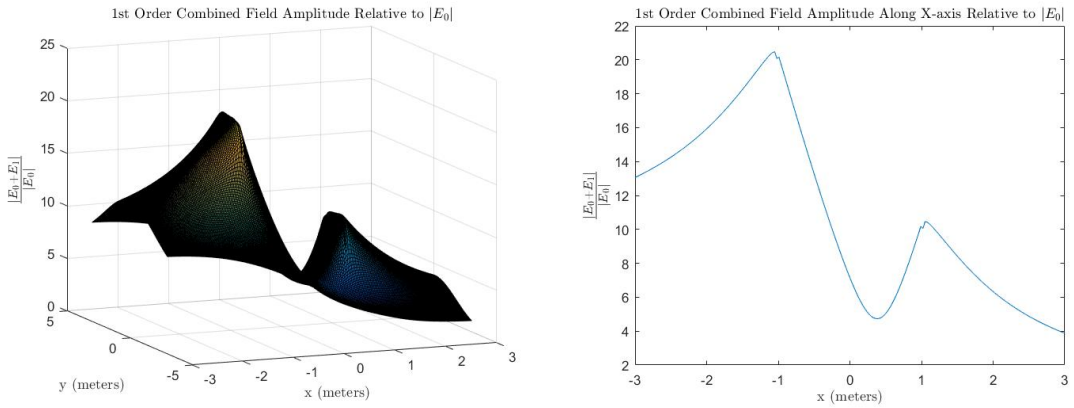

Figure 5.20: Surface plot and plot along the x-axis for of the combined (to first order) electric field amplitude, relative to incident field amplitude, for the square structure simulation, with meshsize 0.03 meter, wavenumber 0.02 m^{-1}, half side lengths 1 and 2 meters.

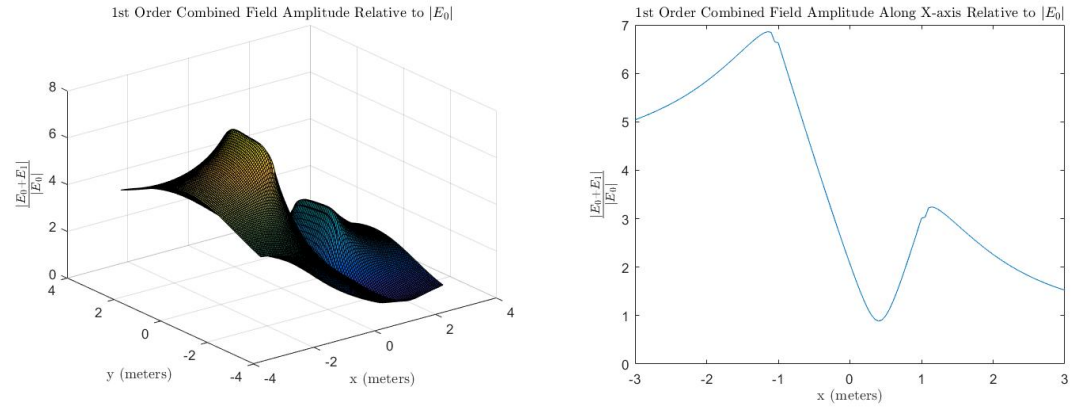

Figure 5.21: Surface plot and plot along the x-axis for of the combined (to first order) electric field amplitude, relative to incident field amplitude, for the square structure simulation, with meshsize 0.05 meter, wavenumber 0.02 m^{-1}, half side lengths 1 and 2 meters.

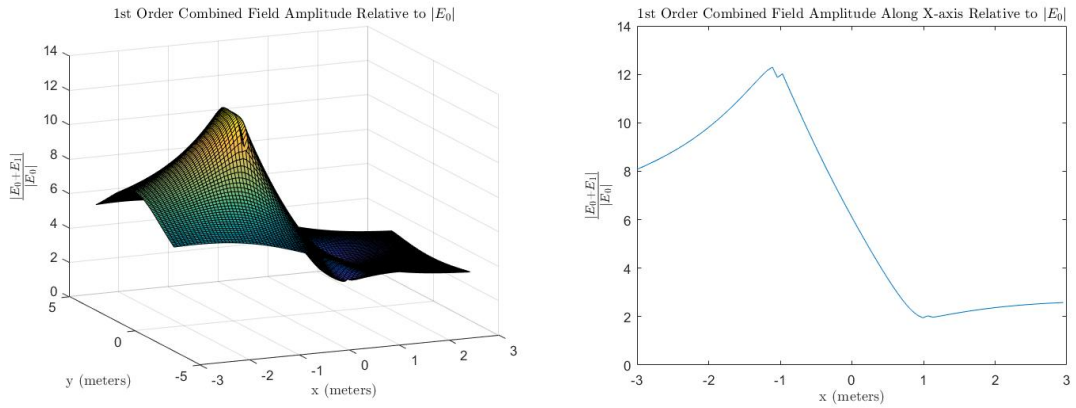

Figure 5.22: Surface plot and plot along the x-axis for of the combined (to first order) electric field amplitude, relative to incident field amplitude, for the square structure simulation, with meshsize 0.07 meter, wavenumber 0.02 m^{-1}, half side lengths 1 and 2 meters.

In addition to these findings, we observe combined field amplitudes dependent on wavenumber as per the cylindrical structure. Also noted is the breakdown of the simulation similar to that of Figures 5.10, 5.18, and 5.19 upon the incident wavelength lowering to within three orders of magnitude of the meshsize.

CHAPTER 6:
Conclusions

Here we will consider the results of the approach to electromagnetic scattering pursued through Chapters 4 and 5, and outline possibilities for future work.

6.1 Effectiveness of the Iterative Approach

Although well–grounded in the fundamental relations of classical electromagnetism, implementation of a Neumann series approximation for the response electric and magnetic fields can be problematic when applied to exotic structures such as TO-based CDEW electromagnetic redirection structures. The divergence in the material susceptibility required for even the simple ideal structures we have examined here can lead to considerable variation in the results of our numerical calculations depending on mesh size and incident wavenumber. For this reason, it is likely that, in order to attain convergence of numerical results, a meshsize finer than possible on the hardware employed for this study should be used, or analyses should be restricted to reduced material parameter structures such as those studied in Section 5.2. Regardless, powerful hardware would also be required to begin analyzing the numerical results for second and higher order responses. These higher order results would be of value in addressing the remaining issues of series convergence and the extreme incident wavenumber dependence of our results.

Due to practical engineering concerns, a real-world CDEW redirection structure will feature neither a continuously varying susceptibility, nor a susceptibility with any components diverging as a particular bounding surface is approached. Studies such as [3] and [13] have examined the linear response of layered structures, designed to approximate the cylindrical redirection device proposed in [9] and analyzed in Chapter 3 above.

6.2 Future Work

Opportunities for follow-on research are plentiful. As mentioned, attaining a convergent first order response and analyzing the numerical computations for second and higher order

response fields may be possible with access to greater computing power than was available for this work. In addition, once the higher order responses have been well characterized, and assuming that the Neumann series is shown to converge, the efficacy of the approach may be tested via experiment using the layered structures which have been shown to closely mimic the theorized linear behavior of TO-based devices. Such experimental work could be carried out as an extension to the metamaterials research currently being done by Professors James Luscombe and Dragoslav Grbovic of the NPS Physics Department.

Beyond these refinements, there is considerable theoretical ground which may be analyzed through the approach taken here. In order to be considered a successful extension of current theory, this iterative approach should allow us to predict observed phenomena. Miller's rule, an empirical method of attaining higher order electric susceptibilities in regular non-magnetic structures (i.e., crystals) from the lower electric susceptibilities, has been shown to be effective in predicting the nonlinear optical behavior of these structures. If valid, the approach taken here to nonlinear optical responses should reduce to Miller's rule in the appropriate material regime. As a further test of the predictive power of our approach, we should be able to show the appearance of well-known nonlinear optical effects such as frequency doubling and the Kerr effect in appropriate media.

APPENDIX A:
Green Functions

Green functions relevant to the iterative approach of chapter 5 of this work will be derived here.

A.1 The Green function for the two dimensional Helmholtz equation

The homogenous Helmholtz equation is given as

$$\nabla^2 f + k_0^2 f = 0 \tag{A.1}$$

where f is the function of interest and k_0 is a known parameter. The Green function for this equation is therefore given as the solution to

$$\nabla^2 G\left(\vec{r},\vec{r}'\right) + k_0^2 G\left(\vec{r},\vec{r}'\right) = \delta\left(\vec{r}-\vec{r}'\right) \tag{A.2}$$

Performing a Fourier transform and applying the sifting property of the Dirac delta function,

$$\int_{-\infty}^{\infty} \left(\nabla^2 G\left(\vec{r},\vec{r}'\right) + k_0^2 G\left(\vec{r},\vec{r}'\right)\right) e^{-i\vec{k}\cdot\vec{r}} d^2\vec{r} = \int_{-\infty}^{\infty} \delta\left(\vec{r}-\vec{r}'\right) e^{-i\vec{k}\cdot\vec{r}} d^2\vec{r} \tag{A.3}$$

$$\int_{-\infty}^{\infty} \nabla^2 G\left(\vec{r},\vec{r}'\right) e^{-i\vec{k}\cdot\vec{r}} d^2\vec{r} + \int_{-\infty}^{\infty} k_0^2 G\left(\vec{r},\vec{r}'\right) e^{-i\vec{k}\cdot\vec{r}} d^2\vec{r} = e^{-i\vec{k}\cdot\vec{r}'} \tag{A.4}$$

From Green's second identity,

$$\int_D \left(f\nabla^2 g - g\nabla^2 f\right) dA = \int_{\partial D} \left(f\left(\nabla g\cdot\vec{n}\right) - g\left(\nabla f\cdot\vec{n}\right)\right) dl \tag{A.5}$$

where D is the domain of the functions f and g, ∂D is the bounding set to that domain, and $\vec{n}$ is the normal to the bounding set. Thus,

$$\int_D f\nabla^2 g dA = \int_D g\nabla^2 f dA - \int_{\partial D}\left(g\frac{\partial f}{\partial n} - f\frac{\partial g}{\partial n}\right)dl \tag{A.6}$$

where $\dfrac{\partial f}{\partial n} = \nabla f \cdot \vec{n}$ and similar for $\dfrac{\partial g}{\partial n}$. Taking $f = e^{-i\vec{k}\cdot\vec{r}}$ and $g = G$, and furthermore taking D as the entire x-y plane, and assuming that G falls off at least as fast as $\dfrac{1}{r}$, assuming a value of zero in the large r limit,

$$\int_{-\infty}^{\infty} e^{-i\vec{k}\cdot\vec{r}}\nabla^2 G\left(\vec{r},\vec{r}'\right)dA = \int_{-\infty}^{\infty} G\left(\vec{r},\vec{r}'\right)\nabla^2\left(e^{-i\vec{k}\cdot\vec{r}}\right)dA \tag{A.7}$$

$$\int_{-\infty}^{\infty} e^{-i\vec{k}\cdot\vec{r}}\nabla^2 G\left(\vec{r},\vec{r}'\right)dA = -k^2\int_{-\infty}^{\infty} G\left(\vec{r},\vec{r}'\right)e^{-i\vec{k}\cdot\vec{r}}dA \tag{A.8}$$

$$\int_{-\infty}^{\infty} e^{-i\vec{k}\cdot\vec{r}}\nabla^2 G\left(\vec{r},\vec{r}'\right)dA = -k^2\int_{-\infty}^{\infty} G\left(\vec{r},\vec{r}'\right)e^{-i\vec{k}\cdot\vec{r}}dA \tag{A.9}$$

The two-dimensional Fourier transform of the Laplacian of the Green function is thus simply the Fourier transform of the Green function multiplied by $-k^2$, where k is the Fourier transform parameter. Inserting this result into (A.7), with $G\left(\vec{k},\vec{r}'\right) = \int_{-\infty}^{\infty} G\left(\vec{r},\vec{r}'\right)e^{-i\vec{k}\cdot\vec{r}}d^2\vec{r}$,

$$\left(k_0^2 - k^2\right)\tilde{G}\left(\vec{k},\vec{r}'\right) = e^{-i\vec{k}\cdot\vec{r}'} \tag{A.10}$$

$$\tilde{G}\left(\vec{k},\vec{r}'\right) = \frac{e^{-i\vec{k}\cdot\vec{r}'}}{k_0^2 - k^2} \tag{A.11}$$

The Green function may now be attained by inverse Fourier transforming the above expression.

$$G\left(\vec{r},\vec{r}'\right)=\frac{1}{(2\pi)^2}\int_{-\infty}^{\infty}\frac{e^{-i\vec{k}\cdot\vec{r}'}}{k_0^2-k^2}e^{i\vec{k}\cdot\vec{r}}d^2\vec{k} \tag{A.12}$$

$$G\left(\vec{r},\vec{r}'\right)=\frac{1}{(2\pi)^2}\int_{-\infty}^{\infty}\frac{e^{i\vec{k}\cdot(\vec{r}-\vec{r}')}}{k_0^2-k^2}d^2\vec{k} \tag{A.13}$$

In Cartesian coordinates in k-space (this integral may also be performed in cylindrical coordinates),

$$G\left(\vec{r},\vec{r}'\right)=\frac{-1}{(2\pi)^2}\int_{-\infty}^{\infty}\int_{-\infty}^{\infty}\frac{e^{i\left(k_x\rho_x+k_y\rho_y\right)}}{k_0^2-k_x^2-k_y^2}dk_x\,dk_y \tag{A.14}$$

where $\vec{\rho}\equiv\vec{r}-\vec{r}'$.

$$G\left(\vec{r},\vec{r}'\right)=\frac{1}{(2\pi)^2}\int_{-\infty}^{\infty}e^{ik_y\rho_y}\int_{-\infty}^{\infty}\frac{e^{ik_x\rho_x}}{k_x^2-\left(k_0^2-k_y^2\right)}dk_x\,dk_y \tag{A.15}$$

$$G\left(\vec{r},\vec{r}'\right)=\frac{1}{(2\pi)^2}\int_{-\infty}^{\infty}e^{ik_y\rho_y}\int_{-\infty}^{\infty}\frac{e^{ik_x\rho_x}}{\left(k_x+\sqrt{k_0^2-k_y^2}\right)\left(k_x-\sqrt{k_0^2-k_y^2}\right)}dk_x\,dk_y \tag{A.16}$$

The denominator of the k_x integral has simple poles given by $k_x=\pm\sqrt{k_0^2-k_y^2}$. If k_0 is greater than k_y, these poles lie on the real k_x-axis. If k_0 is less than k_y, the poles lie on the imaginary k_x-axis. If $k_0=k_y$, there is a single pole of second order at the origin. We will evaluate (A.16) case by case.

A.1.1 Case 1: $|k_0|>\left|k_y\right|$

The integrand of the k_x integral has poles on the real k_x line at $k_x=\pm\sqrt{k_0^2-k_y^2}$. We will evaluate it via a contour in the complex k_x plane comprised of a large semicircle in the upper half of the plane, taking $\sqrt{k_0^2-k_y^2}\rightarrow\sqrt{k_0^2-k_y^2}+i\varepsilon$,

Taking $f(z) = \dfrac{e^{iz\rho_x}}{\left(z+\sqrt{k_0^2-k_y^2}+i\varepsilon\right)\left(z-\sqrt{k_0^2-k_y^2}-i\varepsilon\right)}$, we note that the poles of $f(z)$ now lie at $\sqrt{k_0^2-k_y^2}+i\varepsilon$ and $-\sqrt{k_0^2-k_y^2}-i\varepsilon$, and that therefore only the simple pole $\sqrt{k_0^2-k_y^2}+i\varepsilon$ lies within our contour. From the residue theorem,

$$2\pi i Res\left(f\left(z=\sqrt{k_0^2-k_y^2}+i\varepsilon\right)\right) = \int_{-R}^{R} f(k_x)\,dk_x + \int_{C_R} f(z)\,dz \tag{A.17}$$

where C_R denotes the semicircle in the upper half plane of radius R.

$$= \int_{-R}^{R} f(k_x)\,dk_x + \int_{C_R} \frac{e^{iz\rho_x}}{\left(z+\sqrt{k_0^2-k_y^2}+i\varepsilon\right)\left(z-\sqrt{k_0^2-k_y^2}-i\varepsilon\right)}\,dz \tag{A.18}$$

Taking $z = Re^{i\theta}$ on C_R,

$$= \int_{-R}^{R} f(k_x)\,dk_x + \int_{0}^{\pi} \frac{e^{iRe^{i\theta}\rho_x}}{\left(Re^{i\theta}+\sqrt{k_0^2-k_y^2}+i\varepsilon\right)\left(Re^{i\theta}-\sqrt{k_0^2-k_y^2}-i\varepsilon\right)} iRe^{i\theta}\,d\theta \tag{A.19}$$

$$= \int_{-R}^{R} f(k_x)\,dk_x + \int_{0}^{\pi} \frac{iRe^{i\theta+i\rho_x R(\cos(\theta)+i\sin(\theta))}}{\left(Re^{i\theta}+\sqrt{k_0^2-k_y^2}+i\varepsilon\right)\left(Re^{i\theta}-\sqrt{k_0^2-k_y^2}-i\varepsilon\right)}\,d\theta \tag{A.20}$$

$$= \int_{-R}^{R} f(k_x)\,dk_x + \int_{0}^{\pi} \frac{iRe^{i\theta+i\rho_x R\cos(\theta)}e^{-\rho_x R\sin(\theta)}}{\left(Re^{i\theta}+\sqrt{k_0^2-k_y^2}+i\varepsilon\right)\left(Re^{i\theta}-\sqrt{k_0^2-k_y^2}-i\varepsilon\right)}\,d\theta \tag{A.21}$$

As $R \to \infty$, the second integral approaches a value of zero by Jordan's lemma, since $\sin(\theta) \geq 0$ on $\theta = [0, \pi]$.

$$2\pi i Res\left(f\left(z=\sqrt{k_0^2-k_y^2}+i\varepsilon\right)\right)=\int_{-\infty}^{\infty}\frac{e^{ik_x\rho_x}}{\left(k_x+\sqrt{k_0^2-k_y^2}+i\varepsilon\right)\left(k_x-\sqrt{k_0^2-k_y^2}-i\varepsilon\right)}dk_x \tag{A.22}$$

The residue of $f(z)$ at the simple pole $\sqrt{k_0^2-k_y^2}+i\varepsilon$ may be computed as

$$Res\left(f\left(z=\sqrt{k_0^2-k_y^2}+i\varepsilon\right)\right)=\lim_{z\to\sqrt{k_0^2-k_y^2}+i\varepsilon}\left[\left(z-\sqrt{k_0^2-k_y^2}-i\varepsilon\right)f(z)\right] \tag{A.23}$$

$$=\lim_{z\to\sqrt{k_0^2-k_y^2}+i\varepsilon}\left[\left(z-\sqrt{k_0^2-k_y^2}-i\varepsilon\right)\frac{e^{iz\rho_x}}{\left(z+\sqrt{k_0^2-k_y^2}+i\varepsilon\right)\left(z-\sqrt{k_0^2-k_y^2}-i\varepsilon\right)}\right] \tag{A.24}$$

$$=\lim_{z\to\sqrt{k_0^2-k_y^2}+i\varepsilon}\left[\frac{e^{iz\rho_x}}{z+\sqrt{k_0^2-k_y^2}+i\varepsilon}\right] \tag{A.25}$$

$$Res\left(f\left(z=\sqrt{k_0^2-k_y^2}+i\varepsilon\right)\right)=\frac{e^{i\rho_x\left(\sqrt{k_0^2-k_y^2}+i\varepsilon\right)}}{2\left(\sqrt{k_0^2-k_y^2}+i\varepsilon\right)} \tag{A.26}$$

Inserting this result into (A.22),

$$\int_{-\infty}^{\infty}\frac{e^{ik_x\rho_x}}{\left(k_x+\sqrt{k_0^2-k_y^2}+i\varepsilon\right)\left(k_x-\sqrt{k_0^2-k_y^2}-i\varepsilon\right)}dk_x=2\pi i\frac{e^{i\rho_x\left(\sqrt{k_0^2-k_y^2}+i\varepsilon\right)}}{2\left(\sqrt{k_0^2-k_y^2}+i\varepsilon\right)} \tag{A.27}$$

$$\int_{-\infty}^{\infty} \frac{e^{ik_x\rho_x}}{\left(k_x+\sqrt{k_0^2-k_y^2}+i\varepsilon\right)\left(k_x-\sqrt{k_0^2-k_y^2}-i\varepsilon\right)}\,dk_x = \pi i \frac{e^{i\rho_x\left(\sqrt{k_0^2-k_y^2}+i\varepsilon\right)}}{\sqrt{k_0^2-k_y^2}+i\varepsilon} \tag{A.28}$$

Taking $\varepsilon \to 0$,

$$\int_{-\infty}^{\infty} \frac{e^{ik_x\rho_x}}{\left(k_x+\sqrt{k_0^2-k_y^2}\right)\left(k_x-\sqrt{k_0^2-k_y^2}\right)}\,dk_x = \pi i \frac{e^{i\rho_x\left(\sqrt{k_0^2-k_y^2}\right)}}{\sqrt{k_0^2-k_y^2}} \tag{A.29}$$

A.1.2 Case 2: $|k_0| < |k_y|$

In this case, $f(z)$ has simple poles at $k_x = \pm i\sqrt{k_y^2-k_0^2}$. Again closing our contour with a large semicircle in the upper half plane, only $i\sqrt{k_y^2-k_0^2}$ lies within the contour. From the residue theorem,

$$2\pi i\, Res\left(f\left(z = i\sqrt{k_y^2-k_x^2}\right)\right) = \int_{-R}^{R} f(k_x)\,dk_x + \int_{C_R} f(z)\,dz \tag{A.30}$$

where $f(z) = \frac{e^{iz\rho_x}}{\left(z+i\sqrt{k_y^2-k_0^2}\right)\left(z-\sqrt{k_y^2-k_0^2}\right)}$ and C_R is again the semicircle of radius R in the upper half plane, centered at the origin. Taking $z = Re^{i\theta}$ on C_R,

$$= \int_{-R}^{R} f(k_x)\,dk_x + \int_0^{\pi} \frac{e^{iRe^{i\theta}\rho_x}}{\left(Re^{i\theta}+i\sqrt{k_y^2-k_0^2}\right)\left(Re^{i\theta}-i\sqrt{k_y^2-k_0^2}\right)} iRe^{i\theta}\,d\theta \tag{A.31}$$

$$= \int_{-R}^{R} f(k_x)\,dk_x + \int_0^{\pi} \frac{iRe^{i\theta+iR(\cos(\theta)+i\sin(\theta))\rho_x}}{\left(Re^{i\theta}+i\sqrt{k_y^2-k_0^2}\right)\left(Re^{i\theta}-i\sqrt{k_y^2-k_0^2}\right)}\,d\theta \tag{A.32}$$

$$= \int_{-R}^{R} f(k_x)\, dk_x + \int_0^{\pi} \frac{iRe^{i\theta + i\rho_x R\cos(\theta) - \rho_x R\sin(\theta)}}{\left(Re^{i\theta} + i\sqrt{k_y^2 - k_0^2}\right)\left(Re^{i\theta} - i\sqrt{k_y^2 - k_0^2}\right)} d\theta \tag{A.33}$$

Again the integral over C_R approaches zero as $R \to \infty$, by Jordan's lemma.

$$2\pi i Res\left(f\left(z = i\sqrt{k_y^2 - k_0^2}\right)\right) = \int_{-\infty}^{\infty} \frac{e^{i\rho_x k_x}}{\left(k_x + i\sqrt{k_y^2 - k_0^2}\right)\left(k_x - i\sqrt{k_y^2 - k_0^2}\right)} dk_x \tag{A.34}$$

Since the pole at $i\sqrt{k_y^2 - k_0^2}$ is of order one, it may be computed as

$$Res\left(f\left(z = i\sqrt{k_y^2 - k_0^2}\right)\right) = \lim_{z \to i\sqrt{k_y^2 - k_0^2}} \left[\left(z - i\sqrt{k_y^2 - k_0^2}\right) f(z)\right] \tag{A.35}$$

$$= \lim_{z \to i\sqrt{k_y^2 - k_0^2}} \left[\left(z - i\sqrt{k_y^2 - k_0^2}\right) \frac{e^{i\rho_x z}}{\left(z + i\sqrt{k_y^2 - k_0^2}\right)\left(z - i\sqrt{k_y^2 - k_0^2}\right)}\right] \tag{A.36}$$

$$= \lim_{z \to i\sqrt{k_y^2 - k_0^2}} \left[\frac{e^{i\rho_x z}}{z + i\sqrt{k_y^2 - k_0^2}}\right] \tag{A.37}$$

$$= \frac{e^{i\rho_x\left(i\sqrt{k_y^2 - k_0^2}\right)}}{2i\sqrt{k_y^2 - k_0^2}} \tag{A.38}$$

$$= \frac{e^{-\rho_x\sqrt{k_y^2 - k_0^2}}}{2i\sqrt{k_y^2 - k_0^2}} \tag{A.39}$$

Inserting this result into (A.34),

$$\int_{-\infty}^{\infty} \frac{e^{i\rho_x k_x}}{\left(k_x + i\sqrt{k_y^2 - k_0^2}\right)\left(k_x - i\sqrt{k_y^2 - k_0^2}\right)} = 2\pi i \left(\frac{e^{-\rho_x\sqrt{k_y^2 - k_0^2}}}{2i\sqrt{k_y^2 - k_0^2}}\right) \tag{A.40}$$

$$\int_{-\infty}^{\infty} \frac{e^{i\rho_x k_x}}{\left(k_x + i\sqrt{k_y^2 - k_0^2}\right)\left(k_x - i\sqrt{k_y^2 - k_0^2}\right)} = \frac{\pi e^{-\rho_x\sqrt{k_y^2 - k_0^2}}}{\sqrt{k_y^2 - k_0^2}} \tag{A.41}$$

A.1.3 Case 3: $|k_0| = |k_y|$

In this case, our k_x integral reduces to

$$\int_{-\infty}^{\infty} \frac{e^{ik_x\rho_x}}{k_x^2}\, dk_x \tag{A.42}$$

Moving the (now second-order) singularity off of the real axis as for case 1, we consider

$$\int_C \frac{e^{iz\rho_x}}{(z + i\varepsilon)(z - i\varepsilon)}\, dz \tag{A.43}$$

where C is once more the large semicircle in the upper half plane. By the residue theorem,

$$2\pi i\, Res\left(f(z = i\varepsilon)\right) = \int_{-R}^{R} \frac{e^{ik_x\rho_x}}{(k_x + i\varepsilon)(k_x - i\varepsilon)}\, dk_x + \int_{C_R} \frac{e^{iz\rho_x}}{(z + i\varepsilon)(z - i\varepsilon)}\, dz \tag{A.44}$$

where $f(z) = \dfrac{e^{iz\rho_x}}{(z + i\varepsilon)(z - i\varepsilon)}$. Taking $z = Re^{i\theta}$ on C_R,

$$= \int_{-R}^{R} \frac{e^{ik_x\rho_x}}{(k_x + i\varepsilon)(k_x - i\varepsilon)}\, dk_x + \int_0^{\pi} \frac{e^{i\rho_x Re^{i\theta}}}{\left(Re_i^{i\theta}\varepsilon\right)\left(Re^{i\theta} - i\varepsilon\right)} iRe^{i\theta}\, d\theta \tag{A.45}$$

$$= \int_{-R}^{R} \frac{e^{ik_x\rho_x}}{(k_x + i\varepsilon)(k_x - i\varepsilon)}\, dk_x + \int_0^{\pi} \frac{iRe^{i\theta} e^{i\rho_x R(\cos(\theta) + i\sin(\theta))}}{\left(Re^{i\theta} + i\varepsilon\right)\left(Re^{i\theta} - i\varepsilon\right)}\, d\theta \tag{A.46}$$

$$= \int_{-R}^{R} \frac{e^{ik_x\rho_x}}{(k_x+i\varepsilon)(k_x-i\varepsilon)}\,dk_x + \int_0^{\pi} \frac{iRe^{i\theta+i\rho_x R\cos(\theta)-\rho_x R\sin(\theta)}}{\left(Re^{i\theta}+i\varepsilon\right)\left(Re^{i\theta}-i\varepsilon\right)}\,d\theta \tag{A.47}$$

As previously, the integral over C_R approaches zero as $R \to \infty$ by Jordan's lemma.

$$\int_{-\infty}^{\infty} \frac{e^{ik_x\rho_x}}{(k_x+i\varepsilon)(k_x-i\varepsilon)}\,dk_x = 2\pi i\,Res\left(f(z=i\varepsilon)\right) \tag{A.48}$$

The pole at $z = i\varepsilon$ is simple, and therefore

$$\int_{-\infty}^{\infty} \frac{e^{ik_x\rho_x}}{(k_x+i\varepsilon)(k_x-i\varepsilon)}\,dk_x = 2\pi i \lim_{z\to i\varepsilon}\left[(z-i\varepsilon)\frac{e^{i\rho_x z}}{(z+i\varepsilon)(z-i\varepsilon)}\right] \tag{A.49}$$

$$\int_{-\infty}^{\infty} \frac{e^{ik_x\rho_x}}{(k_x+i\varepsilon)(k_x-i\varepsilon)}\,dk_x = 2\pi i \lim_{z\to i\varepsilon}\left[\frac{e^{i\rho_x z}}{(z+i\varepsilon)}\right] \tag{A.50}$$

$$\int_{-\infty}^{\infty} \frac{e^{ik_x\rho_x}}{(k_x+i\varepsilon)(k_x-i\varepsilon)}\,dk_x = 2\pi i\left(\frac{e^{i\rho_x i\varepsilon}}{2i\varepsilon}\right) \tag{A.51}$$

$$\int_{-\infty}^{\infty} \frac{e^{ik_x\rho_x}}{(k_x+i\varepsilon)(k_x-i\varepsilon)}\,dk_x = \frac{\pi e^{-\rho_x\varepsilon}}{\varepsilon} \tag{A.52}$$

This integral therefore does not converge as $\varepsilon \to 0$. We conclude that $k_y = k_0$ is an unphysical value for this system.

A.1.4 Returning to the Green function

From (A.16), taking all allowed values of k_y from the previous three subsections,

$$G\left(\vec{r},\vec{r}'\right) = \frac{1}{(2\pi)^2}\int_{-\infty}^{\infty} e^{ik_y\rho_y}\int_{-\infty}^{\infty} \frac{e^{ik_x\rho_x}}{\left(k_x+\sqrt{k_0^2-k_y^2}\right)\left(k_x-\sqrt{k_0^2-k_y^2}\right)}dk_x\,dk_y \tag{A.53}$$

$$G\left(\vec{r},\vec{r}'\right)=\frac{1}{(2\pi)^2}\int_{|k_y|<|k_0|}\frac{\pi i e^{ik_y\rho_y}e^{i\rho_x\sqrt{k_0^2-k_y^2}}}{\sqrt{k_0^2-k_y^2}}\,dk_y+\frac{1}{(2\pi)^2}\int_{|k_y|>|k_0|}\frac{\pi e^{ik_y\rho_y}e^{-\rho_x\sqrt{k_y^2-k_0^2}}}{\sqrt{k_y^2-k_0^2}}\,dk_y \tag{A.54}$$

$$=\frac{1}{(2\pi)^2}\left(\int_{-\infty}^{-|k_0|}\frac{\pi e^{ik_y\rho_y-\rho_x\sqrt{k_y^2-k_0^2}}}{\sqrt{k_y^2-k_0^2}}\,dk_y+\int_{-|k_0|}^{|k_0|}\frac{\pi i e^{ik_y\rho_y+i\rho_x\sqrt{k_0^2-k_y^2}}}{\sqrt{k_0^2-k_y^2}}\,dk_y\right.$$
$$\left.+\int_{|k_0|}^{\infty}\frac{\pi e^{ik_y\rho_y-\rho_x\sqrt{k_y^2-k_0^2}}}{\sqrt{k_y^2-k_0^2}}\,dk_y\right) \tag{A.55}$$

$$=\frac{1}{(2\pi)^2}\left(\int_{-\infty}^{-|k_0|}\frac{\pi e^{-\rho_x\sqrt{k_y^2-k_0^2}}\left(\cos\left(k_y\rho_y\right)+i\sin\left(k_y\rho_y\right)\right)}{\sqrt{k_y^2-k_0^2}}\,dk_y\right.$$
$$+\int_{-|k_0|}^{|k_0|}\frac{\pi i\left(\cos\left(k_y\rho_y+\rho_x\sqrt{k_0^2-k_y^2}\right)+i\sin\left(k_y\rho_y+\rho_x\sqrt{k_0^2-k_y^2}\right)\right)}{\sqrt{k_0^2-k_y^2}}\,dk_y$$
$$\left.+\int_{|k_0|}^{\infty}\frac{\pi e^{-\rho_x\sqrt{k_y^2-k_0^2}}\left(\cos\left(k_y\rho_y\right)+i\sin\left(k_y\rho_y\right)\right)}{\sqrt{k_y^2-k_0^2}}\,dk_y\right) \tag{A.56}$$

We note now that the first and third integrals above may be combined to yield a single integral which is symmetric about the origin, while the second integral is already symmetric about the origin. Further splitting these integrals into even and odd components,

$$= \frac{1}{(2\pi)^2}\left(\int_{\Gamma_1} \frac{\pi e^{-\rho_x\sqrt{k_y^2-k_0^2}}\cos(k_y\rho_y)}{\sqrt{k_y^2-k_0^2}}\,dk_y + \int_{\Gamma_1} \frac{\pi i e^{-\rho_x\sqrt{k_y^2-k_0^2}}\sin(k_y\rho_y)}{\sqrt{k_y^2-k_0^2}}\,dk_y \right.$$
$$\left. + \int_{-|k_0|}^{|k_0|} \frac{\pi i\cos\left(k_y\rho_y+\rho_x\sqrt{k_0^2-k_y^2}\right)}{\sqrt{k_0^2-k_y^2}}\,dk_y - \int_{-|k_0|}^{|k_0|} \frac{\pi\sin\left(k_y\rho_y+\rho_x\sqrt{k_0^2-k_y^2}\right)}{\sqrt{k_0^2-k_y^2}}\,dk_y \right) \tag{A.57}$$

where Γ_1 is the entire real k_y line except for the interval $[-|k_0|, |k_0|]$, which is symmetric about the origin. Since the second and fourth integrals above are odd in k_y and are integrated symmetrically with respect to the origin, they integrate to zero. We are left with

$$G(\vec{r},\vec{r}') = \frac{1}{(2\pi)^2}\left(\int_{\Gamma_1} \frac{\pi e^{-\rho_x\sqrt{k_y^2-k_0^2}}\cos(k_y\rho_y)}{\sqrt{k_y^2-k_0^2}}\,dk_y + \int_{-|k_0|}^{|k_0|} \frac{\pi i\cos\left(k_y\rho_y+\rho_x\sqrt{k_0^2-k_y^2}\right)}{\sqrt{k_0^2-k_y^2}}\,dk_y \right) \tag{A.58}$$

The remaining integrals are each even and integrated symmetrically with respect to the origin.

$$G(\vec{r},\vec{r}') = \frac{2}{(2\pi)^2}\left(\int_{|k_0|}^{\infty} \frac{\pi e^{-\rho_x\sqrt{k_y^2-k_0^2}}\cos(k_y\rho_y)}{\sqrt{k_y^2-k_0^2}}\,dk_y + \int_{0}^{|k_0|} \frac{\pi i\cos\left(k_y\rho_y+\rho_x\sqrt{k_0^2-k_y^2}\right)}{\sqrt{k_0^2-k_y^2}}\,dk_y \right) \tag{A.59}$$

Without loss of generality, let $\vec{\rho}$ lie along the k_y axis. Then $\rho_x = 0$ and $\rho_y = \rho \equiv |\vec{r}-\vec{r}'|$. We are left with

$$G\left(\vec{r},\vec{r}'\right)=\frac{2}{(2\pi)^2}\left(\int_{|k_0|}^{\infty}\frac{\pi\cos\left(k_y\rho\right)}{k_0\sqrt{\left(\frac{k_y}{k_0}\right)^2-1}}\,dk_y+\int_0^{|k_0|}\frac{\pi i\cos\left(k_y\rho\right)}{k_0\sqrt{1-\left(\frac{k_y}{k_0}\right)^2}}\,dk_y\right) \tag{A.60}$$

Let $u=\dfrac{k_y}{k_0}$. Note that for $k_y\to|k_0|$, $u\to\pm1$.

$$G\left(\vec{r},\vec{r}'\right)=\frac{1}{2\pi^2}\left(\int_1^{\infty}\frac{\pi\cos\left(k_0\rho u\right)}{k_0\sqrt{u^2-1}}\,k_0\,du+\int_0^{\pm1}\frac{\pi i\cos\left(k_0\rho u\right)}{k_0\sqrt{1-u^2}}\,k_0\,du\right) \tag{A.61}$$

Since the second integral above is even in u,

$$G\left(\vec{r},\vec{r}'\right)=\frac{1}{2\pi^2}\left(\int_1^{\infty}\frac{\pi\cos\left(k_0\rho u\right)}{k_0\sqrt{u^2-1}}\,k_0\,du+\int_0^{1}\frac{\pi i\cos\left(k_0\rho u\right)}{k_0\sqrt{1-u^2}}\,k_0\,du\right) \tag{A.62}$$

For the second integral above, let $u=\cos\left(t\right)$.

$$G\left(\vec{r},\vec{r}'\right)=\frac{1}{2\pi}\left(\int_1^{\infty}\frac{\cos\left(k_0\rho u\right)}{\sqrt{u^2-1}}\,du+\int_{\frac{\pi}{2}}^{0}\frac{-i\cos\left(k_0\rho\cos\left(t\right)\right)}{\sqrt{\sin^2\left(t\right)}}\,\sin\left(t\right)\,dt\right) \tag{A.63}$$

$$G\left(\vec{r},\vec{r}'\right)=\frac{1}{2\pi}\left(\int_1^{\infty}\frac{\cos\left(k_0\rho u\right)}{\sqrt{u^2-1}}\,du+i\int_0^{\frac{\pi}{2}}\cos\left(k_0\rho\cos\left(t\right)\right)\,dt\right) \tag{A.64}$$

The first integral above is an integral representation of the Bessel function of the second kind, order 0,

$$\int_1^{\infty}\frac{\cos\left(k_0\rho u\right)}{\sqrt{u^2-1}}\,du=\frac{\pi}{2}N_0\left(k_0\rho\right) \tag{A.65}$$

While the second integral of (A.63) is an integral representation of the Bessel function of the first kind, order 0,

$$\int_0^{\frac{\pi}{2}} \cos\left(k_0 \rho \cos\left(t\right)\right) dt = \frac{\pi}{2} J_0\left(k\rho\right) \tag{A.66}$$

Inserting (A.64) and (A.65) into (A.63),

$$G\left(\vec{r},\vec{r}'\right) = \frac{1}{2\pi}\left(\frac{\pi}{2} N_0\left(k_0\rho\right) + \frac{i\pi}{2} J_0\left(k_0\rho\right)\right) \tag{A.67}$$

$$G\left(\vec{r},\vec{r}'\right) = \frac{i}{4}\left(J_0\left(k_0\rho\right) iN_0\left(k_0\rho\right)\right) \tag{A.68}$$

$$G\left(\vec{r},\vec{r}'\right) = \frac{i}{4} H_0^{(1)}\left(k_0\rho\right) \tag{A.69}$$

where $H_0^{(1)}$ is the first Hankel function of order zero.

THIS PAGE INTENTIONALLY LEFT BLANK

APPENDIX B:
MATLAB Simulations

This appendix will present the MATLAB scripts used to simulate the various TO-derived structures studied in Chapter 5 of this work.

B.1 Cylindrical Cloak in Cartesian Mesh

```
%% An Iterative Approach: Cylindrical Structure with Cartesian Mesh
%%
% Input physical constants
%clearvars;
run('PhysicalConstants.m');
%%
%%
% Input known material values
a = 1;
b = 1.5;
R = (b-a)/b;
%%
% Input meshgrid for the region of interest.
increment = 0.03;
x = cat(2,-b:increment:-increment,increment:increment:b);
y = cat(2,-b:increment:-increment,increment:increment:b);
[X,Y] = meshgrid(x,y);
%%
% Convert to cylindrical coordinates
r = sqrt(X.^2+Y.^2);
origin = size(x,2)/2;
theta = zeros(size(x,2),size(x,2));
for n = 1:1:size(x,2)/2
    for m = 1:1:size(x,2)/2
        theta(n,m) = atan(y(n)/x(m))+pi;
        theta(n+size(x,2)/2,m) = atan(y(n+size(x,2)/2)/x(m))+pi;
        theta(n,m+size(x,2)/2) = atan(y(n)/x(m+size(x,2)/2))+2*pi;
```

```
        theta(n+size(x,2)/2,m+size(x,2)/2) = ...
            atan(y(n+size(x,2)/2)/x(m+size(x,2)/2));
    end
end
%%
% Input the coordinate transformation from $r$ to $r^{'}$.
r_prime = (r-a)./R;
for n = 1:1:size(x,2)
    for m = 1:1:size(x,2)
        if r(n,m) <= a
            r_prime(n,m) = 0;
        end
    end
end
%%
% Input the transformation optics derived susceptibilities. Assume vacuum
% outside of the "shield."
L_11 = zeros(size(x,2),size(x,2));
L_12 = zeros(size(x,2),size(x,2));
L_13 = zeros(size(x,2),size(x,2));
L_22 = zeros(size(x,2),size(x,2));
L_23 = zeros(size(x,2),size(x,2));
L_33 = ones(size(x,2),size(x,2));
L = cell(size(x,2),size(x,2));
Chi_11 = zeros(size(x,2),size(x,2));
Chi_12 = zeros(size(x,2),size(x,2));
Chi_13 = zeros(size(x,2),size(x,2));
Chi_22 = zeros(size(x,2),size(x,2));
Chi_21 = zeros(size(x,2),size(x,2));
Chi_23 = zeros(size(x,2),size(x,2));
Chi_31 = zeros(size(x,2),size(x,2));
Chi_32 = zeros(size(x,2),size(x,2));
Chi_33 = zeros(size(x,2),size(x,2));
for n = 1:1:size(x,2);
    for m = 1:1:size(x,2)
                L_11(n,m) = R+(a/r_prime(n,m))*(sin(theta(n,m)))^2;
                L_12(n,m) = -a*cos(theta(n,m))*sin(theta(n,m))/r_prime(n,m);
                L_22(n,m) = R+(a/r_prime(n,m))*(cos(theta(n,m)))^2;
    end
```

```
end
for n = 1:1:size(x,2)
    for m = 1:1:size(x,2)
        L{n,m} = [L_11(n,m),L_12(n,m),L_13(n,m);L_12(n,m),L_22(n,m),...
            L_23(n,m);L_13(n,m),L_23(n,m),L_33(n,m)];
    end
end
Chi = cell(size(x,2),size(x,2));
for n = 1:1:size(x,2)
    for m = 1:1:size(x,2)
        if r(n,m) > b
            Chi{n,m} = zeros(3,3);
        else if r(n,m) <= a
                Chi{n,m} = zeros(3,3);
            else
                Chi{n,m} = (L{n,m}*((L{n,m}).')).*(r_prime(n,m)/(R*...
                    r(n,m)))-eye(3);
            end
        end
    end
end
for n = 1:1:size(x,2)
    for m = 1:1:size(x,2)
        Chi_11(n,m) = Chi{n,m}(1,1);
        Chi_12(n,m) = Chi{n,m}(1,2);
        Chi_13(n,m) = Chi{n,m}(1,3);
        Chi_21(n,m) = Chi{n,m}(2,1);
        Chi_22(n,m) = Chi{n,m}(2,2);
        Chi_23(n,m) = Chi{n,m}(2,3);
        Chi_31(n,m) = Chi{n,m}(3,1);
        Chi_32(n,m) = Chi{n,m}(3,2);
        Chi_33(n,m) = Chi{n,m}(3,3);
    end
end
%%
% Input the incident fields, as well as the functions $F_1(E_0,H_0)$ and
% $F_2(H_0,E_0)$. Begin by choosing a value for $\omega_0$. Take $10^{11} Hz$.
k_0 = 1e-2;
%%
```

```
% Input the initial (frequency domain) electric field
E0_z = 2*pi.*exp(1i*k_0.*X);
%%
% Compute the tensor contractions appearing in $F_1$ and $F_2$

%%
% Perform the integration indicated in equation (3.40) to obtain the
% first-order response electric field.  Begin on the x-axis outside the
% shield.  That is, let $\vec{r} = -2a\hat{x}$.
rminusrprime = cell(size(x,2),size(x,2));
G1 = cell(size(x,2),size(x,2));
S1 = 3*X.^2.*Y.^4+3*X.^4.*Y.^2-r.^5+X.^6+Y.^6;
S2 = X.^2-2*r.^3+Y.^2;
Chi_22_x = X.*(6*X.^2.*r-r.^3+2*Y.^2)./S1-X.*(12*X.^2.*Y.^2-5*r.^3+6*...
    X.^4+6*Y.^4).*(X.^2+Y.^2-r.^5+2.*X.^2.*r.^3+Y.^4)./(S1.^2);
Chi_12_y = X.*S2./S1-2*X.*Y.^2.*(3*r-1)./S1-X.*Y.^2.*S2.*(12*X.^2.*Y.^2-...
    5*r.^3+6*X.^4+6*Y.^4)./(S1.^2);

for n = 1:1:size(x,2)
    for m = 1:1:size(x,2)
        if r(n,m) > b
            Chi_22_x(n,m) = 0;
            Chi_12_y(n,m) = 0;
        elseif r(n,m) <= a
            Chi_22_x(n,m) = 0;
            Chi_12_y(n,m) = 0;
        end
    end
end
for n = 1:1:size(x,2);
    for m = 1:1:size(x,2);
    rminusrprime{n,m} = sqrt((X(n,m)-X).^2+(Y(n,m)-Y).^2);
    G1{n,m} = besselh(0,1,k_0.*rminusrprime{n,m});
    G1{n,m}(n,m) = 0;
    end
end
%%
% Compute the integral (4.58)
F = cell(size(x,2),size(x,2));
```

```
for n = 1:1:size(x,2)
    for m = 1:1:size(x,2)
        F{n,m} = pi*1i/2*G1{n,m}.*exp(1i*k_0*X).*(k_0^2*Chi_33-1i*k_0* ...
            Chi_22_x+k_0^2*Chi_22+1i*k_0*Chi_12_y);
    end
end
E0_z = 2*pi*exp(1i*k_0*X);
E0_x = 0;
E1_z = zeros(size(x,2),size(x,2));
for n = 1:1:size(x,2)
    for m = 1:1:size(x,2)
        E1_z(n,m) = increment^2*trapz(trapz(F{n,m},2));
    end
end
%%
% Linear approach.
E_0 = 1;
D_x = (Chi_11+1)*E_0;
D_y = (Chi_21)*E_0;
D_r = D_x.*cos(theta)+D_y.*sin(theta);
for n = 1:1:size(x,2)
    for m = 1:1:size(x,2)
        if r(n,m) <=a
            D_r(n,m) = 0;
        end
    end
end
%%
% Streamline plot the linear field
streamline(X,Y,D_x,D_y,-b*ones(1,size(x,2)),y);
%%
% Graphs
h1 = surf(X,Y,Chi_11);
title('$\chi_{xx}$ for Cylindrical Redirection Structure','interpreter',...
    'latex','fontsize',14);
xlabel('x (meters)','interpreter','latex','fontsize',12);
ylabel('y (meters)','interpreter','latex','fontsize',12);
zlabel('$\chi_{xx}$','interpreter','latex','fontsize',14);
figure
```

```
surf(X,Y,abs(E0_z+E1_z)/(2*pi))
xlabel('x (meters)','interpreter','latex');
ylabel('y (meters)','interpreter','latex');
zlabel('$\frac{\left|E_0+E_1\right|}{\left|E_0\right|}$','interpreter',...
    'latex','fontsize',14);
figure
surf(X,Y,abs(E1_z)/(2*pi));
title('1st Order Response Field Amplitude Relative to $\left|E_0\right|$',...
    'interpreter','latex');
xlabel('x (meters)','interpreter','latex');
ylabel('y (meters)','interpreter','latex');
zlabel('$\frac{\left|E_1\right|}{\left|E_0\right|}$','interpreter',...
    'latex','fontsize',14);
```

B.2 Cylindrical Structure in Cylindrical Mesh

```
%% An Iterative Approach: Cylindrical Structure in Cylindrical Mesh
%%
% Input physical constants
clearvars;
%run('PhysicalConstants.m');
%%
% Input known material parameters
a = 1;
b = 1.5;
R = (b-a)/b;
%%
% Input cylindrical meshgrid for the region of interest
rstep = 0.02;
rmax = 2;
phistep = pi/50;
[r,phi] = meshgrid(0:rstep:rmax,0:phistep:2*pi);
%%
% Input relative permittivity in cylindrical coordinates.
eps_rr = ((r-a)./r).^2;
eps_pp = ones(size(r));
eps_zz = (1/R)^2.*ones(size(r));
```

```
for n = 1:1:size(phi,1)
    for m = 1:1:size(r,2)
        if r(n,m)>b
            eps_rr(n,m) = 1;
            eps_pp(n,m) = 1;
            eps_zz(n,m) = 1;
        elseif r(n,m)<=a
            eps_rr(n,m) = 1;
            eps_pp(n,m) = 1;
            eps_zz(n,m) = 1;
        end
    end
end
%%
% Convert to Cartesian coordinates. Compute the susceptibility.
eps_xx = eps_rr.*(cos(phi)).^2+eps_pp.*(sin(phi)).^2;
eps_yy = eps_rr.*(sin(phi)).^2+eps_pp.*(cos(phi)).^2;
eps_xy = (eps_rr-eps_pp).*sin(phi).*cos(phi);
chi_xx = eps_xx-1;
chi_yy = eps_yy-1;
chi_xy = eps_xy;
chi_yx = eps_xy;
chi_zz = eps_zz-1;
%%
% Plot the xx component of the  permittivity for comparison with the purely
% Cartesian approach
h1 = surf(r.*cos(phi),r.*sin(phi),chi_xx);
hold on
title('$\chi_{xx}$ for Cylindrical Redirection Structure','interpreter',...
    'latex','fontsize',14);
xlabel('x (meters)','interpreter','latex','fontsize',12);
ylabel('y (meters)','interpreter','latex','fontsize',12);
zlabel('$\chi_{xx}$','interpreter','latex','fontsize',14);
hold off
%%
% Input incident wavenumber and electric field
k_0 = 1e-1;
E0_z = 2*pi*exp(1i*k_0*r.*cos(phi));
%%
```

```
% Input the terms to be integrated
X = r.*cos(phi);
Y = r.*sin(phi);
S1 = 3*X.^2.*Y.^4+3*X.^4.*Y.^2-r.^5+X.^6+Y.^6;
S2 = X.^2-2*r.^3+Y.^2;
chi_yy_x = X.*(6*X.^2.*r-r.^3+2*Y.^2)./S1-X.*(12*X.^2.*Y.^2-5*r.^3+6*...
    X.^4+6*Y.^4).*(X.^2+Y.^2-r.^5+2.*X.^2.*r.^3+Y.^4)./(S1.^2);
chi_xy_y = X.*S2./S1-2*X.*Y.^2.*(3*r-1)./S1-X.*Y.^2.*S2.*(12*X.^2.*...
    Y.^2-5*r.^3+6*X.^4+6*Y.^4)./(S1.^2);
for n = 1:1:size(r,1)
    for m = 1:1:size(r,2)
        if r(n,m) > b
            chi_yy_x(n,m) = 0;
            chi_xy_y(n,m) = 0;
        elseif r(n,m) <= a
            chi_yy_x(n,m) = 0;
            chi_xy_y(n,m) = 0;
        end
    end
end
rminusrprime = cell(size(r));
G = cell(size(r));
rdphi = phistep*r(1,:);
for n = 1:1:size(r,1)
    for m = 1:1:size(r,2)
        rminusrprime{n,m} = sqrt((X(n,m)-X).^2+(Y(n,m)-Y).^2);
        G{n,m} = -besselh(0,1,k_0.*rminusrprime{n,m});
        G{n,m}(n,m) = 0;
    end
end
F = cell(size(r));
for n = 1:1:size(r,1)
    for m = 1:1:size(r,2)
        F{n,m} = pi*1i/2*G{n,m}.*exp(1i*k_0*X).*(k_0^2*chi_zz-1i*k_0* ...
            chi_yy_x+k_0^2*chi_yy+1i*k_0*chi_xy_y);
    end
end
E1_z = zeros(size(r));
for n = 1:1:size(r,1)
```

```
    for m = 1:1:size(r,2)
        E1_z(n,m) = rstep*trapz(rdphi.*trapz(F{n,m},1));
    end
end
%%
% Graphs
figure;
h2 = surf(X,Y,abs(E1_z+E0_z)/(2*pi));
hold on
title('1st Order Response Field Amplitude Relative to $\left|E_0\right|$',...
    'interpreter','latex');
xlabel('x (meters)','interpreter','latex');
ylabel('y (meters)','interpreter','latex');
zlabel('$\frac{\left|E_0+E_1\right|}{\left|E_0\right|}$','interpreter',...
    'latex','fontsize',14);
title('1st Order Combined Field Amplitude Relative to $\left|E_0\right|$',...
    'interpreter','latex');
hold off
xx = -rmax:rstep:rmax;
E0_c = cat(2,fliplr(E0_z(51,:)),E0_z(1,:));
E1_c = cat(2,fliplr(E1_z(51,:)),E1_z(1,:));
E0_c(size(r,2)+1) = [];
E1_c(size(r,2)+1) = [];
figure
plot(xx,abs(E0_c+E1_c)/(2*pi))
hold on
T = '1st Order Combined Field Along X-axis Relative to $\left|E_0\right|$';
title(T,'Interpreter','latex');
xlabel('x (meters)','interpreter','latex');
ylabel('$\frac{\left|E_0+E_1\right|}{\left|E_0\right|}$','interpreter',...
    'latex','fontsize',14);
hold off
```

B.3 Reduced Material Parameter Cylindrical Structure in Cylindrical Mesh

```
%% An Iterative Approach: Reduced Parameter Cylindrical Structure
```

```
%%
% Input physical constants
clearvars;
%run('PhysicalConstants.m');
%%
% Input known material parameters
a = 1;
b = 1.5;
R = (b-a)/b;
%%
% Input cylindrical meshgrid for the region of interest
rstep = 0.008;
rmax = 2;
phistep = pi/50;
[r,phi] = meshgrid(0:rstep:rmax,0:phistep:2*pi);
%%
% Input relative permittivity in cylindrical coordinates.
eps_rr = ((r-a)./r).^2;
eps_pp = ones(size(r));
eps_zz = (1/R)^2.*ones(size(r));
for n = 1:1:size(phi,1)
    for m = 1:1:size(r,2)
        if r(n,m)>b
            eps_rr(n,m) = 1;
            eps_pp(n,m) = 1;
            eps_zz(n,m) = 1;
        elseif r(n,m)<=a
            eps_rr(n,m) = 1;
            eps_pp(n,m) = 1;
            eps_zz(n,m) = 1;
        end
    end
end
%%
% Convert to Cartesian coordinates. Compute the susceptibility.
eps_xx = eps_rr.*(cos(phi)).^2+eps_pp.*(sin(phi)).^2;
eps_yy = eps_rr.*(sin(phi)).^2+eps_pp.*(cos(phi)).^2;
eps_xy = (eps_rr-eps_pp).*sin(phi).*cos(phi);
chi_xx = eps_xx-1;
```

```
chi_yy = eps_yy-1;
chi_xy = eps_xy;
chi_yx = eps_xy;
chi_zz = eps_zz-1;
%%
% Plot the xx component of the  permittivity for comparison with the purely
% Cartesian approach
h1 = surf(r.*cos(phi),r.*sin(phi),chi_xx);
hold on
title('$\chi_{xx}$ for Cylindrical Redirection Structure','interpreter',...
    'latex','fontsize',14);
xlabel('x (meters)','interpreter','latex','fontsize',12);
ylabel('y (meters)','interpreter','latex','fontsize',12);
zlabel('$\chi_{xx}$','interpreter','latex','fontsize',14);
hold off
%%
% Input incident wavenumber and electric field
k_0 = 1e-1;
E0_z = 2*pi*exp(1i*k_0*r.*cos(phi));
%%
% Input the terms to be integrated
X = r.*cos(phi);
Y = r.*sin(phi);
chi_yy_x = (2*X.*Y.^2).*(3*r-2)./(r.^6);
chi_xy_y = -X.*(2*X.^2.*r-4*Y.^2.*r-X.^2+3*Y.^2)./(r.^6);
for n = 1:1:size(r,1)
    for m = 1:1:size(r,2)
        if r(n,m) > b
            chi_yy_x(n,m) = 0;
            chi_xy_y(n,m) = 0;
        elseif r(n,m) <= a
            chi_yy_x(n,m) = 0;
            chi_xy_y(n,m) = 0;
        end
    end
end
rminusrprime = cell(size(r));
G = cell(size(r));
rdphi = phistep*r(1,:);
```

```
for n = 1:1:size(r,1)
    for m = 1:1:size(r,2)
        rminusrprime{n,m} = sqrt((X(n,m)-X).^2+(Y(n,m)-Y).^2);
        G{n,m} = -besselh(0,1,k_0.*rminusrprime{n,m});
        G{n,m}(n,m) = 0;
    end
end
F = cell(size(r));
for n = 1:1:size(r,1)
    for m = 1:1:size(r,2)
        F{n,m} = pi*1i/2*G{n,m}.*exp(1i*k_0*X).*(k_0^2*chi_zz-1i*k_0* ...
            chi_yy_x+k_0^2*chi_yy+1i*k_0*chi_xy_y);
    end
end
E1_z = zeros(size(r));
for n = 1:1:size(r,1)
    for m = 1:1:size(r,2)
        E1_z(n,m) = rstep*trapz(rdphi.*trapz(F{n,m},1));
    end
end
%%
% Graphs
figure;
h2 = surf(X,Y,abs(E1_z+E0_z)/(2*pi));
hold on
title('1st Order Combined Field Amplitude Relative to $\left|E_0\right|$',...
    'interpreter','latex');
xlabel('x (meters)','interpreter','latex');
ylabel('y (meters)','interpreter','latex');
zlabel('$\frac{\left|E_0+E_1\right|}{\left|E_0\right|}$','interpreter',...
    'latex','fontsize',14);
title('1st Order Combined Field Amplitude Relative to $\left|E_0\right|$',...
    'interpreter','latex');
hold off
xx = -rmax:rstep:rmax;
E0_c = cat(2,fliplr(E0_z(51,:)),E0_z(1,:));
E1_c = cat(2,fliplr(E1_z(51,:)),E1_z(1,:));
E0_c(size(r,2)+1) = [];
E1_c(size(r,2)+1) = [];
```

```
figure
plot(xx,abs(E0_c+E1_c)/(2*pi))
hold on
T = '1st Order Combined Field Along X-axis Relative to $\left|E_0\right|$';
title(T,'Interpreter','latex');
xlabel('x (meters)','interpreter','latex');
ylabel('$\frac{\left|E_0+E_1\right|}{\left|E_0\right|}$','interpreter',...
    'latex','fontsize',14);
hold off
```

B.4 Square Cloak

```
%% An Iterative Approach: Symbolic Method for Square Cloak
%%
% Input physical constants
clearvars;
run('PhysicalConstants.m');
%%
% Input predetermined structure shape. Let $S_1$ and $S_2$ be the inner and
% outer half side lengths, respectively.
s1 = 1;
s2 = 2;
%%
% Input symbolic expression for the electric permittivity, as per Pendry et
% al. Rotate the symbolic expression through $\frac{\pi}{2}$, $\pi$, and
% $\frac{3\pi}{2}$ in order to obtain the permittivity throughout the
% structure.
syms x y z;
a = s2/(s2-s1);
b = symfun(a*y*s1/(x^2),[x y]);
c = symfun(a*(1-s1/x),[x y]);
eps1 = symfun([c/a,-b/a,0;-b/a,(a^2+b^2)/(a*c),0;0,0,a*c],[x y]);
%%
% Input meshgrid for the region of interest.
increment = 0.03;
[X,Y] = meshgrid(-1.5*s2:increment:1.5*s2,-1.5*s2:increment:1.5*s2);
%%
```

```
% Determine numeric values of the permittivity over one quarter of the
% structure, and rotate, as per [8].
A_90 = [0,-1,0;1,0,0;0,0,1];
A_n90 = [0,1,0;-1,0,0;0,0,1];
A_180 = [-1,0,0;0,-1,0;0,0,1];
A_n180 = A_180;
A_270 = [0,1,0;-1,0,0;0,0,1];
A_n270 = [0,-1,0;1,0,0;0,0,1];
eps2 = symfun(A_90* ...
    eps1(dot(A_n90*[x;y;0],[1;0;0]),dot(A_n90*[x;y;0],[0;1;0]))*...
    A_90.',[x y]);
eps3 = symfun(A_180* ...
    eps1(dot(A_n180*[x;y;0],[1;0;0]),dot(A_n180*[x;y;0],[0;1;0]))*A_180.',...
    [x y]);
eps4 = symfun(A_270* ...
    eps1(dot(A_n270*[x;y;0],[1;0;0]),dot(A_n270*[x;y;0],[0;1;0]))*A_270.',...
    [x y]);
chi1 = symfun(eps1(x,y)-eye(3),[x y]);
chi2 = symfun(eps2(x,y)-eye(3),[x y]);
chi3 = symfun(eps3(x,y)-eye(3),[x y]);
chi4 = symfun(eps4(x,y)-eye(3),[x y]);
CHI = cell(size(X,2),size(X,2));
CHI_11 = zeros(size(X,2),size(X,2));
CHI_12 = zeros(size(X,2),size(X,2));
CHI_22 = zeros(size(X,2),size(X,2));
CHI_33 = zeros(size(X,2),size(X,2));
G = cell(size(X,2),size(X,2));
k_0 = 2e-1;
for n = 1:1:size(X,2)
    for m = 1:1:size(X,2)
        if atan2(Y(n,m),X(n,m)) >= -pi/4 && atan2(Y(n,m),X(n,m)) < pi/4
            if abs(X(n,m)) == s1
                CHI{n,m} = zeros(3,3);
            elseif abs(X(n,m)) < s1 && abs(Y(n,m)) < s1
                CHI{n,m} = zeros(3,3);
            elseif abs(X(n,m)) > s2 || abs(Y(n,m)) > s2
                CHI{n,m} = zeros(3,3);
            else
                CHI{n,m} = double(chi1(X(n,m),Y(n,m)));
```

```
65              end
66          end
67          if atan2(Y(n,m),X(n,m)) >= pi/4 && atan2(Y(n,m),X(n,m)) < 3*pi/4
68              if abs(Y(n,m)) == s1
69                  CHI{n,m} = zeros(3,3);
70              elseif abs(X(n,m)) < s1 && abs(Y(n,m)) < s1
71                  CHI{n,m} = zeros(3,3);
72              elseif abs(X(n,m)) > s2 || abs(Y(n,m)) > s2
73                  CHI{n,m} = zeros(3,3);
74              else
75                  CHI{n,m} = double(chi2(X(n,m),Y(n,m)));
76              end
77          end
78          if atan2(Y(n,m),X(n,m)) >= 3*pi/4 || atan2(Y(n,m),X(n,m)) < -3*pi/4
79              if abs(X(n,m)) == s1
80                  CHI{n,m} = zeros(3,3);
81              elseif abs(X(n,m)) < s1 && abs(Y(n,m)) < s1
82                  CHI{n,m} = zeros(3,3);
83              elseif abs(X(n,m)) > s2 || abs(Y(n,m)) > s2
84                  CHI{n,m} = zeros(3,3);
85              else
86                  CHI{n,m} = double(chi3(X(n,m),Y(n,m)));
87              end
88          end
89          if atan2(Y(n,m),X(n,m)) >= -3*pi/4 && atan2(Y(n,m),X(n,m)) < -pi/4
90              if abs(Y(n,m)) == s1
91                  CHI{n,m} = zeros(3,3);
92              elseif abs(X(n,m)) < s1 && abs(Y(n,m)) < s1
93                  CHI{n,m} = zeros(3,3);
94              elseif abs(X(n,m)) > s2 || abs(Y(n,m)) > s2
95                  CHI{n,m} = zeros(3,3);
96              else
97                  CHI{n,m} = double(chi4(X(n,m),Y(n,m)));
98              end
99          end
100         CHI_11(n,m) = CHI{n,m}(1,1);
101         CHI_12(n,m) = CHI{n,m}(1,2);
102         CHI_22(n,m) = CHI{n,m}(2,2);
103         CHI_33(n,m) = CHI{n,m}(3,3);
```

```
        G{n,m} = besselh(0,1,k_0.*sqrt((X(n,m)-X).^2+(Y(n,m)-Y).^2));
        G{n,m}(n,m) = 0;
    end
end
%%
% Compute the derivatives of the susceptibility appearing in (4.60)
chi1_12 = symfun(conj(dot(chi1(x,y)*[0;1;0],[1;0;0])),[x y]);
chi1_12_y = symfun(diff(chi1_12(x,y),y),[x y]);
chi2_12 = symfun(dot(chi2(x,y)*[0;1;0],[1;0;0]),[x y]);
chi2_12_y = symfun(diff(chi2_12(x,y),y),[x y]);
chi3_12 = symfun(dot(chi3(x,y)*[0;1;0],[1;0;0]),[x y]);
chi3_12_y = symfun(diff(chi3_12(x,y),y),[x y]);
chi4_12 = symfun(dot(chi4(x,y)*[0;1;0],[1;0;0]),[x y]);
chi4_12_y = symfun(diff(chi4_12(x,y),y),[x y]);
chi1_22 = symfun(conj(dot(chi1(x,y)*[0;1;0],[0;1;0])),[x y]);
chi1_22_x = symfun(diff(chi1_22(x,y),x),[x y]);
chi2_22 = symfun(dot(chi2(x,y)*[0;1;0],[0;1;0]),[x y]);
chi2_22_x = symfun(diff(chi2_22(x,y),x),[x y]);
chi3_22 = symfun(dot(chi3(x,y)*[0;1;0],[0;1;0]),[x y]);
chi3_22_x = symfun(diff(chi3_22(x,y),x),[x y]);
chi4_22 = symfun(dot(chi4(x,y)*[0;1;0],[0;1;0]),[x y]);
chi4_22_x = symfun(diff(chi4_22(x,y),x),[x y]);
CHI_12_y = zeros(size(X,2),size(X,2));
CHI_22_x = zeros(size(X,2),size(X,2));
for n = 1:1:size(X,2)
    for m = 1:1:size(X,2)
        if atan2(Y(n,m),X(n,m)) >= -pi/4 && atan2(Y(n,m),X(n,m)) < pi/4
            if abs(X(n,m)) == s1
                CHI_12_y(n,m) = 0;
                CHI_22_x(n,m) = 0;
            elseif abs(X(n,m)) < s1 && abs(Y(n,m)) < s1
                CHI_12_y(n,m) = 0;
                CHI_22_x(n,m) = 0;
            elseif abs(X(n,m)) > s2 || abs(Y(n,m)) > s2
                CHI_12_y(n,m) = 0;
                CHI_22_x(n,m) = 0;
            else
                CHI_12_y(n,m) = double(chi1_12_y(X(n,m),Y(n,m)));
                CHI_22_x(n,m) = double(chi1_22_x(X(n,m),Y(n,m)));
```

```
143             end
144         end
145         if atan2(Y(n,m),X(n,m)) >= pi/4 && atan2(Y(n,m),X(n,m)) < 3*pi/4
146             if abs(X(n,m)) == s1
147                 CHI_12_y(n,m) = 0;
148                 CHI_22_x(n,m) = 0;
149             elseif abs(X(n,m)) < s1 && abs(Y(n,m)) < s1
150                 CHI_12_y(n,m) = 0;
151                 CHI_22_x(n,m) = 0;
152             elseif abs(X(n,m)) > s2 || abs(Y(n,m)) > s2
153                 CHI_12_y(n,m) = 0;
154                 CHI_22_x(n,m) = 0;
155             else
156                 CHI_12_y(n,m) = double(chi2_12_y(X(n,m),Y(n,m)));
157                 CHI_22_x(n,m) = double(chi2_22_x(X(n,m),Y(n,m)));
158             end
159         end
160         if atan2(Y(n,m),X(n,m)) >=3*pi/4 || atan2(Y(n,m),X(n,m)) < -3*pi/4
161             if abs(X(n,m)) == s1
162                 CHI_12_y(n,m) = 0;
163                 CHI_22_x(n,m) = 0;
164             elseif abs(X(n,m)) < s1 && abs(Y(n,m)) < s1
165                 CHI_12_y(n,m) = 0;
166                 CHI_22_x(n,m) = 0;
167             elseif abs(X(n,m)) > s2 || abs(Y(n,m)) > s2
168                 CHI_12_y(n,m) = 0;
169                 CHI_22_x(n,m) = 0;
170             else
171                 CHI_12_y(n,m) = double(chi3_12_y(X(n,m),Y(n,m)));
172                 CHI_22_x(n,m) = double(chi3_22_x(X(n,m),Y(n,m)));
173             end
174         end
175         if atan2(Y(n,m),X(n,m)) >= -3*pi/4 && atan2(Y(n,m),X(n,m)) < -pi/4
176             if abs(X(n,m)) == s1
177                 CHI_12_y(n,m) = 0;
178                 CHI_22_x(n,m) = 0;
179             elseif abs(X(n,m)) < s1 && abs(Y(n,m)) < s1
180                 CHI_12_y(n,m) = 0;
181                 CHI_22_x(n,m) = 0;
```

```
            elseif abs(X(n,m)) > s2 || abs(Y(n,m)) > s2
                CHI_12_y(n,m) = 0;
                CHI_22_x(n,m) = 0;
            else
                CHI_12_y(n,m) = double(chi4_12_y(X(n,m),Y(n,m)));
                CHI_22_x(n,m) = double(chi4_22_x(X(n,m),Y(n,m)));
            end
        end
    end
end
F = cell(size(X,2),size(X,2));
for n = 1:1:size(X,2)
    for m = 1:1:size(X,2)
        F{n,m} = pi*1i/2*G{n,m}.*exp(1i*k_0*X).*(k_0^2*CHI_33-1i*k_0*...
            CHI_22_x+k_0^2*CHI_22+1i*k_0*CHI_12_y);
    end
end
E1_z = zeros(size(X,2),size(X,2));
for n = 1:1:size(X,2);
    for m = 1:1:size(X,2)
        E1_z(n,m) = increment^2*trapz(trapz(F{n,m},2));
    end
end
E0_z = 2*pi*exp(1i*k_0*X);
%%
% Graphs
surf(X,Y,CHI_11)
title('$\chi_{xx}$ for Square Structure','interpreter','latex');
xlabel('x (meters)','interpreter','latex');
ylabel('x (meters)','interpreter','latex');
zlabel('$\chi_{xx}$','interpreter','latex','fontsize',14);
figure
surf(X,Y,abs(E0_z+E1_z)/(2*pi))
title('1st Order Combined Field Amplitude Relative to $\left|E_0\right|$',...
    'interpreter','latex');
xlabel('x (meters)','interpreter','latex');
ylabel('y (meters)','interpreter','latex');
zlabel('$\frac{\left|E_0+E_1\right|}{\left|E_0\right|}$','interpreter',...
    'latex','fontsize',14);
```

```
figure
plot(X(101,:),abs(E0_z(101,:)+E1_z(101,:))/(2*pi));
T = '1st Order Combined Field Along X-axis Relative to $\left|E_0\right|$';
title(T,'interpreter','latex');
xlabel('x (meters)','interpreter','latex');
ylabel('$\frac{\left|E_0+E_1\right|}{\left|E_0\right|}$','interpreter',...
    'latex','fontsize',14);
```

THIS PAGE INTENTIONALLY LEFT BLANK

List of References

[1] Office of Naval Research. (2015). Long range broad agency announcement (BAA) for Navy and Marine Corps science and technology. Internet draft. [Online]. Available: http://www.onr.navy.mil/~/media/Files/Funding-Announcements/BAA/2016/N00014-16-R-BA001.ashx. Accessed April 23, 2016.

[2] D. S. J. Pendry and D. Smith, "Controlling electromagnetic fields," *Science*, vol. 312, pp. 1780–1782, June 2006.

[3] D. Schurig *et al.*, "Metamaterial electromagnetic cloak at microwave frequencies," *Science*, vol. 314, pp. 977–979, November 2006.

[4] R. W. Boyd, *Nonlinear Optics*. New York, NY: Academic Press, 2008.

[5] Office of Naval Research. (2015). Directed energy program. Public web page. [Online]. Available: http://www.onr.navy.mil/Science-Technology/Departments/Code-35/All-Programs/air-warfare-352/Directed-Energy.aspx. Accessed April 29, 2016.

[6] G. Kulacki. (2014). An authoritative source on china's military space strategy. Internet draft. [Online]. Available: http://www.ucsusa.org/sites/default/files/legacy/assets/documents/nwgs/China-s-Military-Space-Strategy.pdf#1. Accessed April 29, 2016.

[7] Office of Naval Research. (2015). Counter-directed energy program. Public web page. [Online]. Available: http://www.onr.navy.mil/en/Science-Technology/Departments/Code-35/All-Programs/aerospace-research-351/Counter-Directed-Energy.aspx. Accessed April 29, 2016.

[8] J. Pendry *et al.*, "Design of electromagnetic cloaks and concentrators using form-invariant coodrinate transformations of maxwell's equations," *Photonics and Nanos-tructures – Fundamentals and Applications*, vol. 6, pp. 87–95, Apr. 2008.

[9] T. P. U. Leonhardt, "Transformation optics and the geometry of light," *Progress in Optics*, vol. 53, pp. 1–72, June 2008.

[10] O. Paul and M. Rahm, "Covariant description of transformation optics in nonlinear media," *Optics Express*, vol. 20, pp. 8982–8997, Apr. 2012.

[11] B. P. S. Cummer *et al.*, "Full-wave simulations of electromagnetic cloaking structures," *Physical Review*, vol. 74, May 2000.

[12] A. K. W. Cai, U. Chettiar and V. Shalaev, "Optical cloaking with metamaterials," *Nature Photonics*, vol. 1, pp. 224–227, April 2007.

[13] Y. F. Y. Huang and T. Jiang, "Electromagnetic cloaking by layered structure of homogenous isotropic materials," *Optics Express*, vol. 15, pp. 11 133–11 141, September 2007.

[14] D. R. Smith *et al.*, "Composite medium with simultaneously negative permeability and permittivity," *Physical Review Letters*, vol. 84, September 2006.

[15] E. J. Post, *Formal Structure of Electromagnetics: General Covariance and Electromagnetics*. Mineola, NY: Dover Publications.

[16] J. Luscombe, "Relativity and cosmology," unpublished.

[17] R. Courant and D. Hilbert, *Methods of Mathematical Physics, Volume 1*. New York, NY: Interscience Publishers, 1954.

[18] J. J. Sakurai, *Modern Quantum Mechanics*. Reading, MA: Addison-Wesley Publishing Company, 1994.

Initial Distribution List

1. Defense Technical Information Center
   Ft. Belvoir, Virginia

2. Dudley Knox Library
   Naval Postgraduate School
   Monterey, California